STUDY THERMOELECTRIC PROPERTIES OF DELAFOSSITE $CuFe_{(1-x)}M_{(x)}O_2$ WHEN M= Ga, Al and $0 \leq x \leq 0.5$

YUTTANA HONGAROMKIJ

A THESIS SUMITTED IN PARTIAL FULFILLMENT
OF THE REQUIREMENTS FOR THE DEGREE OF
DOCTOR OF PHILOSOPHY IN APPLIED PHYSICS
FACULTY OF SCIENCE
KING MONGKUT'S INSTITUTE OF TECHNOLOGY LADKRABANG
2016

KMITL-2016-SC-D-030-005

STUDY THERMOELECTRIC PROPERTIES OF DELAFOSSITE $CuFe_{(1-x)}M_{(x)}O_2$ WHEN M= Ga, Al and $0 \leq x \leq 0.5$

YUTTANA HONGAROMKIJ

A THESIS SUMITTED IN PARTIAL FULFILLMENT

OF THE REQUIREMENTS FOR THE DEGREE OF

DOCTOR OF PHILOSOPHY IN APPLIED PHYSICS

FACULTY OF SCIENCE

KING MONGKUT'S INSTITUTE OF TECHNOLOGY LADKRABANG

2016

KMITL-2016-SC-D-030-005

หัวข้อวิทยานิพนธ์	การศึกษาคุณสมบัติเทอร์โมอิเล็กทริกของ ดีลาฟอร์ไซด์ $CuFe_{(1-x)}M_{(x)}O_2$ เมื่อ M= Ga, Al และ $0 \leq x \leq 0.5$
ชื่อนักศึกษา	นาย ยุทธนา หงษ์อารมณ์กิจ
รหัสประจำตัว	53650104
ปริญญา	ปรัชญาดุษฎีบันฑิต
สาขาวิชา	ฟิสิกส์ประยุกต์
พ.ศ.	2559
อาจารย์ที่ปรึกษาวิทยานิพนธ์	ผศ.ดร.เชรษฐา รัตนพันธ์

บทคัดย่อ

จุดประสงค์ของวิทยานิพนธ์นี้ เพื่อศึกษาคุณสมบัติเทอร์โมอิเล็กทริกของสารประกอบโครงสร้างเดลาฟอสไซท์ โดยใช้สารประกอบโครงสร้างหลักเป็น $CuFeO_2$ การสังเคราะห์สารประกอบโครงสร้างเดลาฟอสไซท์ของวิทยานิพนธ์นี้ ทำการสังเคราะห์แทนที่ เหล็ก (Fe) บางส่วนโดยจำนวนเปอร์เซ็นต์ ของสารที่เข้าแทนที่คือ 10%, 30% และ 50% สารที่เข้าแทนที่มี แกลเลี่ยม (Ga) และ อลูมิเนียม (Al) ตามสูตรทางเคมี $CuFe_{(1-x)}M_{(x)}O_2$ เมื่อ M= Ga, Al และ $0 \leq x \leq 0.5$ การเลือกสารประกอบโครงสร้างหลักเป็น $CuFeO_2$ นั้น เนื่องด้วยสารประกอบโครงสร้างหลักนี้มีคุณสมบัติเป็นสารกึ่งตัวนำ ซึ่งเป็นคุณสมบัติที่ตรงตามทฤษฎีของเทอร์โมอิเล็กทริก และ มีค่าการนำไฟฟ้าที่สูงที่สุดในกลุ่มเดียวกันเมื่อเทียบกับ $CuMO_2$ เมื่อ M= โครเมียม (Cr), แมงกานีส (Mn), โคบอลต์ (Co), หรือแม้แต่ อลูมิเนียม (Al), และ แกลเลียม (Ga) การเลือกสารเพื่อแทนที่ โดยวิทยานิพนธ์ นี้เลือก แกลเลี่ยม และอลูมิเนียม เพราะ ขนาดรัศมีอะตอม ของสารที่เลือกมีขนาดเล็กกว่าขนาดรัศมีอะตอมของเหล็ก (Ga^{3+}=0.625, Al^{3+}=0.535, and Fe^{3+}=0.645 A°) เมื่อขนาดรัศมีอะตอมของสารที่แทนมีขนาดเล็กกว่าส่งผลทำให้แลตทิสสเปรซของแต่ละแลตทิสมีระยะห่างน้อยลง ซึ่งยืนยันได้จากผลการวัด X-ray Diffraction (XRD) ทำให้เกิดแลตทิสสเตรน (little Strain) จากการศึกษาพบว่า แลตทิสสเตรน มีผลทำให้ค่าการนำความร้อนลดลง ซึ่งค่าการนำความร้อนนี้แปรผกผันกลับกับค่าประสิทธิ์ภาพเทอร์โมอิเล็กทริก มากกว่านั้น แกลเลียม และ อลูมิเนียม มีน้ำหนักอะตอม (Atomic Mass) ที่แตกต่างกับเหล็ก (Ga=69.723, Al=26.982, and Fe=55.847) การแทนที่ น้ำหนักของอะตอมที่แตกต่างกัน และเมื่อวัสดุได้รับความร้อนทำให้อะตอมเกิดการสั่น (lattice Vibration) ผลต่างของน้ำหนักอะตอม ทำให้เกิด แอนฮาโมนิค (anhamonic) ซึ่ง

หมายความว่า ประสิทธ์ภาพของการนำความร้อนลดลง ส่งผลให้ประสิทธิ์ภาพเทอร์โมอิเล็กทริกเพิ่มขึ้น ผลการวัด ประสิทธ์ภาพของการนำความร้อนของลดลงโดย $CuFeO_2$ 5.5 W/mK เป็น 2.5 w/mK เมื่อแทนที่ แกลเลียมเข้าไป 50 เปอร์เซ็นต์ ($CuFe_{0.5}Ga_{0.5}O_2$).

อีกหนึ่งเหตุผลที่ เลือกสารที่เข้าแทนที่เป็น แกลเลี่ยม (Ga) และ อลูมิเนียม (Al) เพราะ $CuGaO_2$ และ $CuAlO_2$ มีค่า สัมประสิทธิ์ซีแบค ที่สูง เพื่อเพิ่มประสิทธิ์ภาพเทอร์โมอิเล็กทริก แต่อย่างไรก็ตาม ผลที่ตามมาคือค่า การนำไฟฟ้า ลดลงตามอัตราส่วนที่เข้าแทนที่ ค่าสัมประสิทธิ์ซีแบคที่สูงสุด 578 μV/K at 469 K เมื่อแทนที่ แกลเลียมเข้าไป 50 เปอร์เซ็นต์ ($CuFe_{0.5}Ga_{0.5}O_2$) **ค่าการนำไฟฟ้าสูงสุด** 875 $\Omega^{-1}m^{-1}$ of $CuFe_{0.5}Al_{0.5}O_2$ at 849 K ค่า power factor สูงสุดที่ $CuFeO_2$ และ $CuFe_{0.9}Al_{0.1}O_2$ 1.1 $\times 10^{-4}$ W/m-K^2 at 849 K และค่า Dimensionless Figure of Merit สูงสุดที่ $CuFeO_2$ (ZT=0.0086) at 573 K.

คำสำคัญ : เทอร์โมอิเล็กทริก, แลตทิสสเปรซ, แลตทิสสเตรน, แอนฮาโมนิค, สัมประสิทธิ์ซีแบค

Thesis Title	Study Thermoelectric Properties of Delafossite $CuFe_{(1-x)}M_{(x)}O_2$ when M= Ga, Al and $0 \leq x \leq 0.5$
Student Name	Mr. Yuttana Hongaromkij
Student ID	53650104
Degree	Doctor of philosophy
Program	Applied Physics
Year	2016
Thesis Advisor	Assistant Professor Doctor Chesta Ruttanapun

Abstract

The purpose of this thesis is study thermoelectric property of delafossite $CuFe_{(1-x)}M_{(x)}O_2$ when M= Ga, Al and $0 \leq x \leq 0.5$. The $CuFeO_2$ selected is base due to property of its semiconductor and higher electrical conductivity of the group. By general formula of group is $CuMO_2$ by M= Cr, Mn, Co, Al and Ga. The Ga and Al selected because nature oxidation state of its 3^+ and smaller atomic radius (Ga^{3+}=0.625, Al^{3+}=0.535, and Fe^{3+}=0.645 A°). The difference of atomic radius effect to lattice space of each lattice is shortened. Affect to thermal conductivity decreases by Lattice Strain which thermal conductivity decreases meaning is increase thermoelectric efficiency. The Lattice Strain confirms results by X-ray diffraction by main peak shifted or angle of diffraction increases. Moreover the Ga and Al have mass difference (Ga=69.723, Al=26.982, and Fe=55.847). The mass difference affect to vibration of lattice or effect to decreases of thermal conductivity by anhamonic. The measurement results of thermal conductivity decreases with ratio of substitution of Ga and Al. The lowest thermal conductivity is 2.5 W/mK of $CuFe_{0.5}Ga_{0.5}O_2$ at 573 K ($CuFeO_2$ 5.5 W/mK at 573 K).

And the reason one selected Ga and Al because $CuGaO_2$ and $CuAlO_2$ are high value of seebeck coefficient. The measurement results of seebeck coefficient increases with ratio of substitution of Ga and Al. But very low electrical conductivity

because carrier concentration decreases. The higher seebeck coefficient is 578 μV/K of $CuFe_{0.5}Ga_{0.5}O_2$ at 469 K. And higher electrical conductivity is 875 $\Omega^{-1}m^{-1}$ of $CuFe_{0.9}Al_{0.1}O_2$ at 849 K. Maximum power factor this study is $CuFeO_2$ and $CuFe_{0.9}Al_{0.1}O_2$ 1.1 $\times 10^{-4}$ W/m-K^2 at 849 K. And Dimensionless Figure of Merit is $CuFeO_2$ (ZT=0.0086) at 573 K.

Keywords: **Thermoelectric, Lattice Space, Lattice Strain, Anhamonic, Seebeck coefficient**

Acknowledgements

(กิตติกรรมประกาศ)

ความสำเร็จของวิทยานิพนธ์ฉบับนี้ได้รับความกรุณาจากอาจารย์ที่ปรึกษา รศ.ดร. อารีย์ วิเชียรฉาย และ ผศ.ดร.เชรษฐา รัตนพันธ์ ที่ให้คำปรึกษาหัวข้องานวิจัย คำชี้แนะและช่วยแก้ปัญหาจนทำให้งานวิจัยสำเร็จลุล่วงเป็นอย่างดี

ขอขอบคุณคณะกรรมการสอบวิทยานิพนธ์ โดยมี รศ.ดร. อารีย์ วิเชียรฉาย ผศ.ดร.ประธาน บุรณศิริ ดร. วรการ นียากร และ ผศ.ดร.อาภาภรณ์ สกุลการะเวก

ขอขอบคุณ ผศ.ดร.อาภาภรณ์ สกุลการะเวก ให้ความอนุเคราะห์ สารตั้งต้น แกลเลียม ที่ใช้ในวิทยานิพนธ์นี้

ขอขอบคุณ นาย เฉลิมพล รุจรดาวงศ์ ที่ช่วยในการติดตั้งเครื่องมือการเตรียมสาร เตรียมสาร และ ส่งสารตัวอย่างวัดคุณสมบัติ

ขอขอบคุณ นาย วัชรินทร์ สามิตร ช่วยวาดโครงสร้างอะตอม เพื่อง่ายต่อความเข้าใจและส่งตีพิมพ์ในระดับนานาชาติ นาย ยอดยิ่ง หมวกงาม ที่ช่วยใช้โปรแกรมคณิตศาสตร์ คำนวณสมการที่มีหลายตัวแปร

ขอขอบคุณ ดร.เกษญา วัชรนุกูล ช่วยทบทวนเนื้อหาบทความก่อนตีพิมพ์ในระดับนานาชาติ ช่วยปรับแก้ภาษาบทความตีพิมพ์ในระดับนานาชาติ ช่วยปรับแก้ภาษาให้เหมาะสมในวิทยานิพนธ์ฉบับนี้

ขอขอบคุณ ดร.จริยา บัวเจริญ ช่วยอธิบายคำศัพท์เฉพาะด้านในเชิงเคมี

ขอขอบคุณ ดร.อัชยา เทพพิทักษ์ศักดิ์ และ ว่าที่ ดร.รุ่งโรจน์ เมาลานนท์ ปรับแก้ภาษาให้เหมาะสมในวิทยานิพนธ์ฉบับนี้

สำหรับคุณงามความดีอันใดที่เกิดจากวิทยานิพนธ์ฉบับนี้ ข้าพเจ้าขอมอบให้กับ บิดามารดา ญาติพี่น้อง และทุกคนที่เป็นกำลังใจ ตลอดจนครู อาจารย์ที่ได้ประสาทวิชาความรู้และถ่ายทอดประสบการณ์ที่ดีให้แก่ข้าพเจ้า

ยุทธนา หงษ์อารมณ์กิจ

6 ธันวาคม 2559

Table of Contents

List of Tables

List of Figures

List of Abbreviations

Electrical Potential (Voltage)	V
Temperature	T
Seebeck Coefficient	S
Thermal Power	Q
Peltier Coefficient	Π
Current Density	J
Efficiency	η
Power	P
Current	I
Road	R_L
Electrical Resistivity	ρ
Thermal Conductivity	κ
Dimensionless Figure of merit	ZT
Electrical Conductivity	σ
Carrier Concentration	n
Mobility	μ
Energy	E
Density of State of Energy E	$g(E)$
Probability of occupation of a state of energy E	$p(E)$
Mass	m

Fermi Energy	E_F
Boltzmann Constant	k
Planck's Constant	h
Fermi Integral	F_r
Relaxation Time	τ
Electronic Thermal Conductivity	κ_{el}
Lattice Thermal Conductivity	κ_{ph}
Specific Heat	C
Velocity of Sound	V_s
Phonon Frequency	ω
Umklapp Temperature	θ_u
Debye Temperature	θ_D
Thermal Expansion Coefficient	α
Grunesen Constant	γ
Melting Point Temperature	T_m
Mean Atomic Weight	A
Relaxation Time frequency for two scattering process	ν_0
Upper limit of distribution of Lattice vibration	ν_m
Wavelength of X-ray Beam	λ
Thermal Diffusion	α_d
Kinetic Energy	K
Binning Energy	B

Work Function	W
Absorbance	A_a
Energy Gap	E_g
Intensity of light	I
Molar extinction coefficient	α_M
Full width half maximum	$\beta_{1/2}$
Thermal Resistivity	K
Thermal Resistivity by substitution impurity	A
Intrinsic thermal resistivity	B
Cross Section of Phonon Scattering	Γ_i
Internal Energy	U
Work Done	W_d
Entropy	$S_{entropy}$
Energy edge conduction band	E_c
Energy edge conduction band	E_v

Chapter 1

Introduction

1.1 Research Motivation

Energy is necessary for life and industry. The demand for consuming energy is drastically increasing. The primary energy source is fossil fuel such as coal, petroleum and nature gas [1]. In contrast to an increase in the demand for energy, the rate of discoveries of energy sources (fossil fuels) decreases. To overcome this problem, environment implication with method converse is used to change fossil fuels to energy. Many researchers have been searching for renewable energy sources such as biofuel, wind, solar, hydroelectric and thermoelectric power. These sources of energy release very little or no releasing toxic gases such as carbon dioxide and sulfur dioxide into the environment [1, 2]. Recently, renewable of energy sources has been found to decrease fuel fossil usage approximately 19% [1-5] However, to compete with fossil fuel energy, improvement in efficiency of generating electric power from renewable energy sources is crucial. This requires improvement in science and engineering.

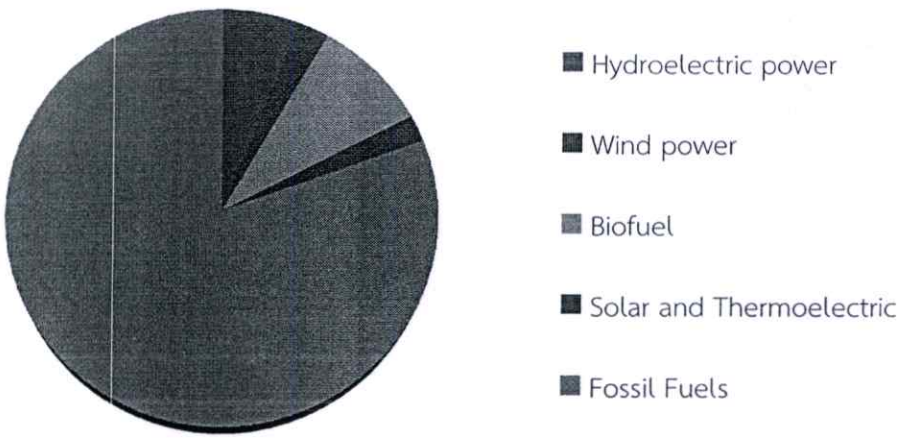

Figure 1.1 Global energy sources.

Waste-heat losses from industrial processes are unprofitable. In general, the energy about 20-70 percent, depending on a nature of industrial process cannot be

avoided. Therefore the suitable solution is to convert this waste-heat into electrical energy again.

This study focuses on clean energy source based on thermoelectric method. The most famous groups of material for thermoelectric generator are $(Bi,Sb)_2Te_3$, $Bi_2(Te,Se)_3$ and PbTe [1, 6]. The advantage of this group is that it provides high efficiency but it is toxic, low operating temperature and easily oxidized [7, 8]. The thermoelectric efficiency of this group as a function of temperature is shown in figure 1.2 [9] .Tellurium (Te) material is the main of component of this group, this is the one problem because Tellurium (TE) is one of the rarest materials and thus [1, 7], very high cost. It is necessary to find the alternative component which still maintain or increase the conversion efficiency. I. Terasaka [10] reported ZT at 300 K of 0.264 based on $NaCo_2O_4$. The main limitation of $NaCo_2O_4$ is a volatility of Na and hygroscopicity of the material [8]. Since we are interested in improving the delafossite oxide structure to achieve better thermoelectric property, $CuFeO_2$ was used as the base structure in the work. The advantages of the delafossite oxide based on $CuFeO_2$ are very low toxicity, low cost high operating temperature.

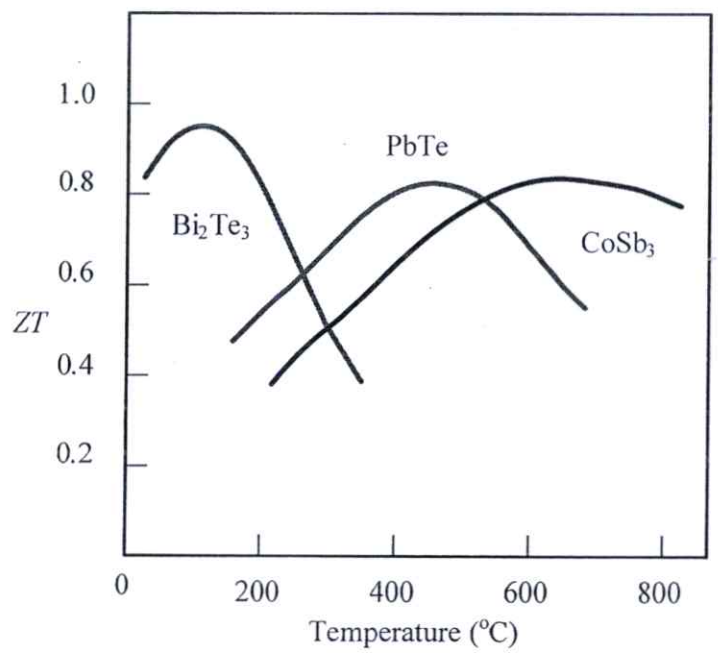

Figure 1.2 Thermoelectric Efficiency plots with temperature

Typical delafossite-type oxides have the chemical formula AMO_2, in which A= Cu, Pt, Pd, Ag and M=Cr, Fe, Al, Co, Ga and so on [11-12]. The unit cell of this structure is hexagonal, the oxygen atoms are bonded to the A site atoms in a dumbbell configuration and the edge sharing layer M atoms are octahedral configured as MO_6, as shown in figure 1.3 [13].

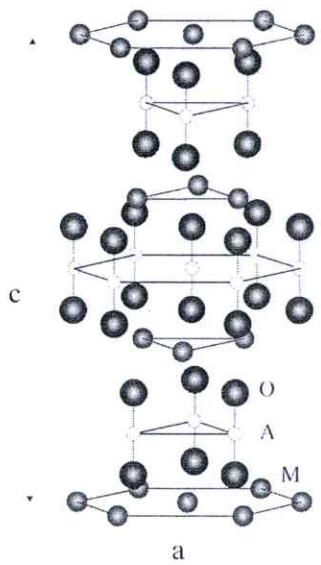

Figure 1.3 Delafossite structure AMO_2 (A, M and O is circle yellow, red and blue)

Delafossite-structure A-site, Pt and Pd improved the electrical conductivity because was metallic conductor affect to Seebeck coefficient low value [14-15] and starting material expensive. Ions in A-site were Cu and Ag, property show semiconductor [8-12]. The resistivity of Ag is much higher than Cu, therefore Cu was selected into A-site because high electrical conductivity [12, 16] and cheap.

Delafossite-structure M-site, and M=Cr, Fe, Al, Co, Ga and so on [11-12]. Among of M-site large electrical conductivity by Cu A-site was Fe ($CuFeO_2$) and resistivity of compound show in table 1.1. Therefore $CuFeO_2$ selected into base because electrical property mainly governed by mixed valence of Cu^{1+}/Cu^{2+} and Fe^{2+}/Fe^{3+} [16-19].

Table 1.1 Resistivity of compound delafossite

Compound	Resistivity (Parallel axis)
$PtCoO_2$	$1x10^{-3}$ Ohm-cm
$PdCoO_2$	$2.1x10^{-3}$ Ohm-cm
$CuFeO_2$	$3x10^{3}$ Ohm-cm
$AgFeO_2$	$2x10^{10}$ Ohm-cm

K.Park et al [8] reported $CuAl_{1-x}Fe_xO_2$ ($0 \leq x \leq 0.2$) provided the highest value of power factory (1.1×10^{-4} $W/m^{-1}K^{-2}$) at x=0.1 and 1140 K. Chesta.R [20] reported $Cu_{1-x}Pt_xFeO_2$ ($0.0 \leq x \leq 0.05$) had the high dimensionless figure of merit (ZT) at x=0.05 was 0.05 and the power factor of 2.0×10^{-4} $W/m^{-1}K^{-2}$. It is observed that the power factor and the ZT were high because of the high electrical conductivity while Seebeck coefficient estimation was not changed at x=0. The higher electrical conductivity is the more thermal conductivity increases in the series.

K. Kei Hayashi et al. [21] reported that $CuFe_{1-x}Ni_xO_2$ ($0 \leq x \leq 0.05$) had the maximum ZT = 0.14 at x = 0.01 at 1100 K. In this case, the dimensionless figure of merit was high at x=0.01 due to low thermal conductivity because electrical conductivity of x=0.01, 0.02 and 0.03 was approximately the same value. Though, Seebeck coefficient showed high at x=0.00. The interrelationship of three parameters (Seebeck coefficient, electrical conductivity and thermal conductivity) is related to functions carrier. The value of Seebeck coefficient decreases as the carrier increases while electrical conductivity and total thermal conductivity increase. The total thermal conductivity (κ) can be generated by electronic and lattice (phonon), $\kappa=\kappa_e+\kappa_l$ [22, 24]. One parameter that is not dependent to electrical conductivity and has very slight effect to Seebeck coefficient is lattice thermal conductivity.

This aim of this work is to improve thermoelectric material base $CuFeO_2$ by substitution Aluminum (Al) and Gallium (Ga) [25] in the Iron (Fe) of this structure in order to increase the efficiency by reducing thermal conductivity.

1.2 Objectives of the study

1.2.1 To study delafossite oxide structure of $CuFeO_2$.

1.2.2 To study delafossite oxide structure of $CuFe_{1-x}M_xO_2$ when M= Al, Ga and x=0.1, 0.3 and 0.5.

1.2.3 To study Seebeck coefficient and electrical conductivity of $CuFeO_2$ and $CuFe_{1-x}M_xO_2$ when M= Al, Ga and x=0.1, 0.3 and 0.5.

1.2.4 To study thermal conductivity of $CuFeO_2$ and $CuFe_{1-x}M_xO_2$ when M= Al, Gaand x=0.1, 0.3 and 0.5.

1.2.5 To study thermoelectric property of $CuFeO_2$ and $CuFe_{1-x}M_xO_2$ when M= Al, Ga and x=0.1, 0.3 and 0.5.

1.3 Scope of the study

1.3.1 Fabricate delafossite oxide structure of $CuFeO_2$.

1.3.2 Fabricate delafossite oxide structure of $CuFe_{1-x}M_xO_2$ when M= Al, Ga and x=0.1, 0.3 and 0.5.

1.3.3 Characterize Seebeck coefficient, electrical conductivity and thermal conductivity of $CuFeO_2$.

1.3.4 Characterize Seebeck coefficient, electrical conductivity and thermal conductivity of $CuFe_{1-x}M_xO_2$ when M= Al, Ga and x=0.1, 0.3 and 0.5.

1.3.5 Analyze thermoelectric property of $CuFeO_2$ and $CuFe_{1-x}M_xO_2$ when M= Al, Ga and x=0.1, 0.3 and 0.5.

1.4 Benefits of the study

1.4.1 New compound of delafossite oxide structure.

1.4.2 Knowledge of new compound to Seebeck coefficient and electrical conductivity.

1.4.3 Knowledge of new compound to thermal conductivity.

1.4.4 Knowledge of new compound to thermoelectric property.

1.4.5 This work can be a reference in thermoelectric new material.

Chapter 2

Theory and Literature Reviews

2.1 Theory

2.1.1 Basic Principle

The thermoelectric effect is the direct conversion of thermal energy to electrical energy and vice versa. The conversion of thermal energy into electrical energy is first discovered and described by Seebeck in 1822. After that, in 1834, Jean Charles Athanase Peltier expanded the work to heat reverse (absorbed or expel) at a junction between two dissimilar conductors when a current pass through the junction (electrical energy converse to thermal energy) [26].

The Seebeck effect description to the electromotive force set up with open circuit condition and temperature difference between junction of two dissimilar conductor wires *a* and *b*, as showed in figure 2.1 [27-29]. The voltage (*dV*) can be generated proportional to the temperature difference (*dT*).

$$dV \propto dT = S_{a,b}dT \qquad (2.1)$$

When $S_{a,b}$ is Seebeck Coefficient or Thermoelectric Power. The magnitude of $S_{a,b}$in general depend on the both (a and b) of material and on the difference temperature of the junction.

$$S_{a,b} = \lim_{T->0} \frac{\Delta V}{\Delta T} = \frac{dV}{dT} \qquad (2.2)$$

Jean Charles Athanase Peltier discover and reported relation of heat reverse (absorbed or expel) at a junction between two dissimilar conductors when a current pass through the junction (electrical energy converse to thermal energy) [28-29]. This process is called the Peltier Effect. Peltier was found the reversible heat absorbed per unit time and unit cross-section area with current density passing dissimilar conductor *a* and *b* in figure 2.2 [29]. If a current flow from n-type material to the p-type, the dominate carriers in both material move away from the junction and carry away heat. The junction becomes cold because the electrical current pump heat away from the junction [28, 29].

$$Q_P = \Pi_{a,b} J \qquad (2.3)$$

When $\Pi_{a,b}$ Peltier coefficient and J is current density

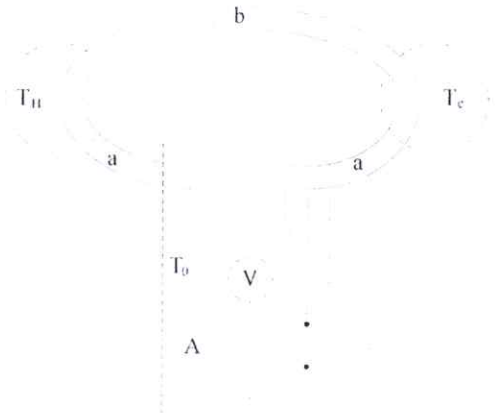

Figure 2.1 Thermoelectric circuit composed dissimilar two conductor material *a* and *b*

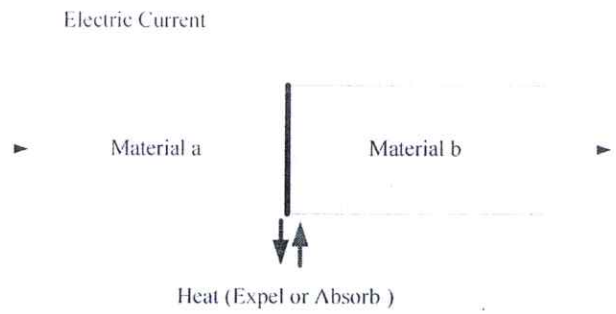

Figure 2.2 Current applied to conductor effect to heat (absorbs or expel)

2.1.2 Conversion Efficiency

Conversion efficiency (η) is defined as the ratio of the electrical power output (P) to the thermal power input at the hot side (Q). The maximum efficiency in a load R_L as shown figure 2.3 [28, 29].

$$\eta = P/Q \qquad (2.4)$$

According to figure 2.3, emf V_0 and road R_L evaluate electrical power output (P) is

$$P = I^2 R_L$$

where I is the electrical current and R_L is the load resistance.

In the thermoelectric generator device, when the heat is applied at one side of the materials. This leads to an increase of the kinetic energy of the charge carriers in both legs of the device. Difference in thermal energy difference leads to diffusion of the charge carriers from hot end to the cold end as shown in figure 2.3. The charge carriers can be accumulated at the cold end. Therefore, connecting between two cold sides of the materials generating current flows around the loop.

The thermal power input (Q) is the heat applied at the hot junction [28]. By assuming the material is homogeneous, Seebeck coefficient (S), electrical resistivity (ρ) and thermal conductivity (κ) are temperature-independent. Three main effects that related to a reduction of the thermal power input are from

1. The heat is absorbed by the material at hot junction, or usually referred to as Peltier heat (Q_1), which can be calculated by

$$Q_1 = -\Pi I$$

2. Joule heat (Q_2) generated in the element go to the hot junction.

$$Q_2 = -\left(\frac{I^2}{2}\right)[\rho_a + (\frac{\rho_b}{A})]$$

3. Processes of thermal conduction (Q_3).Heat transferred from the hot side to the cold side via thermal conduction [1-8].

$$Q_3 = (\kappa_a + A\kappa_b)\Delta T/L$$

where L is the length and A is the cross section area of material, assuming both of sides is equal in length and cross section area. Therefore

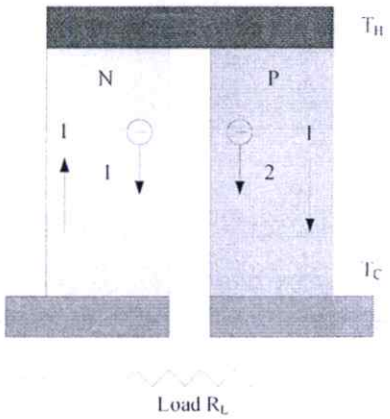

Figure 2.3 Thermoelectric generator p-type and n-type and load R_L.

$$\eta = \frac{I^2 R}{\{(\kappa_a + \kappa_b A)\left(\frac{\Delta T}{L}\right) - \left(\frac{I^2}{2}\right)\left[\rho_a + \left(\frac{\rho_b}{A}\right)\right] - \Pi I\}} \tag{2.5}$$

where$I = \frac{-S_{ab}\Delta T}{\{R_L + \left(\rho_a + \left(\frac{\rho_b}{A}\right)\right)L\}}$Equation 2.5 can be maximums with respect to the two adjustable parameters A and R. And $\overline{T} = (T_h + T_c)/2$ therefore

$$\eta_{max} = \left(\frac{\Delta T}{T_h}\right)\left[\left(1 + \overline{T}Z\right)^{\frac{1}{2}} - 1\right] / \left[\left(1 + \overline{T}Z\right)^{\frac{1}{2}} + \left(\frac{T_c}{T_h}\right)\right] \tag{2.6}$$

$$Z = \frac{(S_{ab})^2}{[(\rho_a \kappa_a)^{1/2} + (\rho_b \kappa_b)^{1/2}]^2} \tag{2.7}$$

where Z in equation is referred to as the figure of merit for the thermoelectric material, $S_{a,b}$ is the Seebeck coefficient, $\rho_{a,b}$ is the electrical resistivity and κ_a and κ_b is the total thermal conductivities of the material a and b respectively. If a single material is used, the figure of merit can be simplified as,

$$Z = \frac{S^2}{\rho\kappa} = \frac{S^2\sigma}{\kappa}$$

Where σ is the electrical conductivity. According to equation 2.6 and 2.7, it can be seen that the efficiency is proportional to $(\frac{\Delta T}{T_h})$ and depended with material parameter thought the combination *Z*.

2.1.3 Figure of Merit

The figure of merit is a critical parameter for evaluating thermoelectric material performance. The maximum efficiency of thermoelectric generator is limited by the figure of merit($ZT = \frac{S^2\sigma}{\kappa}T$). In the ideal material, large value of Seebeck coefficient (S), electrical conductivity (σ) and small value thermal conductivity (κ) are desired. However, in reality interrelations of these parameters are the nature of a material. The Seebeck coefficient value is inversely proportional to the electrical conductivity value. The thermal conductivity is also related with the electrical conductivity due to charge carrier related thermal conductivity figure 2.4 [28, 29] illustrates the evolution of S, σ and κ as a function of the carrier concentration. The optimum Seebeck coefficient is achieved where carrier concentration is within a range of semiconductor.

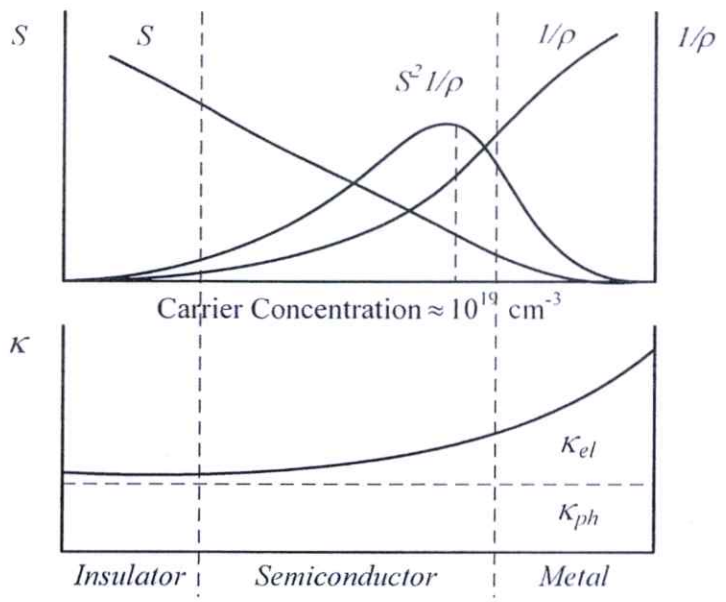

Figure 2.4 Evolution of S, σ, κ and ZT as a function of the carrier concentration.

2.1.4 Electrical Conductivity [30-33]

The electrical conductivity, σ, is defined as the current density, J, per the electric field, E,.

$$\sigma = \frac{J}{E} \tag{2.8}$$

Necessary to specify E sufficient to small so that Ohm's law. Refer the Ohm's law must be electrical conductivity independent with E and it establish electrical conductivity, σ, is

$$\sigma = ne\mu \tag{2.9}$$

where n is the carrier concentration or electron per unit volume, e is the charge of an electron and μ is the electron mobility.

2.1.4.1 Carrier Concentration (n)

The charge carriers in the conduction band and valance band move randomly in all direction due to its kinetic energy depended on the energy of the occupied state. The number of electron (dn) in a band between energy E and E+dE is depended on the density of states in the energy interval and the probability of occupation of a state of energy E. Thus

$$dn = g(E)dEp(E) \tag{2.10}$$

where g(E)dE is the density of states in the energy interval E and E+dE and p(E) is the probability of occupation of a state of energy E.

The density of states, g(E)dE

The nature of electron motion in a potential free space is characterized by quantum numbers n_x, n_y and n_z. The result of quantum number, the density of the electron state between energy interval E and E+dE is.

$$g(E)dE = 4\pi\left(\frac{2m}{h^2}\right)^{\frac{3}{2}} E^{1/2}dE$$

Probability of occupation of a state of energy E, p(E)

According to Fermi-Dirac statistic which obeys the Pauli Exclusion Principle. The occupation probability for a state of energy E is

$$p(E) = \frac{1}{e^{\frac{E-E_f}{kT}} + 1}$$

where E_f is the Fermi energy, T is the temperature and k is the Boltzmann constant.

Thus $$n = \int dn = 4\pi \left(\frac{2m}{h^2}\right)^{\frac{3}{2}} \int_0^{\infty} E^{\frac{1}{2}} \left[1 + exp\left(\frac{E-E_f}{kT}\right)\right]^{-1} dE$$

By substituting $\frac{E}{kT} = \xi$ and $\frac{E_f}{kT} = \eta$ into the above equation and normalize the energy, we obtain:

$$n = \frac{4}{\sqrt{\pi}} \left(\frac{2\pi mkT}{h^2}\right)^{\frac{3}{2}} \int_0^{\infty} \frac{\xi^{\frac{1}{2}} d\xi}{e^{\xi - n} + 1}$$

where $F_{r(n)}$ is the Fermi integral and $F_{r(n)} = \int_0^{\infty} \xi^r \frac{1}{e^{\xi-\eta+1}} d\xi$

Thus $$n = 4\pi^{\frac{-1}{2}} \left(\frac{2\pi mkT}{h^2}\right)^{\frac{3}{2}} F_{\frac{1}{2}(n)} \qquad (2.11)$$

The value of $F_{\frac{1}{2}(n)}$ is dependent upon with η or $\frac{E_f}{kT}$. Since as the carrier concentration of material varies proportions are with the temperature and the location of the Fermi energy.

2.1.4.2 Mobility

The mobility of electron is defined as the electron drift velocity, (V), per field strength, E. As The velocity of electron is directly proportional with the relaxation time, (τ), where $\upsilon = (\frac{eE}{m})\tau$. Thus, mobility can be described in term of relaxation time by,

$$\mu = \frac{V}{E} = \frac{e\tau}{m} \qquad (2.12)$$

Two main effects that could reduce the relaxation time, and thus the mobility are:

- Crystal defects such as impurity atoms, dislocation and surface scattering.

- Second cased by lattice vibration of the atom.

2.1.5 Seebeck Coefficient [34, 35]

The Seebeck coefficient value is a constant value of each material at a particular temperature. If we refer back to figure 2.3, the temperature gradient between two plates could lead to induced voltage (Seebeck effect) according to equation 2.2. Seebeck coefficient is a constant value which measures the magnitude of the induced voltage which results from a thermal gradient or,

$$E_x = S\frac{dT}{dx} \tag{2.13}$$

where E_x is an electric field results from temperature gradient

In microscopic order, this effect can be described by Boltzmann transport equation.

$$\left[\frac{df(E)}{dt}\right]_{field} + \left[\frac{df(E)}{dt}\right]_{collision} = 0 \tag{2.14}$$

Only consider p(E) change as a results of external field and rewritten eq (2.14) is.

$$\left[\frac{dp(E)}{dt}\right]_{field} = -\left[\frac{dp(E)}{dt}\right]_{collision} = -\frac{p(E)-p_0(E)}{\tau} \tag{2.15}$$

The rate of change of the occupational probability for a state of energy E resulting from the external field was considered earlier in the development of electrical conductivity.

In this case, the disturbed field is the temperature gradient which in turn establishes an electrical field. Therefore, the effect of both the temperature gradient and electrical field on $dp(E)/dt$ is given by,

$$-\frac{p(E)-p_0(E)}{\tau} = \frac{\partial p}{\partial E}\frac{\partial E}{\partial v}\frac{dv_x}{dt} + \frac{\partial p}{\partial E}\frac{\partial E}{\partial T}\frac{dT}{dx}v_x \qquad (2.16)$$

For an electron $\frac{dv_x}{dt} = -\frac{eE}{m}$ and $\frac{dx}{dt} = v_x$

$$p(E) = p_0(E) + \frac{eE}{m}\tau\frac{\partial p(E)}{\partial E}\frac{\partial E}{\partial v_x} - \tau v_x\frac{\partial p}{\partial E}\frac{\partial E}{\partial T}\frac{dT}{dx} \qquad (2.17)$$

The current density, J, in from definition of the Seebeck coefficient = 0. Therefore

$$-e\int v_x p(E)g(E)dE = 0$$

By substituting the value of p(E) from eq 2.16 into eq. 2.17 and limiting the integral from E=0 to infinity,

$$-e\int_0^\infty g(E)v_x p_0(E)dE - \frac{e^2E}{m}\int_0^\infty v_x\tau\frac{\partial p}{\partial E}\frac{\partial E}{\partial v_x}g(E)dE + e\frac{dT}{dx}\int_0^\infty v_x^2\tau\frac{\partial p}{\partial E}\frac{\partial E}{\partial T}g(E)dE = 0 \qquad (2.18)$$

Thus

$$S = \left[\frac{E}{\frac{dT}{dx}}\right]_{J=0} = \frac{\int_0^\infty v_x^2\tau\frac{\partial P\partial E}{\partial E\partial T}g(E)d(E)}{\frac{e}{m}\int_0^\infty v_x\tau\frac{\partial P}{\partial E}\frac{\partial E}{\partial v_x}g(E)d(E)} \qquad (2.19)$$

The value of $\frac{\partial E}{\partial T}$ determine from $\frac{\partial E}{\partial T} = \frac{\partial p}{\partial T}\Big/\frac{\partial p}{\partial E}$

Thus $$S = \frac{1}{eT}\left[E_f - \frac{\int_0^\infty E^2\tau\frac{\partial p}{\partial E}g(E)dE}{\int_0^\infty E\tau\frac{\partial p}{\partial E}g(E)dE}\right] \qquad (2.20)$$

Substituting $\tau = aE^b$ and $g(E) = 4\pi\left(\frac{2m}{h^2}\right)^{\frac{3}{2}}E^{\frac{1}{2}}$ and rewritten eq 2.20

$$S = \frac{1}{eT}\left[E_f - \frac{\int_0^\infty E^{b+5/2}\frac{\partial p}{\partial E}dE}{\int_0^\infty E^{b+3/2}\frac{\partial p}{\partial E}dE}\right] \qquad (2.21)$$

And express in term of Fermi integral.

$$S = \frac{1}{eT}\left[E_f - \frac{kT\left(b+\frac{5}{2}\right)F_{b+\frac{3}{2}}(\eta)}{\left(b+\frac{3}{2}\right)F_{b+\frac{3}{2}}(\eta)}\right] \qquad (2.22)$$

The equation 2.21 is the general expression for the Seebeck coefficient in a piece of material. This equation indicates that the Seebeck coefficient depends upon the location of the Fermi energy of material and type of scattering mechanism of carrier concentration.

2.1.6 Thermal Conductivity [36-41]

Thermal conductivity of material is a measure of the transport of energy through material due to temperature gradient. In material the heat flux at a point is directly proportional to the temperature gradient at that point. The quantity of heat flow (q_r) pass a unit cross section in a unit time when temperature gradient $(\frac{dT}{dx})$ is given by,

$$q_r = -\kappa \frac{dT}{dx} \tag{2.23}$$

where κ is the thermal conductivity. Thermal conductivity is a property to conduct heat via microscopic collisions. The process is also known as a diffusion process. The entities diffusing are capable of absorbing and releasing heat energy. The thermal conductivity consists of two components, lattice vibration (κ_{ph}) or phonon and free electron transport(κ_{el}) according to,

$$\kappa = \kappa_{el} + \kappa_{ph} \tag{2.24}$$

2.1.6.1Electronic Thermal Conductivity(κ_{el})

According to equation 2.22 and 2.23, by assuming one dimensional heat transfer, heat energy transported by electrons is given by,

$$\kappa_{el} = -q_r \frac{dT}{dx} \tag{2.25}$$

The element heat flux densitydq_r, which depends upon the number of electrons dn between energy interval E and EdE and the velocity of electron is given by,

$$q_r = \int dq_r = \int_0^\infty v_x E g(E) p(E) dE \tag{2.26}$$

By substitution the density of the electron state between energy interval E and E+dE (g(E)dE) and probability of occupation of a state of energy E (p(E)).

Assuming an external applied temperature gradient is zero, the heat flow can be given by,

$$q_r = \int_0^\infty v_x E g(E) \left[e\frac{\tau E_x}{m}\frac{\partial p}{\partial E}\frac{\partial E_x}{\partial v_x} - \tau v_x \frac{\partial p}{\partial E}\frac{\partial E}{\partial T}\frac{dT}{dx} \right] dE \quad (2.27)$$

By substitution E_x from equation 2.19

$$q_r = \frac{2e}{3m}\frac{1}{eT}\frac{dT}{dx}\left[\left[E_f - \frac{\int_0^\infty E^2 \frac{\partial p}{\partial E} g(E)dE}{\int_0^\infty E\tau \frac{\partial p}{\partial E} g(E)dE} \right] \int_0^\infty E^2 \tau \frac{\partial p}{\partial E} g(E)dE - \right.$$

$$\left. \frac{2}{2mT}\frac{dT}{dx}\int_0^\infty E^2 \tau (E_f - E)\frac{\partial p}{\partial E} g(E)dE \right] \quad (2.28)$$

Let $\tau = aE^b$ and $g(E)dE = AE^{1/2}dE$ where $A = \frac{4\pi}{h^3}(2m)^{3/2}$

Thus

$$\frac{q_r}{\frac{dT}{dx}} = -\frac{2aA}{3mT}\frac{\left[\int_0^\infty E^{b+\frac{5}{2}}\frac{\partial p}{\partial E}dE\right]^2}{\int_0^\infty E^{b+\frac{3}{2}}\frac{\partial p}{\partial E}dE}$$

$$+\frac{2aA}{3mT}\int_0^\infty E^{b+7/2}\frac{\partial p}{\partial E}dE \quad (2.29)$$

And

$$\kappa_{el} = \frac{2}{3m}\frac{4}{\sqrt{\pi}}\left(\frac{2\pi mkT}{h^2}\right)^2 \frac{a}{T}(kT)^b (kT)^2$$

$$\left[\frac{\left(b+\frac{7}{2}\right)\left(b+\frac{3}{2}\right)F_{b+\frac{5}{2}}F_{b+\frac{1}{2}} - \left(b+\frac{5}{2}\right)^2 F_{b+3/2}^2}{\left(b+\frac{3}{2}\right)F_{b+1/2}} \right] \quad (2.30)$$

Equation 2.30 is general of electron contribution to thermal conductivity and this equation depended with location Fermi energy and type of scattering mechanism of carrier.

2.6.1.2 Lattice Thermal Conductivity(κ_{ph})

The theory of lattice thermal conductivity can be explaining much method, so deepened on precise, range of temperature and imperfection of material. In this section, ten main methods to estimate the lattice thermal conduction are presented.

- Krumhans and Williams Concept [37, 42]

  Krumhans and William concept is a simple method of estimate the thermal conductivity by employing the classical kinetic theory of gases formula.

$$\kappa = \frac{1}{3} Cvl \qquad (2.31)$$

  where C is the specific heat capacity at constant volume, V is the velocity of sound in material and l is the mean free path.

- Peierls Concept [37, 43]

  In an ideal crystal, the mean free path at 0K would be infinite. At higher temperatures, phonon-phonon scattering (or Umklapp) is the main process limiting the mean free path. The phonon-phonon scattering arises from the three-phonon processes either two phonon frequency ω_1, ω_2 and momentumq_1, q_2.Phonon-phonon scattering follows energy conservation and the wave vector is conserved with a reciprocal lattice vector. The phonon-phonon scattering processes, where two phonons with frequency ω_1, ω_2collide producing an outgoing phonon atω_3, is giving by,

$$q_1 + q_2 = q_3 + Q$$
$$\bar{h}\omega_1 + \bar{h}\omega_2 = \bar{h}\omega_3 \qquad (2.32)$$

  where Q is the reciprocal lattice vector or recalls occur in all momentums in the crystal. If Q=0, this process is called Normal process. This process follows the law of conservation of energy and momentum, as shown in figure 2.5a. If Q ≠ 0, the process is called Umklapp scattering by Peierls. The collision of phonon 1 and phonon 2 in a case of Umklapp scattering does not follow the low of conservation of momentum. In fact, the phonon velocity reverses as shown in figure 2.5b. A theory of Peierls to the thermal conductivity is inversely proportional to the excitation of the lowest energy phonon.

Roughly call this case is Umklapp processes and approximate relation in equation 2.32.

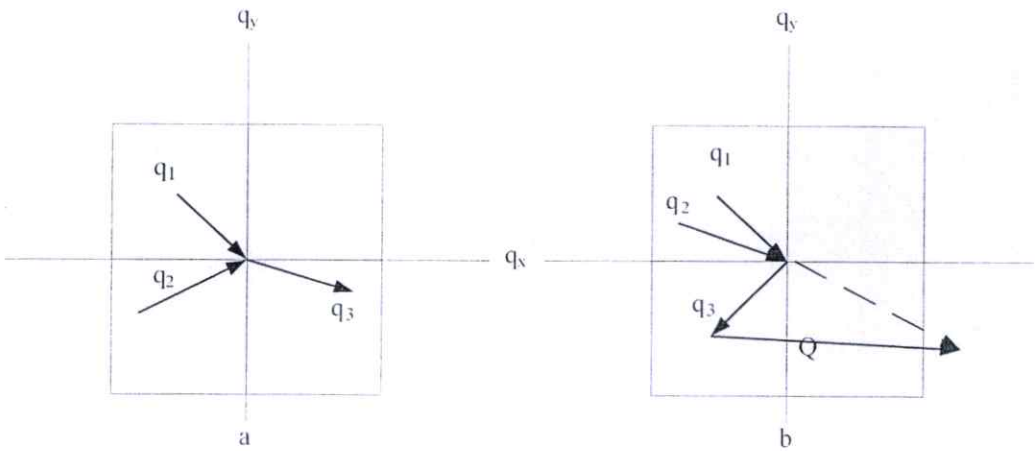

Figure 2.5 Three Phonon processes (a) Conservation in Normal-Processes (b) Umklapp Processes

Peierls showed that the temperature dependence of the lattice thermal conductivity is given by,

$$\kappa_{ph} = \kappa_0 \exp(\frac{\theta_u}{T} - 1) \qquad (2.33)$$

where θ_u is the Umklapp temperature ($\sim 1/2\theta_D$). This indicates that at high temperature, the thermal conductivity is inversely proportional to temperature ($\kappa \propto T^{-1}$)

- **Dugdale and MacDonald Concept [37, 44]**

The phonon-phonon scattering arises from an anharmonic in the lattice potential, coupling between different phonons, also limit the value of the mean free path. Anharmonic of the potential is inversely proportional to the thermal expansions coefficient (α) and Grunesen

constant(γ). Dugdale and MacDonald expressed the mean free path of phonon as,

$$l = \frac{a}{\alpha\gamma T} \tag{2.34}$$

where a is the lattice constant. Thus by substituting eq. 2.34 into eq. 2.31, the lattice thermal conductivity is given by,

$$\kappa_{ph} \approx \frac{1}{3} Cv \frac{a}{\alpha\gamma T} \tag{2.35}$$

- Liebfried and Schlomann Concept [37, 45]

  Liebfried and Schlomann equation is one of the most common method used to predict the thermal lattice conductivity. Using the Liebfried and Schlomann equation:

$$\kappa_{ph} \approx \frac{M a\, \theta_D^3}{T\gamma^2} \tag{2.36}$$

  Where M is the average atomic mass and θ_D is the Debye temperature. It would be expected that material of a high mean atomic mass would have high lattice thermal conductivity. However, But mass dependence with $(a\theta_D^3)$ affect to thermal conductivity fall with increases mass as show in figure 2.6.The figure shows a κ_{ph} dependence on mass difference and degree of ionic to the bonding.

- Spitzer Concept [37, 46}

  He has compiled a list of lattice thermal conductivity for more than 200 semiconductors and found a closed correlation between lattice thermal conductivity and chemical bonding of the crystal. The results agreed with Liebfried and Schlomann theory.

- Klemens Concept [37, 47]

  His prediction lattice thermal conductivity by use relationship and give the following.

$$\kappa_{ph} \approx T_m^{3/2} \rho^{2/3} A^{-7/6} T^{-1} \qquad (2.37)$$

Where T_m is the melting point, ρ is the density and A is the mean atomic weight.

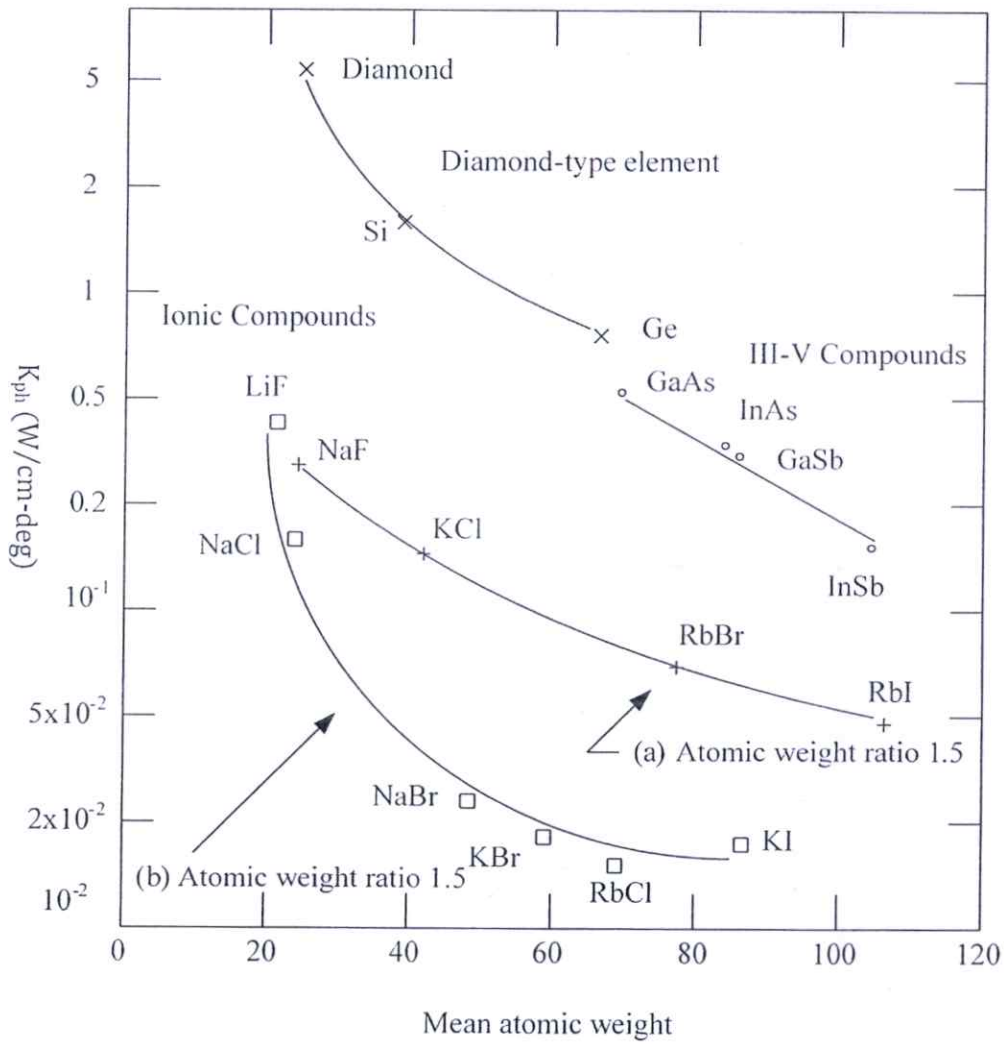

Figure 2.6 The lattice thermal conductivity as a function of mean atomic weight for covalent and ionic bonding crystals.

- Keyes Concept [37, 48]

Keyes use Klemans relationship was plot as show in figure 2.7. That showed general of material selected from the lower rows of the periodic table, so showed lowest lattice thermal conductivity.

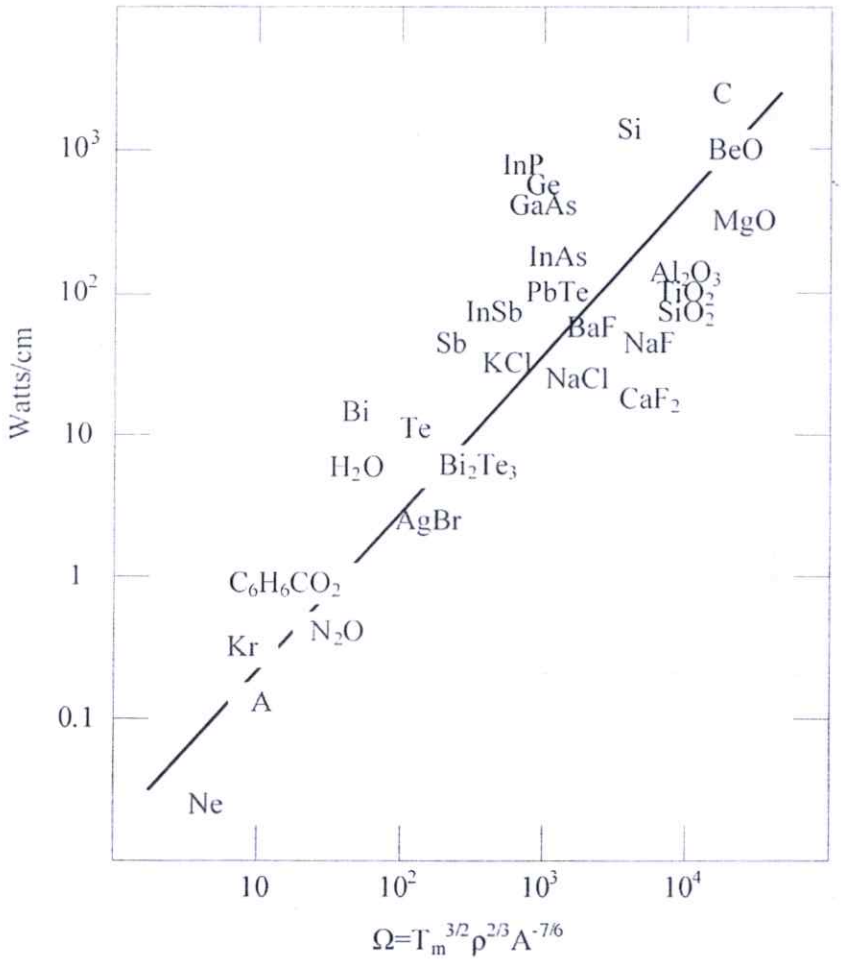

Figure 2.7 Function dependence of lattice thermal conductivity on melting temperature

- Slack Concept [37, 49]

Liebfried - Schlomann equation is valid for one atom per unit cell only. Slack extended the work of Liebfried and Schlomann to calculate lattice thermal conductivity at high temperature a large number of atoms per unit cell on the acoustic and optical phonon. He also calculated the minimum thermal conductivity for a variety of

crystal structures. Static imperfections in the lattice can also be an important source of phonon scattering. Other effects that decrease lattice thermal conductivity are from,

1. Imperfection from impurity.
2. Mass fluctuation (Isotopes, Solid Solution, Alloys or lattice vacancies)
3. Absence of long range order (Glasses or Amorphous structure)
4. Crystal boundaries

- Tavernier Concept [37, 50]

He has dealt with effect of disorder mass fluctuation and fined the transverse phonon following equation 2.38.

$$\kappa_{ph} \propto T_m^{5/6} \rho^{2/3} \Omega^{-2/3} T^{-1/3} \qquad (2.38)$$

where $\Omega^{-2/3}$ is the degree of mass fluctuation. As would be expected, this mechanism gives rise to weaker temperature dependence than that for Umklapp scattering but again shows the minimum conductivity is near the melting point. Writing Klemens' and Tavernier's equation.

- Goldsmid Concept [37, 51]

The concept of Goldsmid combined the effects of Umklapp processes and scattering by imperfection into one equation,

$$\kappa_{ph} = \kappa_u \left(\frac{\nu_0}{\nu_m}\right) tan^{-1}\left(\frac{\nu_m}{\nu_0}\right) \qquad (2.39)$$

where κ_u is the thermal conductivity in the absence of imperfection scattering, ν_0 is the frequency at which the relaxation time for the two scattering processes and ν_m is the upper limit of distribution of lattice vibration frequency. He compared this relation with experiment behavior for a number of alloys, as shown in figure 2.8.

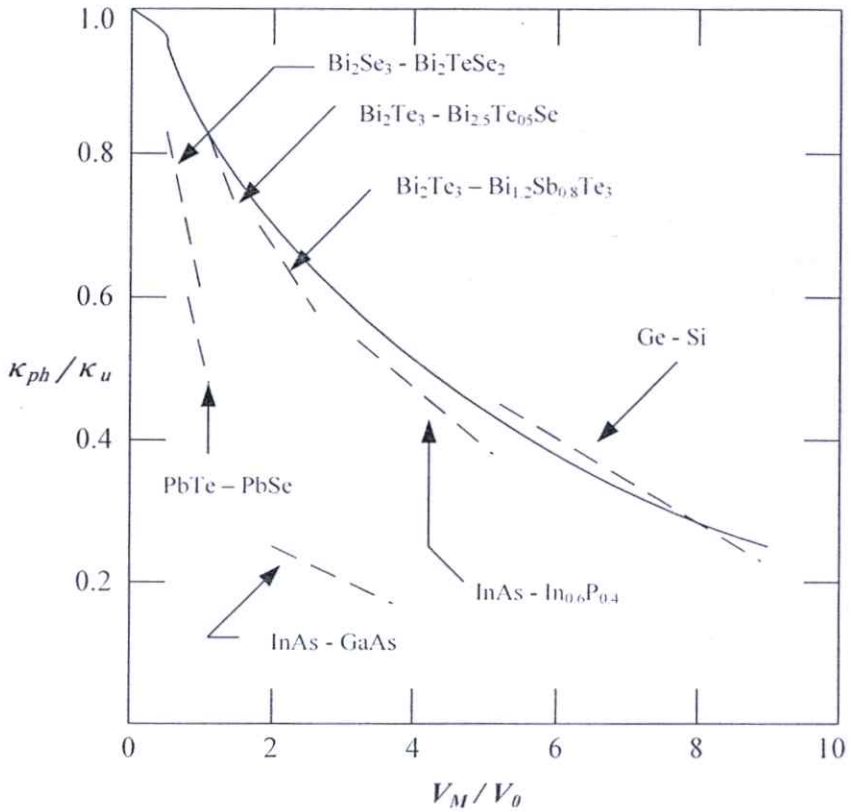

Figure 2.8 Function dependence of lattice thermal conductivity on melting temperature

2.2 Literature Reviews

Many researchers in the world for find new material compound and/or development technique conversion thermal energy into electrical energy. They have tired changing ratio of compound or vary material. Some of reported contribution on thermoelectric by some researcher have been given below.

- Tomohiro Nozaki, Kei Hayashi and Tsuyoshi Kajitani reported thermoelectric property of delafossite-type oxide $CuFe_{1-x}Ni_xO_2$ ($0 \leq x \leq 0.05$). The results show maximum ZT = 0.14 of x=0.01 at 1100 K. The reason of maximum ZT at x= 0.01 due to lowest thermal conductivity (estimate 4 W/mK at 1100 K) of this series. Seebeck coefficient show maximum at x=0.00at 1100 K. The Seebeck coefficient sharp rise above 1000 K because reduction of hole carrier

by partial oxygen loss. And electrical conductivity higher of series approximate same at x= 0.01, 0.02 0.03 (18 S/cm). Cause of electrical conductivity increase due to carrier increase. While electrical conductivity reduce of x=0.04 and 0.05 because impurity phase.

- M. Lalanne, A. Barnabe, F. Mathieu and Ph. Tailhades reported effect of oxygen nonstoichiometry on the stability of the delafossite phase. The doubt of phase delafossite and spinal phase (oxygen exceed) of $CuFe_{1-x}Cr_xO_2$ and $CuFe_{0.2}Ga_{0.8}O_2$.Conclusion Cr^{3+} and Cu^{2+} do not match into the pure octahedral land mixed octahedral/tetrahedral therefore M-site by chromium ions tend to stabilize to stoichiometry delafossite phase. Incase Ga (ionic radius Ga^{3+}= 0.625 A°, Cr^{3+}=0.615 and Fe^{3+}=0.645) ionic radius Ga^{3+} a little bit difference from Cr^{3+} and Fe^{3+} but mixed spinal delafossite because stabilization of the gallium ions in the tetrahedral sites. And the copper ions are mostly pure with octahedral layer. Therefore method of synthesis M-site of delafossite by gallium required more energetic activation to form phase. The results above can be support by reported of Sumio Kato, Ryu Fujimaki, Masataka Ogasawara, Takashi Wakabayashi, Yuunosuke Nakahara and Shinichi Nakata. And title is Oxygen storage capacity of $CuMO_2$ (M= Al, Fe, Mn, Ga) with delafossite structure.
- R. Bruce Gall, Nathqan Ashmore, Meagen, A. Marquardt, Xiaoli Tan, David P. Cann reported synthesis, microstructure and electrical properties of the delafossite compound $CuGaO_2$. The compound show ceramic p-type conductivity therefore high Seebeck coefficient (780 μV/K at room temperature) and electrical conductivity was 0.0033 S/cm. The Seebeck coefficient was high estimate 3 times compare $CuFeO_2$ but electrical conductivity less than 900 time. (Seebeck coefficient and electrical conductivity of $CuFeO_2$ estimate 261 μV/K, 3 S/cm, (Ref. of compares, Chesta Rattanapun $Cu_{1-x}Pt_xFeO_2$ journal of Alloys and Compounds).
- T.K. Le, D. Flahaut, H. Martinez, N. Andreu, D. Gonbeau, E. Pachoud, D. Pelloquin, A. Maignan reported electronic structure of the $CuRh_{1-x}Mg_xO_2$ thermoelectric material: An X-ray photoelectron spectroscopy

study. In discussion explain the very different value of electrical resistivity and Seebeck coefficient of $CuRhO_2$ and $CuCrO_2$.The author description by XPS, $CuCrO_2$ does not show Cu^{2+}whereas $CuRhO_2$ exhibit Cu^{2+}/Cu^{+} this is the reason affect electrical conductivity and Seebeck coefficient. In case of $CuRh_{1-x}Mg_xO_2$ (x=0-0.04-0.1) effect of Cu^{+}/Cu^{2+} and Mg^{2+} affect to chemical formula change to $Cu^{+}_{(1-2x)}Cu^{2+}_{x}Rh^{3+}_{(1-2y)}Rh^{4+}_{y}Mg^{2+}_{(x+y)}O_2$. These results contribute to electrical conductivity.

- K. Park, K.Y. Ko, H.-C. Kwon, S. Nahm reported improvement in thermoelectric property of $CuAlO_2$ by adding Fe_2O_3. The results show higher value power factor $1.1x10^{-4}$ W/mK^2 of x=0.1 at 1140 K. At x=0.1 shows higher of group because Fe lead to increases density affect to increases in the time electron scattering event of charge carrier and individual grains enhance electron moving toward. The value of Seebeck coefficient of x=0.1 is lowest of group because high carrier concentration this nature of property thermoelectric materials.
- K. Park, K.Y. Ko, W.-S. Seo reported Effect of partial substitution of Ca for Al on the microstructure and high-temperature thermoelectric properties of $CuAlO_2$. The results shows highest power factor of group $7.82x10^{-5}$ $Wm^{-1}K^{-2}$ of x=0.1 at 1140 K ($CuAlO_2$ shows Seebeck coefficient 500 μV/K, electrical conductivity 0.75 1/Ωcm and power factor $1.9x\ 10^{-5}$ at 525 K) . The electrical conductivity higher of group was x=0.1 because divalent of Ca^{2+} affect to increase carrier concentration (hole), increase density and grain size. While Seebeck coefficient higher of group was x=0.1 which against nature because in the nature the Seebeck coefficient values increases with carrier concentration decrease but this case both (Seebeck coefficient and electrical conductivity) increases. The reasons of Seebeck coefficient increase authors explain similar $Bi_{2.3-x}Pb_xSr_{2.6}Co_2O_y$effect by strong electron-electron correlation in the CoO_2 sheet. But don't have detailed ideas to fully explain.
- ChestaRuttanapun, AreeWichainchai, WutthisakPrachamon, AnuchaYangthaisong, AnekCharoemphakdee, TosawatSeetawan

reported $Cu_{1-x}Pt_xFeO_2$ ($0.0 \leq x \leq 0.05$). The results show highest dimensionless figure of merit 0.05 of x=0.05 at 960 K. The Seebeck coefficient higher of group at room temperature was x=0.00 and approximate same values at 960 K. While electrical conductivity higher at x=0.05 and lowest of group was x=0.00, the author descript effect of carrier increases by platinum substitution into copper. Because behavior of platinum ions (Pt^+) d^9 ions improve electrical conductivity, different copper (Cu^+) was d^{10} ions therefore Pt^+ affect to improve electrical conductivity. The thermal conductivity higher of group was x=0.05 and lowest x=0.00at 960 K.

- Fang Zhi-Jie, Shi Li-Jie and Liu Yong-Hui reported electronic structure and native defects in transparent conducting of $CuScO_2$ and $CuYO_2$ by calculation. The results show p-type and oxygen rich importance to play conductivity.
- Masashi Hasegawa, Ikuol Nagawa, Masayuki Tanaka, Ichimin Shirotani and Humihiko Takei reported thermoelectric power of $PdCoO_2$. The results show 2-4 μV/K(temperature 100-400 K)and Co showed valence 3+. And Masashi Hasegawa, Tohru Higuchi, Masayuki Tanaka, Takeyo Tsukamoto, Shik Shin and Humihiko Takei reported properties anisotropic of electrical resistivity by electrical resistivity of perpendicular c-axis are lowest parallel c-axis. The result is coincide D.B. Rogers, R.D. Shannon, C.T. Prewitt and J.L. Gillson.
- Masahiro Yasukawa, Kaoru Ikeuchi, Toshio Kono, Kazushige Ueda and Hideo Hosono reported thermoelectric property of $AgIn_{1-x}Sn_xO_2$. The results shows n-type of both (x=0.00 and 0.05), electrical conductivity and Seebeck coefficient measured between 373-673 K, the power factor increases two order due to affect from electrical conductivity increases.
- Qinggang Meng, Shanfu Lu, Sunhui Lu, Yan Xiang reported thermoelectric property of $CuCr_{1-x}Mg_xO_2$ ($0 \leq x \leq 0.15$). The results show p-type, porosity decreases, electrical conductivity increases up to 10.34 S/cm at room temperature compared undope and highest power factor 1.37×10^{-4} $Wm^{-1}K^{-2}$ at x=0.1 470 K.

- Yasuhiro Ono, Ken-ichi Satoh, Tomohiro Nozaki, Tsuyoshi Kajitani reported structure, Magnetic and thermoelectric property of $CuCr_{1-x}Mg_xO_2$ ($0 \le x \le 0.05$). The results show power factor maximum at x=0.03, thermal conductivity show 6-10 Wm-1K-1 at 300 K and maximum dimensionless figure of merit (ZT)=0.04 of x=0.03 at 950 K.
- Kei Hayashi, Ken-ichi Sato, Tomohiro Nozaki, Tsuyoshi Kajitani reported effect of doping on thermoelectric properties of delafossite-type oxide $CuCrO_2$. The results show single dope of Mg, Zn, Ca, Ni and Co, lowest of power factor was Mg doped and higher were $CuCrO_2$. And next prepare double doped $CuCr_{0.97-x}Mg_{0.03}M_xO_2$ (M=Zn, Ca, Ni and Co)($0 \le x \le 0.05$). Effect double dope of $CuCr_{0.97-x}Mg_{0.03}Ni_xO_2$ x=0.04 show maximum electrical conductivity 45 S/cm at 1000K, Seebeck coefficient 225 μV/K, thermal conductivity higher than Mg doped and maximum dimensionless figure of merit (ZT)=0.10.
- Chesta Ruttanapun, Phumin Jindajitawat, Prathan Buranasiri, Warawoot Thowladda, Warakarn Neeyakornreported High temperature thermoelectric properties of delafossite $CuBO_2$. The results show high Seebeck coefficient 950 μV/K and decreases to 450 μV/K when temperature increases (650 to 830 K). While electrical conductivity show low 0.004 S/cm and increases to 0.038 S/cm when temperatures increases (650 to 830 K). And thermal conductivity show 9 W/m-K and decreases to 3 W/m-K when temperature increase (300 to 960 K).
- T. Nozaki, K. Hayashi and T. Kajitani reported Mn-Substitution Effect on Thermal Conductivity of delafossite-Type Oxide $CuFeO_2$.The results shows thermal conductivity of $CuFe_{1-x}Mn_xO_2$ series is lower $CuFe_{1-x}Cr_xO_2$ series and minimum at x=0.5. Although grain boundary of $CuFe_{0.5}Cr_{0.5}O_2$ is smaller $CuFe_{0.5}Mn_{0.5}O_2$, normally smallest grain boundary must to poor thermal conductivity. But experiment result is contrast. The reason of author is large lattice strain of $CuFe_{0.5}Mn_{0.5}O_2$ due to distorted of octahedral structure in compound.
- B. Abeles reported Lattice Thermal Conductivity of Disorder Semiconductor Alloys at High Temperature. The results show relaxation time depended on frequency ω as ω^4 for strain and mass

point defects and ω^2 for normal and Umklapp three-phonon anharmonic processes. The thermal conductivity is expressed in term of the lattice parameter and mean atomic weight of the alloy and its constituents. It is found that the large thermal resistivity of Ge-Si alloys is predominate due to mass defect scattering, whereas that of (Ga, In). As alloy is mainly due to strain scattering.

- C.G. Sivan Pillai and A.M. George reported Thermal Conductivity of Superconducting $La_{2-x}Sr_xCuO_4$ (x=0.10, 0.15 and 0.20) and Semiconducting $Gd_{2-x}Sr_xCuO_4$ (x=0.00, 0.10, 0.15 and 0.20) at High Temperature. The results show, in case of the La-oxides is highly anomalous, showing a linear increases with temperature which cannot be explained either by a two level system (TLS) or a hopping fraction model and seems to be determined mainly by thermally-generated electronic defect in addition to configuration disorder. In contrast, the conductivity of the Gd-oxides follows a T^{-1} relation and also decreases with increasing strontium content. The conductivity dependence on temperature and strontium concentration is found to arise from enhanced phonon scattering due to mass difference and lattice strain.
- Takuya Kurotori and Sunao Sugihara reported Thermoelectric Properties of $CuAl_{1-x}M_xO_2$ (M=Zn, Ca). The results show power factors were the highest near 850 K for the samples of $CuAl_{0.999}Zn_{0.001}O_2$ ($6.8x10^{-5}$ $Wm^{-1}K^{-2}$), $CuAl_{0.999}Ca_{0.001}O_2$ (7.4x10-5 $Wm^{-1}K^{-2}$), $CuAlO_2$ ($6.6x10^{-5}$ $Wm^{-1}K^{-2}$), the electrical conductivity and Seebeck coefficient of the all sample estimate same value so cannot improve from base. Which thermal conductivity lowest of series was $CuAl_{0.999}Zn_{0.001}O_2$ (5 $Wm^{-1}K^{-1}$) affect to high ZT of group$7.5x10^{-6}$ K^{-1} (approximate 1.7 time from base).
- Masahiro Yasukawaa and Kaoru Ikeuchi reported thermoelectric properties of delafossite-type layered oxides $AgIn_{1-x}Sn_xO_2$. The results show solubility limited x=0.05 in this synthesis. The Seebeck coefficient of this group shows negative (n-type) and increasing with increases temperature, maximum at x=0.05 100 μV/K of 673 K. The electrical conductivity increases with Sn content and increasing with

temperature increases. The reasons of increases of electrical conductivity were electron donor affect from Sn. Effect of increases electrical conductivity (5-mol %) by Sn affect to increases power factor estimate 2 order of magnitude to 10^{-6}-10^{-5} $Wm^{-1}K^{-2}$.

- P.G. Klemens reported the scattering of Low-Frequency Lattice Waves by Static Imperfection. The results description phonon scattering from static imperfection interaction of polycrystalline.
  1. Scattering by a substitution atom of difference mass
  2. Scattering by an atom of difference binding force
  3. Scattering by an elastic strain field
  4. Scattering by the elastic strain field around a point imperfection
  5. Scattering by imperfection
  6. Scattering by single dislocation
  7. Scattering by grain boundaries
- Sumio Kato, Ryu Fujimaki, Masataka Ogasawara and Takashi Wakabayashi reported Oxygen storage capacity of $CuMO_2$ (M=Al, Fe, Mn, Ga) with a delafossite-type structure. The results show, when temperature increases up to 500 °C $CuMnO_2$ and $CuFeO_2$ and can store oxygen approximate 0.2 mol-O/mol, which $CuGaO_2$ and $CuAlO_2$ stored oxygen 0.015 mol-O/mol. Next temperature increases up to 800 °C the $CuAlO_2$ and $CuFeO_2$ stored oxygen same value 0.13, $CuMnO_2$ 0.21 and $CuGaO_2$ 0.25mol-O/mol. This results implied $CuGaO_2$ difficult form phase delafossite structure because capacity oxygen storage. The results accord with M. Lalanne and coworker.
- Michael Snure and AshutoshTiwan reported $CuBO_2$: A p-type transparent oxide. The results of electrical conductivity show semiconductor property and temperature dependence. At room temperature electrical conductivity of this sample was 1.65 Scm^{-1} and Seebeck coefficient approximate 725 μV/K. The polycrystalline sample was high power factor compared $CuAlO_2$. But nature of boron is operating at low temperature.
- Chesta Ruttanapun reported Optical and electrical properties of delafossite $CuBO_2$ p-type transparent conducting oxide. The results

show electrical conductivity at room temperature 4.12×10^{-4} S/m and Seebeck coefficient approximates 950 μV/K at 645 K.

Table 2.1 Conclusion solid state reaction method for ternary copper base oxide with delafossite structure [52].

Synthesis Method	Formula	Temperature °C	Atmosphere	Ref
Solid State Reaction	$CuAlO_2$	1050	Vacuum/Air	[52-54]
	$CuCrO_2$	1000-1050	Air	[52,55,56]
	$CuEuO_2$	900	Argon/Vacuum	[52,57,58]
	$CuFeO_2$	1050	Vacuum/Air	[52,59,60]
	$CuGaO_2$	1050	Argon/Vacuum	[52,53,61]
	$CuLaO_2$	1000	Argon/Vacuum	[52,58,62]
	$CuNdO_2$	900	Argon/Vacuum	[52,57,58]
	$CuPrO_2$	900	Argon/Vacuum	[52,57,58]
	$CuSmO_2$	900	Argon/Vacuum	[52,57,58]

Chapter 3

Research methodology and Characterization tools

This chapter explain to the fabrication method, how to confirm the samples too objectively and characterization tools to investigate $CuFe_{1-x}M_xO_2$ when M= Al, Ga and x=0.0, 0.1, 0.3 and 0.5. After fabrication characterization is X-Ray Powder Diffraction (XRD) for confirm polycrystalline structure phase compared Joint Committee on Powder Diffraction Standard 39-0246 [63] (JCPDS, PDF 39-0246), Energy-Dispersive X-Ray Spectroscopy (EDX) confirm for exist of compound in the samples (Qualitative Analysis) and percent ratio of compound in the samples (Quantitative Analysis), Scanning Electron Microscope (SEM) study of the morphology of materials surface at the micro level. And final study thermoelectric property by measured thermal conductivity and power factor (Seebeck coefficient and electrical resistance).

3.1 Fabrication method

3.1.1 Starting Material

The starting material for this research is bulk prepare to $CuFe_{1-x}M_xO_2$ when M= Al, Ga and x=0.1, 0.3 and 0.5.

(1) CuO (≥ 99%, Sigma-Aldrich)

(2) Fe_2O_3 (≥ 99%, Sigma-Aldrich)

(3) Ga_2O_3 (≥ 99.99%, Sigma-Aldrich)

(4) Al_2O_3 (≥ 99%, Sigma-Aldrich)

Figure 3.1 Starting materials

3.1.2 Equipment tool

(1) Polyethylene bottle and Zirconia balls

(2) Agate Mortar

(3) Furnace

(4) Hydraulic

(5) Mould (flat pellet diameter 12mm and rectangular column 20x3x5 mm)

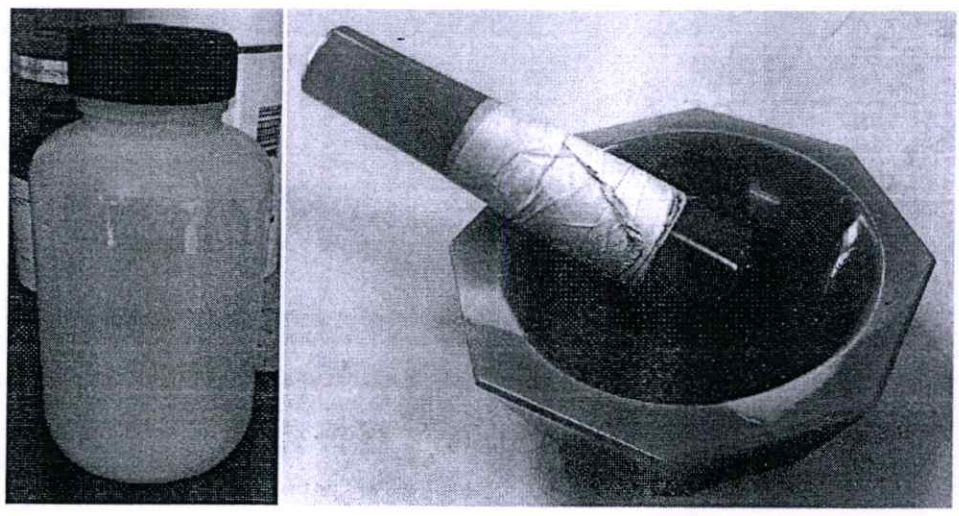

Figure 3.2 Polyethylene bottle, Zirconia balls and Agate Mortar

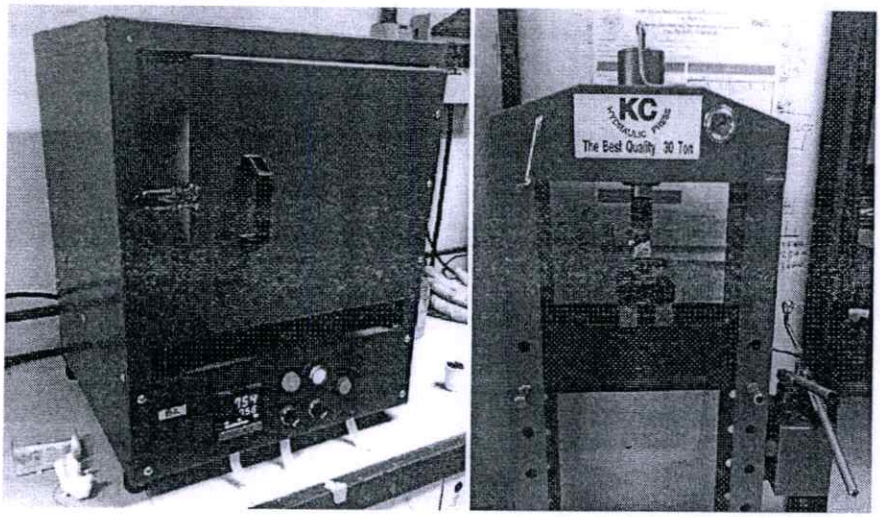

Figure 3.3 Furnace and Hydraulic

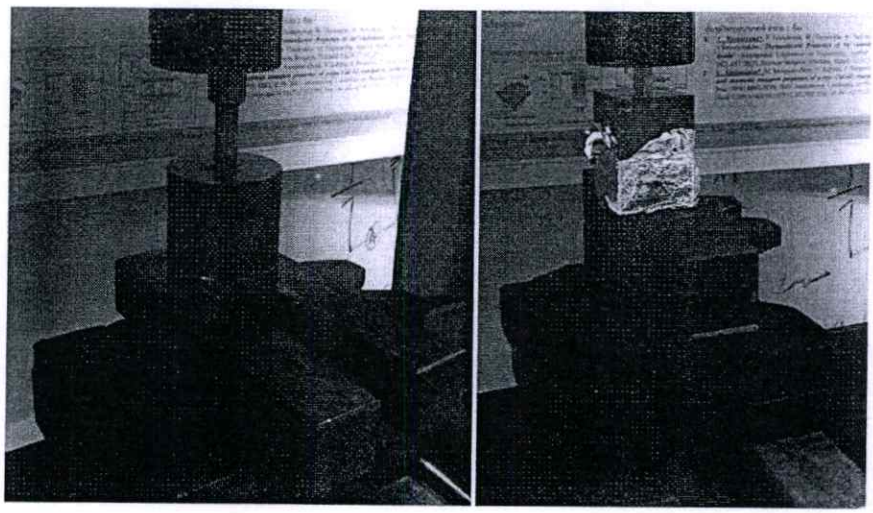

Figure 3.4 Mould (flat pellet diameter 12mm and rectangular column 20x3 mm)

3.1.3 Fabrication procedure

(1) Calculate weight of starting material following equation

$$2CuO + (1-x)Fe_2O_3 + 2(x)M_2O_3 \longrightarrow 2CuFe_{(1-x)}M_{(x)}O_2 + 1/2O_2$$

When M= Al, Ga and x=0.0, 0.1, 0.3 and 0.5

(2) Mixed all starting material after weight into polyethylene bottle, Zirconia balls and distill water. Milling the bottle 24 hour and separate water by heat 100° C.

(3) After separate distill water finish grinding material sample by agate mortar ensure homogeneous.

(4) Sintering by furnace

- Incase $CuFe_{(1-x)}Ga_{(x)}O_2$, x=0.1, 0.3 and 0.5. Atmosphere is in the argon and sintering 1050° C, 20 hour. The vacuum system and argon feed supply equipment show in figure 3.5.
- Incase $CuFe_{(1-x)}Al_{(x)}O_2$, x=0.1, 0.3 and 0.5. Sinter in normal atmosphere and sintering 1050° C, 20 hour.

(5) Grinding material sample, pellet to flat diameter and rectangular column show in figure 3.6.

(6) Repeat step 5 in two times.

(7) Complete fabrications all samples.

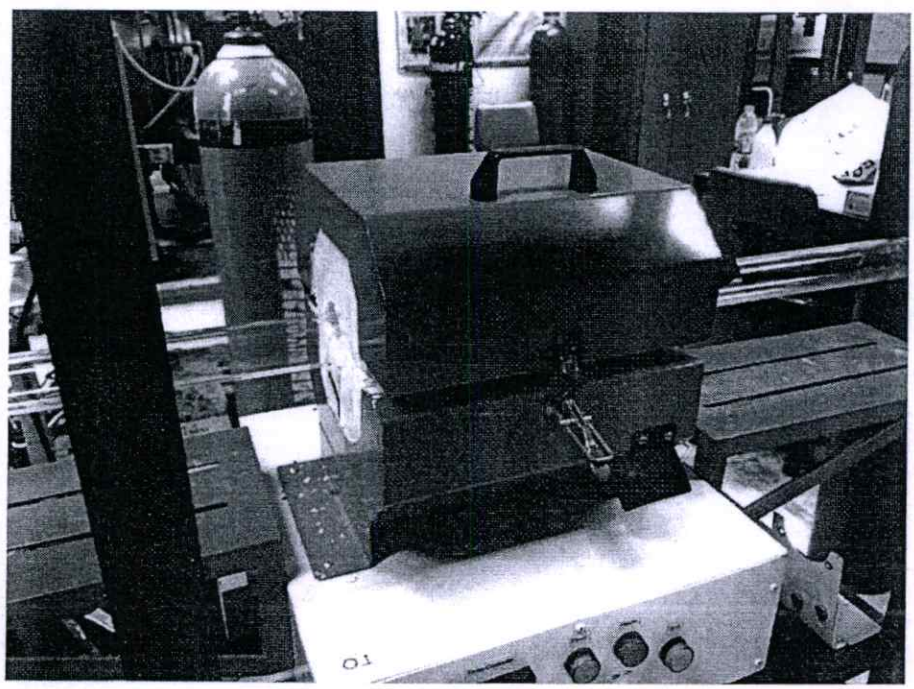

Figure 3.5 Vacuum system and Argon feed supply

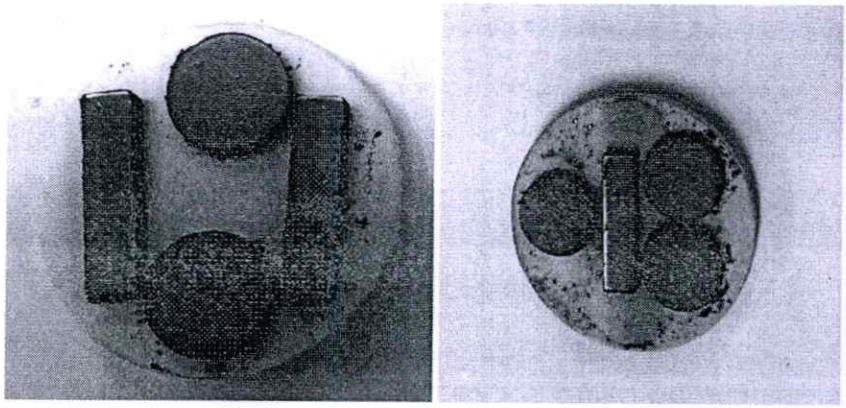

Figure 3.6 Example sample pellet to flat diameter and rectangular column

3.2 Characterization tool

After fabricating, confirm the phase structure of polycrystalline samples by X-Ray Powder Diffraction (XRD) Bruker, D8 Advance (X-ray source $\lambda_{CuK\alpha}$=1.5406 A° and 2θ = 10-80, step=0.02).

3.2.1 X-Ray Powder Diffraction (XRD) technique [64]

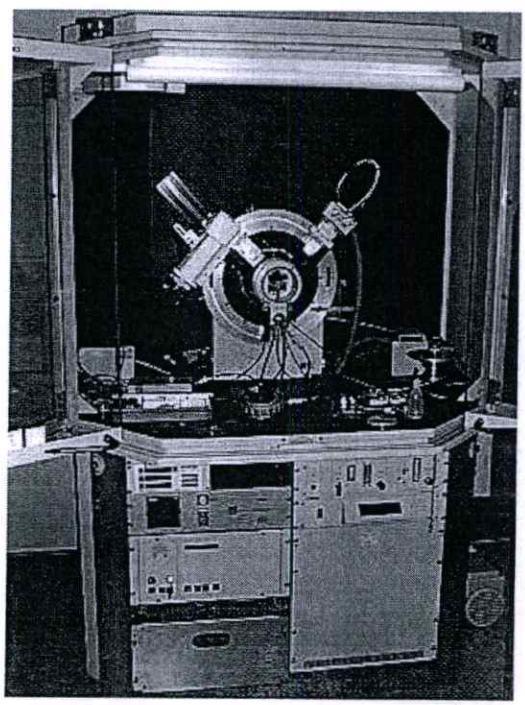

Figure 3.7 X-Ray Diffraction (Bruker, D8 Advance)

X-ray diffraction (XRD) is a method of analyzing the structure by range of structure from several micrometers to ten of nanometers. The basic physics of XRD show figure 3.7 and 3.8 explain by Bragg's equation.

$$2dsi\ n\theta = n\lambda \qquad (3.1)$$

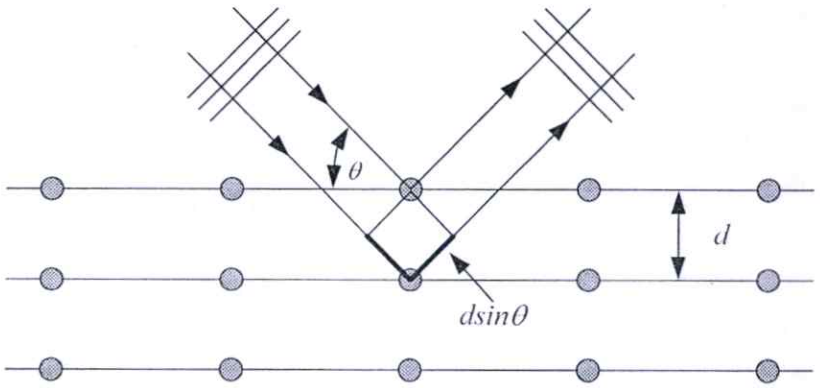

Figure 3.8 X-ray diffraction principles

Where d is the distance between adjacent planes in the set (hkl), θ is the Bragg's angle, n is the integral number and λ is the wavelength of the incident X-ray beam.

The X-ray are scattered by adjacent planed in crystal. Each atom in the crystal its diffraction beam X-ray showed a diffraction pattern. The angles of diffraction pattern are calculated to the unit cell. Because wavelength diffraction by atom and distance of each atom equal $n\lambda$ affect to height of peak or line intensity [41-42]. And a relative of intensities of line can deduce the number of atoms per unit cell.

In case hexagonal unit cell is characterized by two variable parameters a and c by d-spacing type hexagonal show figure3.9 and equation3.2.

$$\left(\frac{1}{d^2} = \frac{4}{3}\left(\frac{h^2+hk+k^2}{a^2}\right) + \frac{l^2}{c^2}\right) \qquad 3.2$$

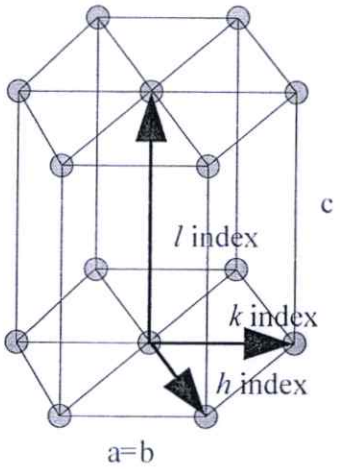

Figure 3.9 The hexagonal unit cell

- Combination Bragg's equation 3.1 and the plane-spacing equation give.

$$sin^2\theta = \frac{\lambda^4}{4}\left[\frac{4}{3}\frac{(h^2+hk+k^2)}{a^2} + \frac{l^2}{c^2}\right] \qquad 3.3$$

For $CuFeO_2$ delafossite reference structure to Joint Committee on Powder Diffraction Standard (JCPDS) number 39-0246.

$CuFeO_2$: Copper Iron Oxide [25].
JCPDS # 39-0246, Wavelength = 1.54056
Molecular Weight : 151.39
Volume : 136.88
S.G. : R3m (166)
Cell Parameter
a=3.034 c=17.16
Mineral Name : Delafossite, synthesis

2θ	Intensity	h	k	l
15.473	10	0	0	3
31.237	60	0	0	6
34.507	9	1	0	1
35.699	100	0	1	2
40.200	22	1	0	4
43.331	3	0	1	5
47.666	7	0	0	9
55.229	20	0	1	8
61.008	20	1	1	0
64.828	12	1	0	10
65.154	12	0	0	12
70.104	12	0	1	11
72.724	7	2	0	2
75.619	3	0	2	4

3.2.2 Scanning Electron Microscopy (SEM) and Energy-Dispersive X-Ray Spectroscopy (EDX)

The surface topology, microstructure characterization and composition of sample were investigated by using a field emission gun Scanning Electron Microscope (SEM), which is integrated with an Energy Dispersive X-Ray spectroscopy (EDX) by a Zeiss EVO MA10 [65] show in figure 3.10.

Diagram of scanning electron microscope show in figure 3.11 by beam electron is generated by Electron gun. The electron beam is accelerated by high voltage and passed through apertures and electromagnetic lens to produce a small electron beam. The scan coils perform scan beam of electron and collected by a suitably position detector.

For the technique of energy dispersive X-ray spectroscopy is analyzing energy emitted by the matter. Electron high energy beam focused into the sample, electrons in the sample are stimulated and electron of next shell moving instead. The difference of energy in the shell must to emit and it released with the element.

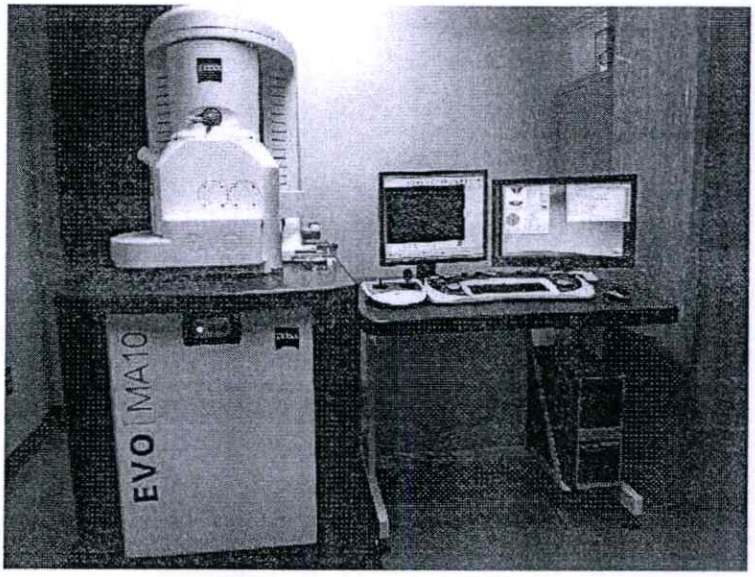

Figure 3.10 Energy-Dispersive X-Ray Spectroscopy and Scanning Electron Microscopy by Zeiss EVO MA10

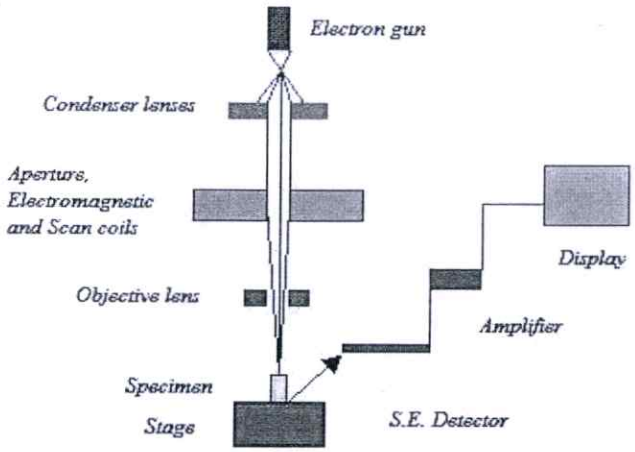

Figure 3.11 Diagram Scanning Electron Microscopy

Both of results of XRD and EDX for confirm samples were delafossite structure and confirm physical of substitution of aluminum and gallium into iron.

3.2.3 Thermal Conductivity (κ)

The thermal characterizations were carried out on flat samples of approximately 12-mm diameter and 2–3-mm thickness using a NETZSCH LFA 477 Nano-Flash thermal diffusivity analyzer [66] show in figure 3.12. The flash source used xenon flash lamp for heat a sample. And result temperature rise on the rear surface of the sample detected by infrared detector. Curve of temperature versus with time can be determining thermal diffusion. The specific heat capacity used technique compares temperature with a reference standard. By pulse flash lamp source into the sample and reference standard. The specific heat of the sample affect to difference temperature between samples with a reference standard. These techniques determine specific heat. The κ results were evaluated via the relation $\kappa = \alpha_d d C_p$.

where α_d, d and C_p are the thermal diffusivity, the density, and the specific heat of the sample, respectively. The values of α and C_p for the samples were obtained by measurements over a temperature range of 298 to 573 K. The bulk density determined by Archimedes method.

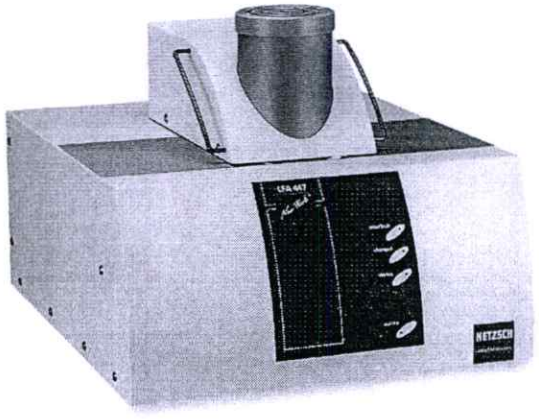

Figure 3.12 Laser Flash NETZSCH LFA 447 Nano-Flash

3.2.4 Seebeck Coefficient and Electrical Resistance

The Seebeck coefficient and electrical resistance measured by the ULVAC ZEM-3 [67] show in figure 3.13 and shape of the sample as rectangular bar and sizes approximate 20x2x3 mm shows in figure 3.14.

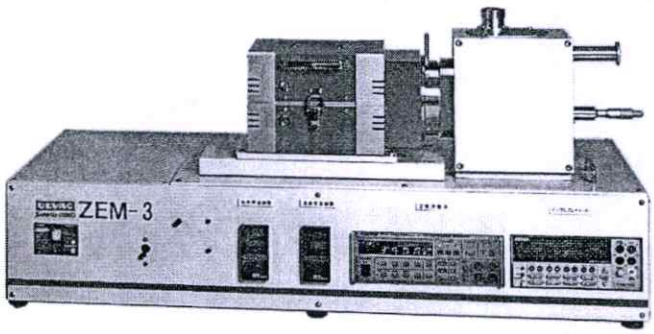

Figure 3.13 ULVAC ZEM-3 for Seebeck coefficient and electrical resistance measurement

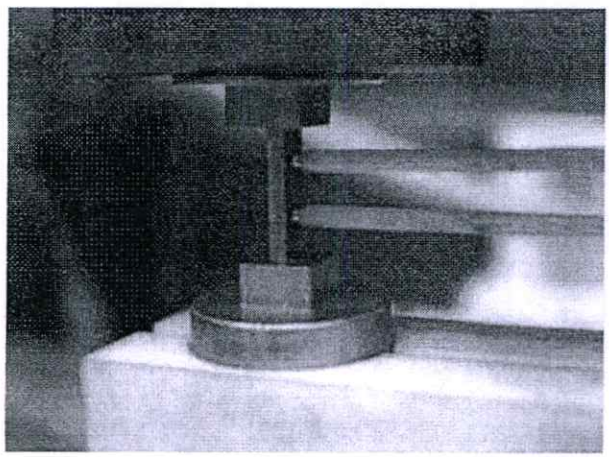

Figure 3.14 Shape and setup technique Seebeck coefficient and electrical resistance measurement

The principle of measurement is a sample setup in a vertical following figure 3.14 and 3.15, [67] upper and lower block in the heating furnace (ambient temperature). While heater in the lower block for product temperature gradient. Seebeck coefficient is measured by the measuring the temperatures T_1 and T_2 with the thermocouples contacted side of the sample following by measured of the thermal electromotive force between the wires on the side of thermocouples.

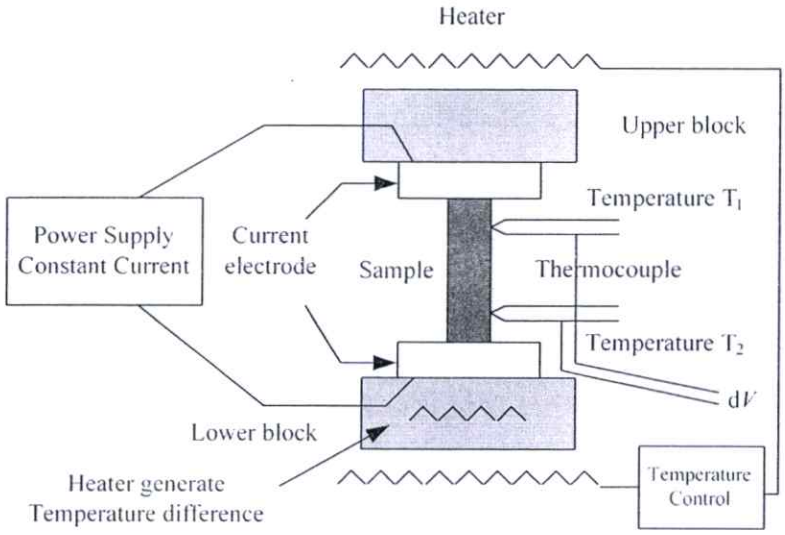

Figure 3.15 Diagram Seebeck coefficient and electrical resistance measurement

The electric resistance is measured by the four-terminal dc method. A constant current is applied to both ends of the sample to measure and determine voltage drop between the wires of the thermocouple by correction the thermo-electromotive force between the leads.

3.2.5 X-ray Photoelectron Spectroscopy (XPS)

The X-ray Photoelectron Spectroscopy (XPS) to study the composition of element, binning energy and interpret for oxidation the state of each element such as Cu^{1+} or Cu^{2+} and Fe^{2-} or Fe^{3+} the results is can explain the electrical property.

The binding energy analyzes from kinetic energy of photoelectron, by a beam of X-ray stimulant. The energy of photoelectron can indicate the element due to particular characteristic energy. The relative of binning energy and kinetic energy as follow in equation 3.2, the principle of measurement and the instrument are shown in figure 3.16 and 3.17, respectively [68]. The chemical state with a binding energy of element showed in table 3.1.

Table 3.1 Chemical state and Binding Energy of element.

Chemical State	Binding Energy
Cu^{1+}	~ 933 eV
Cu^{2+}	~ 934 eV
Fe^{2+}	~ 709 eV
Fe^{3+}	~ 711 eV
O^{2+}	~ 532 eV
Ga^{3+}	~ 1117 eV
Al^{3+}	~ 74 eV

$$Ki = hv - Bi - W \tag{3.2}$$

Where *Ki* is kinetic energy, *hv* is energy of beam X-ray, *Bi* is binning energy *and* W is work function of electron energy analyzer.

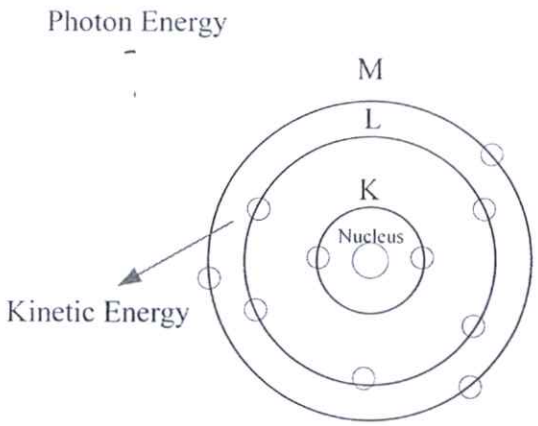

Figure 3.16 Principle of X-ray Photoelectron Spectroscopy

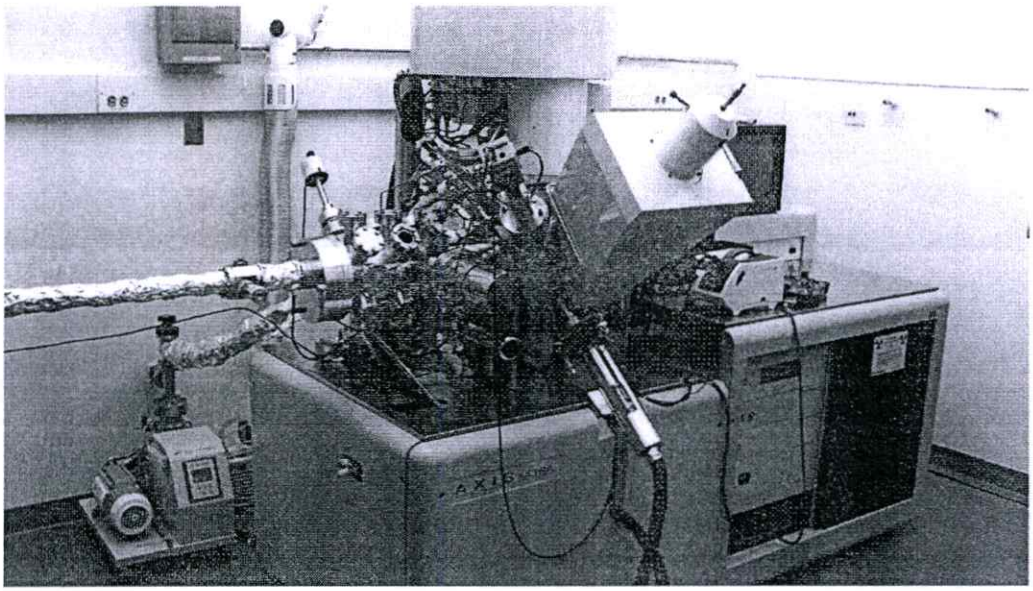

Figure 3.17 Chemical Composition and Binding Energy characterize by AXIS Ultra DLD, Kratos Analytical Ltd.

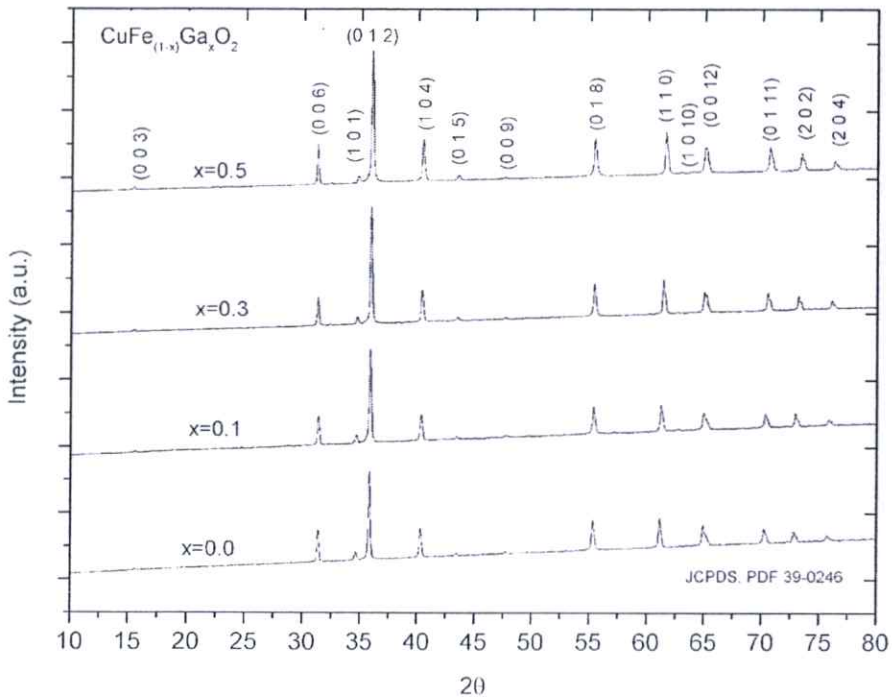

Figure 4.1 The XRD pattern of the $CuFe_{(1-x)}Ga_{(x)}O_2$ (x=0, 0.1, 0.3 and 0.5)

All XRD peaks were shifted when the x component increased. This happens because the substitution of gallium into iron sites caused the BO_6 octahedral to shrink, which the results in a decrease in edge length (a-axis decrease) owing to the smaller ionic radius of Ga^{3+} (0.625Å) compared with that of Fe^{3+} (0.645Å) [12]. Moreover, the length of the c-axis decreased due to the shrink of the bond length of the O-A-O layers and the BO_6 octahedral layers became slightly edge distortion. The effect of a and c parameters affect to volume of delafossite structure to decrease. This means that the lattice parameters *a* and *c* of $CuFe_{1-x}Ga_xO_2$ decreased with the increasing of x content as shown in figure.4.2. Therefore, when x component increases, that all of XRD peaks were shifted or the angle of diffraction increases. Figure 4.3 shows that the main peak (0 1 2) shifted from 35.84° to 35.96°, as the x content increased from 0.0 to 0.5. This was caused by the corresponding shortening of the distance between the adjacent (012) planes [25, 28] and the particle size using Scherrer equation $Size = \frac{0.94\lambda}{\cos\Theta\beta_{1/2}}$ calculate this peak.

Where λ is wavelength of x-ray diffraction source (X-ray source λ Cu K α = 1.5406 Å), $\beta_{1/2}$ is full width half maximum (FWHM) and θ is Bragg's angle. The results showed table 4.1.

Table 4.1 Particle size of $CuFe_{1-x}Ga_xO_2$

Particle size of$CuFe_{1-x}Ga_xO_2$	
x=0.0	43 nm
x=0.1	43 nm
x=0.3	44 nm
x=0.5	45 nm

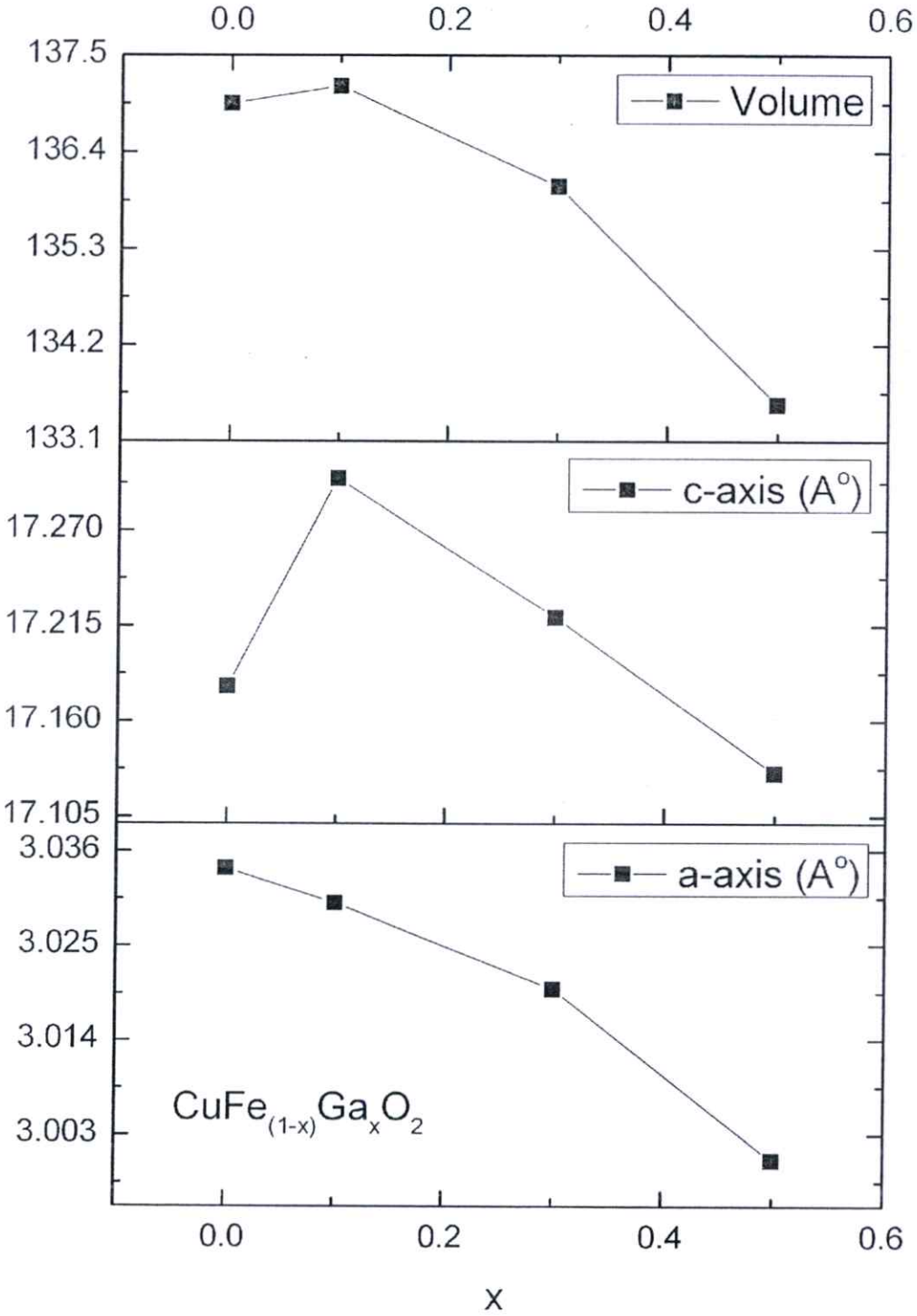

Figure 4.2 Lattice parameter a-axis and c-axis functions with Ga (x= 0, 0.1, 0.3, and 0.5)

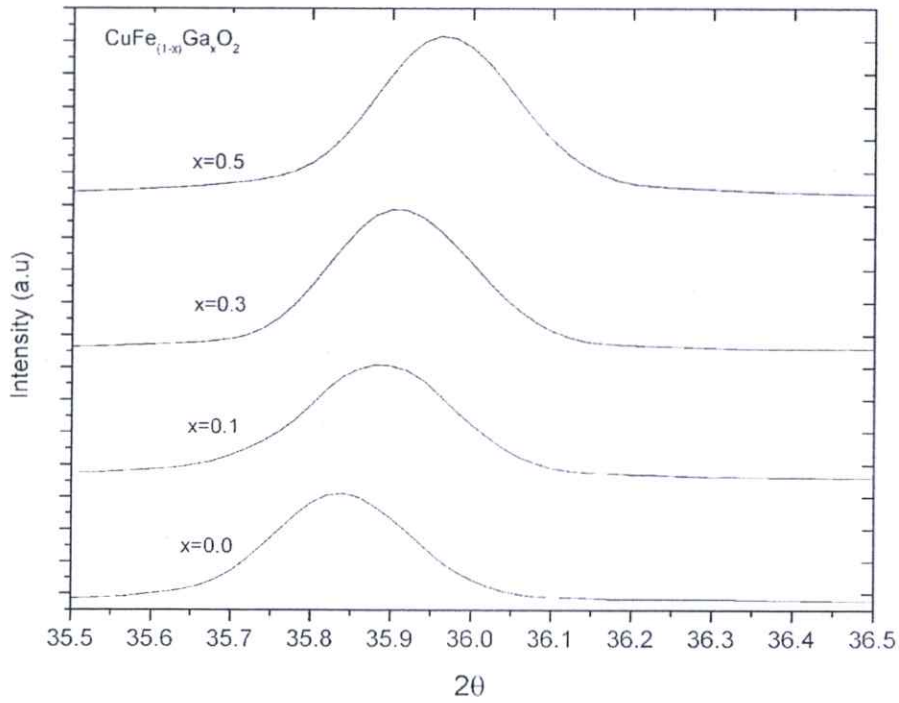

Figure 4.3 Main peak (0 1 2) functions with Ga (x= 0, 0.1, 0.3, and 0.5)

The energy dispersive x-ray spectroscopy results of each x contents (0.1, 0.3 and 0.5) showed in figure. 4.4, 4.5 and 4.6. All sample showed oxygen to exceed 8-9%, iron 100%, 94% and 95%, copper 91%, 90% and 89%, gallium 100%, 93% and 90% at x=0.1, 0.3 and 0.5 respectively.

Both of results of x-ray diffraction and energy dispersive x-ray spectroscopy to confirm the samples were delafossite structure by substation iron with gallium.

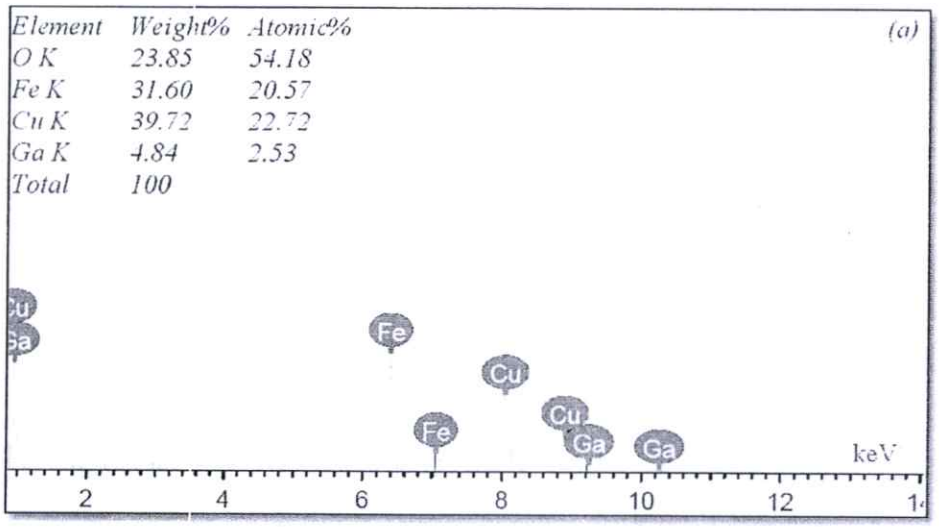

Figure 4.4 Energy dispersive spectroscopy of $CuFe_{(1-x)}Ga_{(x)}O_2$ (x=0.1)

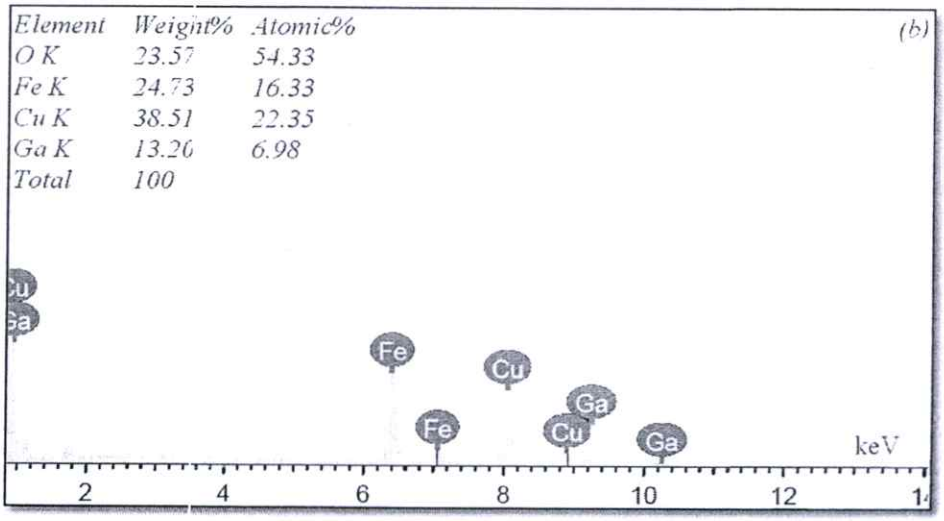

Figure 4.5 Energy dispersive spectroscopy of $CuFe_{(1-x)}Ga_{(x)}O_2$ (x=0.3)

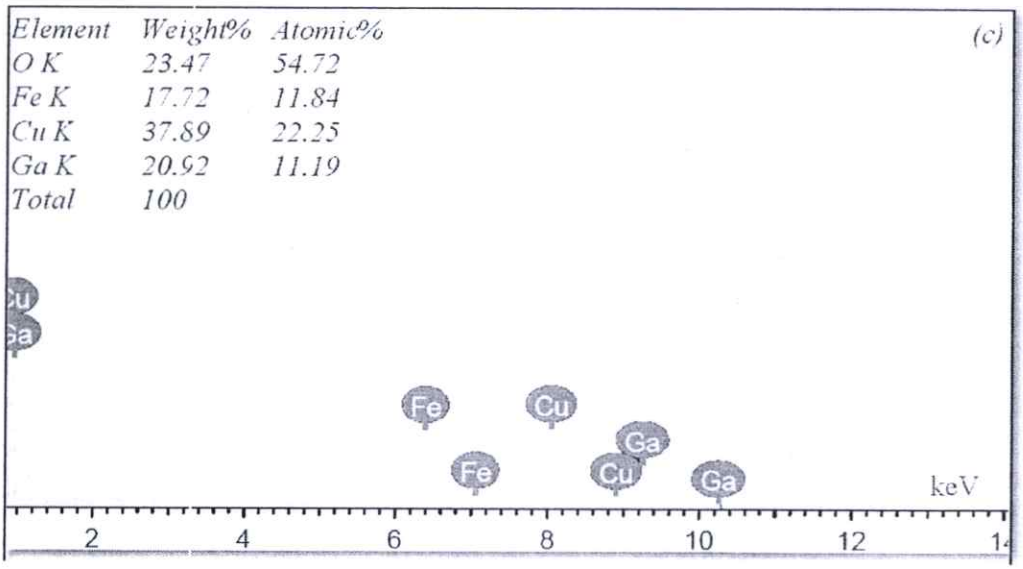

Figure 4.6 Energy dispersive spectroscopy of $CuFe_{(1-x)}Ga_{(x)}O_2$ (x=0.5)

4.1.2 Results of $CuFe_{1-x}Al_xO_2$ where x= 0.1, 0.3 and 0.5

The X-ray diffraction patterns of all Al contents (x= 0.1, 0.3 and 0.5) were shown in figure. 4.7. All of the patterns exhibited the peaks of delafossite with space group $R\bar{3}m$ (166), in accordance with JCPDS PDF 39-0246 and 75-2361 [70]. The XRD pattern confirmed that non-impurity phase peaks in these samples, that corresponding with the remaining of starting material were not found. Thereby, the results confirming that pure phase delafossite was formed. The mains peak of series shifted to right side likewise series of Ga. But this series was shifted higher than because atomic radius of Al (0.534 Å) smallest Ga (0.625Å). Figure 4.8 shows the main peak (0 1 2) of Al series. Figure 4.9 shows length of a-axis, c-axis and volume of Al series, so that a-axis and c-axis were decreased when content of Al increases. Therefore, the effect of delafossite volume decreases.

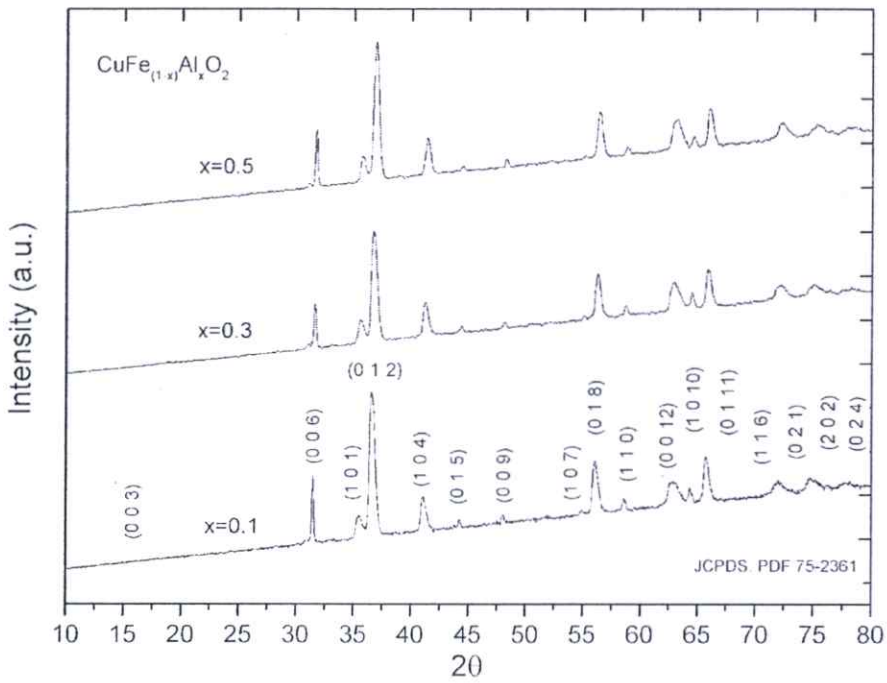

Figure 4.7 The XRD pattern of the $CuFe_{(1-x)}Al_{(x)}O_2$ (x=0.1, 0.3 and 0.5)

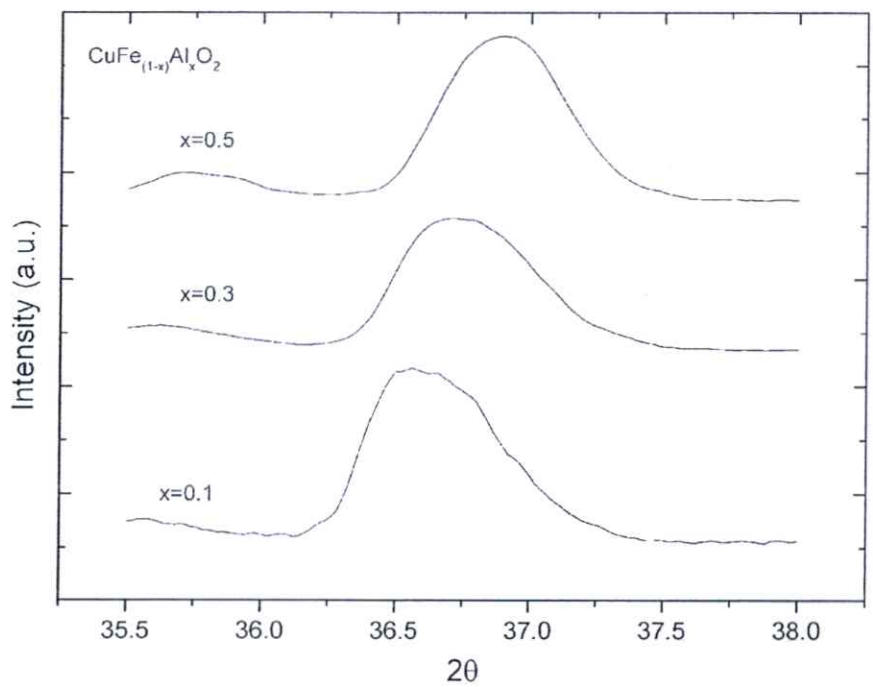

Figure 4.8 Main peak (0 1 2) functions with Al (x= 0.1, 0.3, and 0.5)

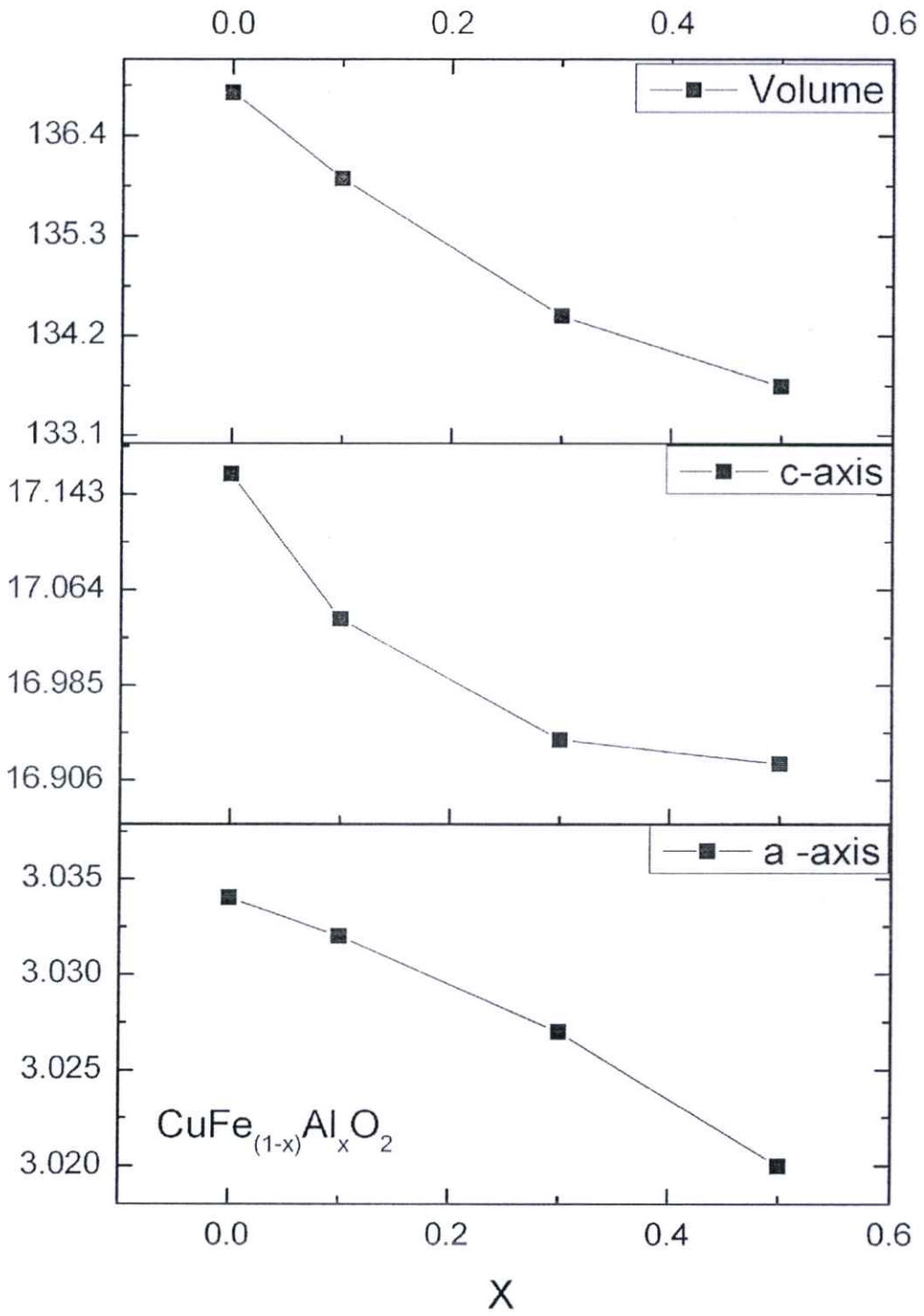

Figure 4.9 Lattice parameter a-axis and c-axis functions with Al (x= 0.1, 0.3, and 0.5)

The energy dispersive x-ray spectroscopy results of each x contents (0.1, 0.3 and 0.5) showed in figure. 4.10, 4.11 and 4.12. All of samples showed oxygen to exceed 7-8%, iron 102%, 136% and 135%, copper 85%, 70% and 68%, aluminum 70%, 97% and 108% at x=0.1, 0.3 and 0.5 respectively.

Both of results of x-ray diffraction and energy dispersive x-ray spectroscopy to confirm the samples were delafossite structure by substation iron with aluminum.

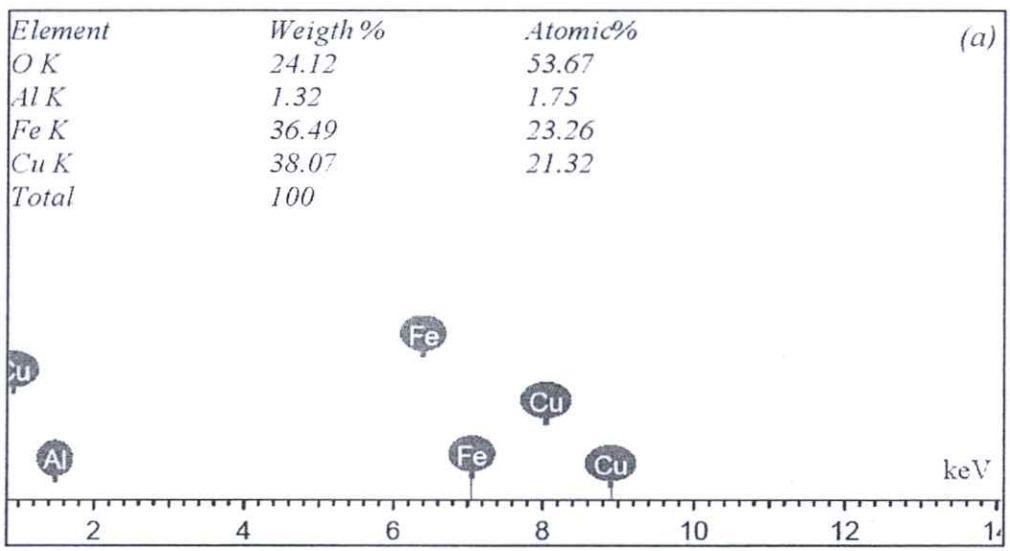

Figure 4.10 Energy dispersive spectroscopy of $CuFe_{1-x}Al_xO_2$ (x=0.1)

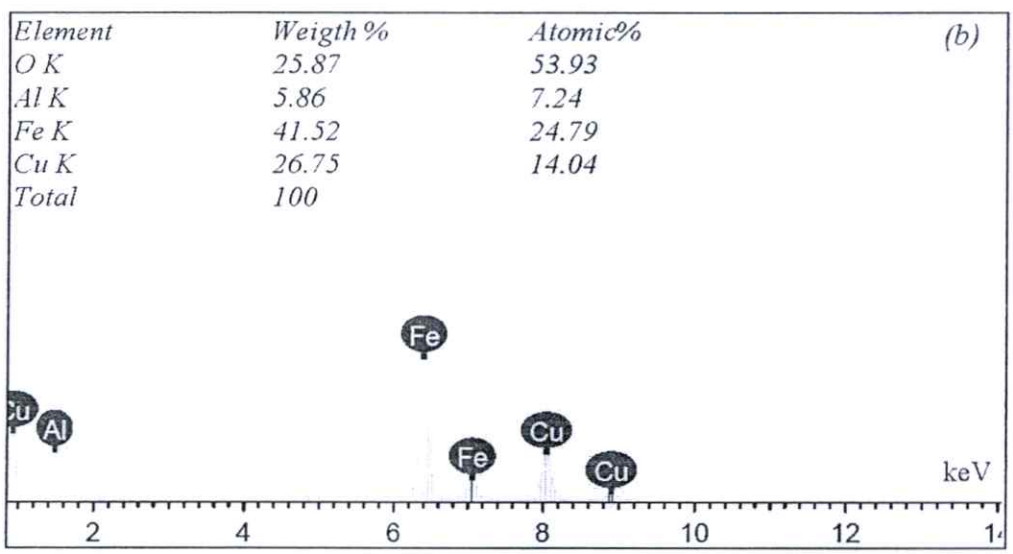

Figure 4.11 Energy dispersive spectroscopy of $CuFe_{1-x}Al_xO_2$ (x=0.3)

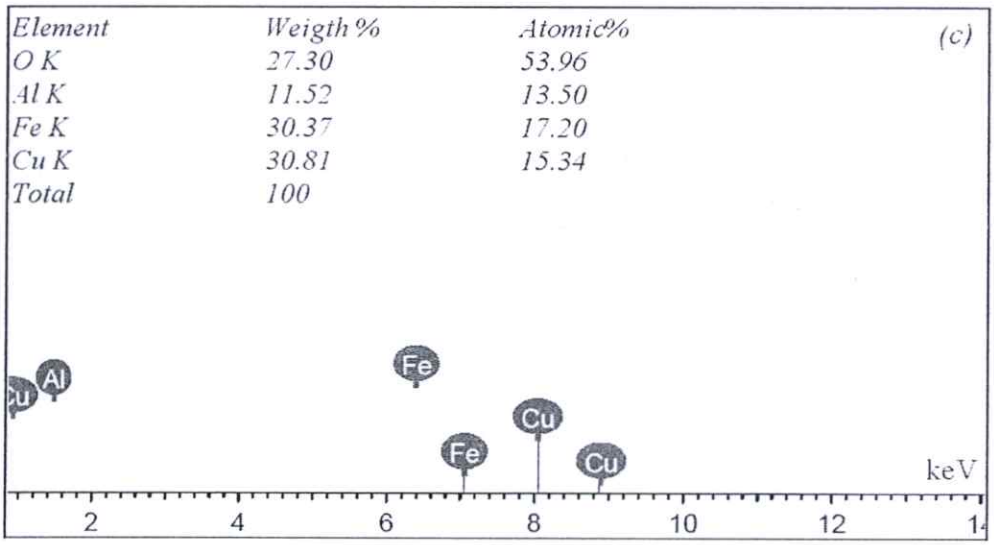

Figure 4.12 Energy dispersive spectroscopy of $CuFe_{1-x}Al_xO_2$ (x=0.5)

4.2 Results and discussion of Thermal Conductivity

Thermal conductivity describes the transport of energy in the form of heat through a body of mass as the result of a temperature gradient. And thermal conductivity effect to efficient of thermoelectric. One of possible way to increases efficiency of thermoelectric is decreases of thermal conductivity. The thermal conductivity every samples were measured by NETZSCH LFA 477 Nano-Flash thermal diffusivity analyzer and recording by step of 50 K from room temperature to 573 K, the results of all samples show figure 4.13 and 4.14.

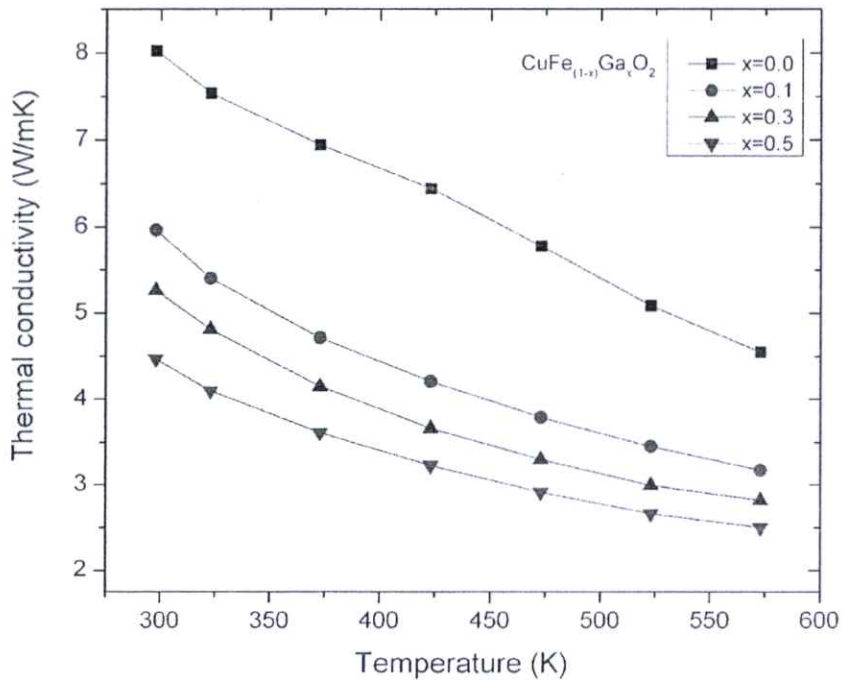

Figure 4.13 Thermal conducivity of the $CuFe_{1-x}Ga_xO_2$ (x=0.0, 0.1, 0.3 and 0.5)

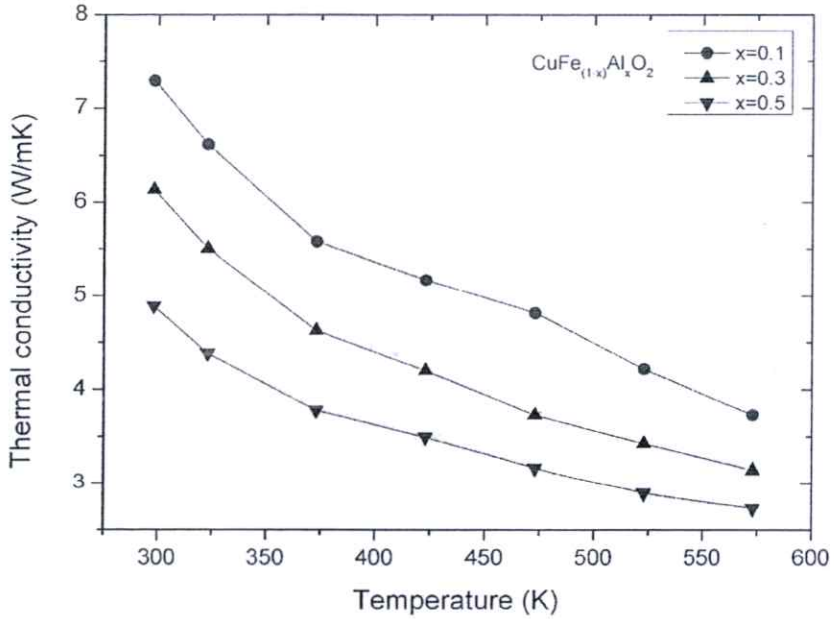

Figure 4.14 Thermal conducivity of the $CuFe_{1-x}Al_xO_2$ (x=0.1, 0.3 and 0.5)

4.2.1 Discussion of Thermal Conductivity

The thermal conductivity decreases with increasing of material substitute (Ga and Al) and temperature. The thermal conductivity results showed the samples of x=0.5 ($CuFe_{0.5}Ga_{0.5}O_2$ and $CuFe_{0.5}Al_{0.5}O_2$) which the lowest of thermal conductivity was $CuFe_{0.5}Ga_{0.5}O_2$.

The concept description of elastic scattering of phonon (phonon scattering) by static imperfection and apply it to substitution impurity, vacancy, dislocation and grain boundary were described by P.G. Klemens [71]. In this case vacancy and dislocation do not affect to thermal conductivity because iron was substituted by Ga and Al.

4.2.1.1 Discussion of Thermal Conductivity by Grain Boundary

The grain boundary was considers to effect of thermal conductivity, which $CuFeO_2$ was grain boundary reference to compared with all series of $CuFe_{1-x}Ga_xO_2$ and $CuFe_{1-x}Al_xO_2$. The grain size image of series $CuFe_{1-x}Ga_xO_2$ (x=0.0, 0.1, 0.3 and 0.5) shows in figure 4.15, 4.16, 4.17 and 4.18. The smallest grain size of the samples was approximately 5–8 μm at x = 0.5. The grain size of the x = 0.0, 0.1 and x = 0.3 samples was approximately 6–9 μm. Thus, the grain size of the x = 0.1, 0.3 and 0.5 $CuFe_{1-x}Ga_xO_2$ samples was not effected to significantly affect their thermal conductivity compared with that of $CuFeO_2$.

The grain size image of series $CuFe_{1-x}Al_xO_2$ (x=0.1, 0.3 and 0.5) shows in figure 4.19, 4.20 and 4.21. The grain sizes of this series approximated 3-7 μm. Therefore this was confirming that the size of grain did not affect significantly to thermal conductivity. The results showed the comparison of 2-series between $CuFe_{1-x}Ga_xO_2$ and $CuFe_{1-x}Al_xO_2$ when x=0.0, 0.1, 0.3 and 0.5 that the lowest thermal conductivity was $CuFe_{0.5}Ga_{0.5}O_2$.

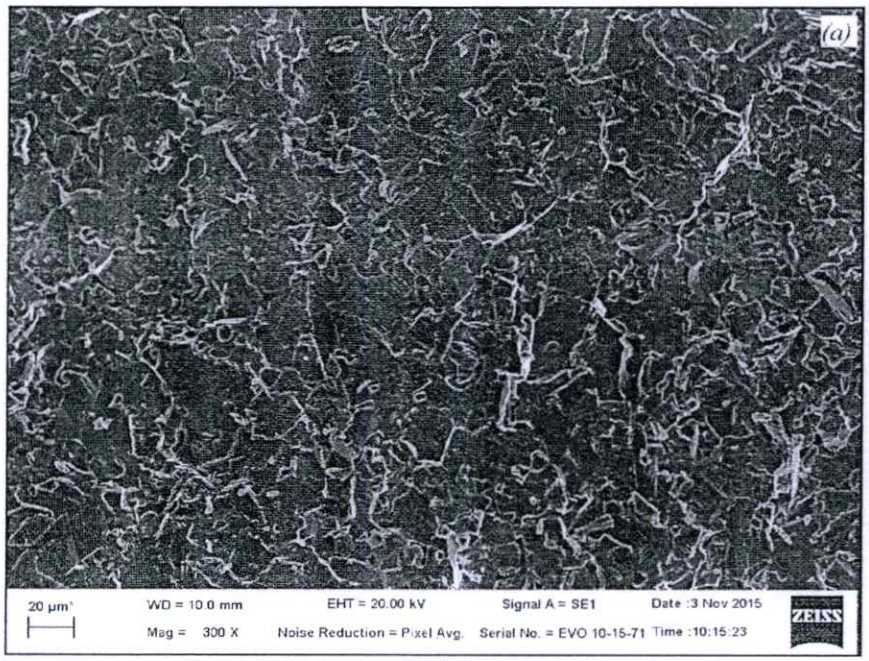

Figure 4.15 Scanning Electron Microscope image of $CuFeO_2$

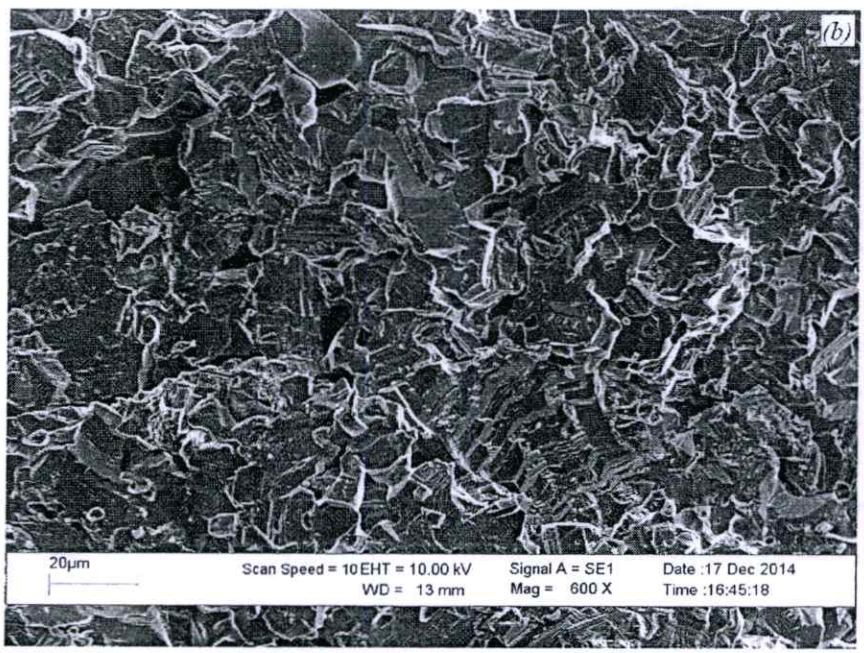

Figure 4.16 Scanning Electron Microscope image of $CuFe_{0.9}Ga_{0.1}O_2$

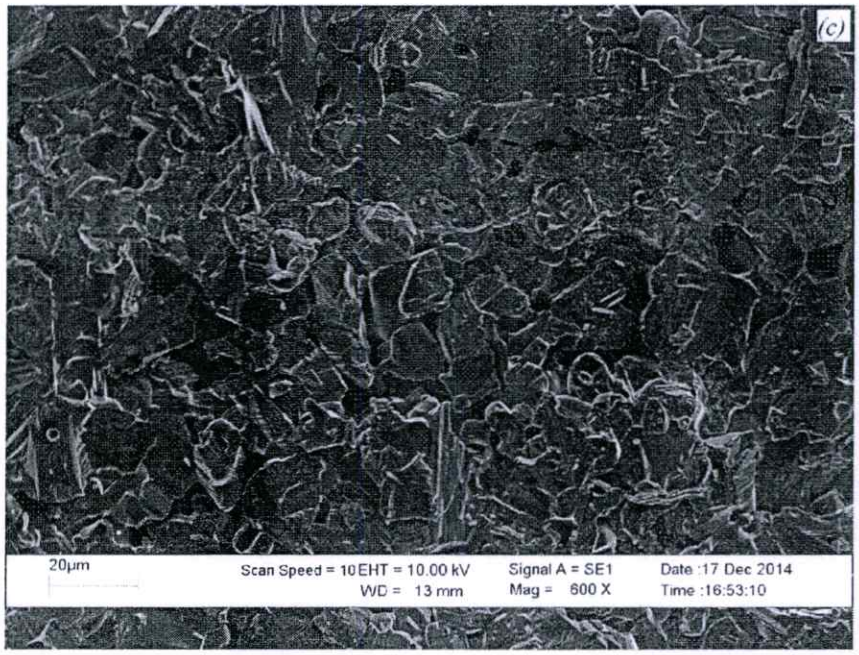

Figure 4.17 Scanning Electron Microscope image of $CuFe_{0.7}Ga_{0.3}O_2$

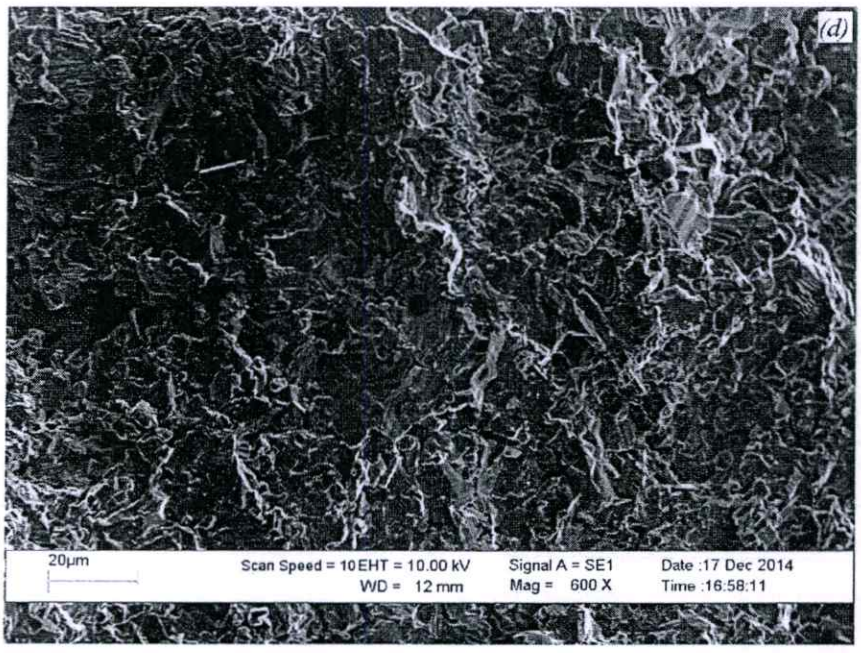

Figure 4.18 Scanning Electron Microscope image of $CuFe_{0.5}Ga_{0.5}O_2$

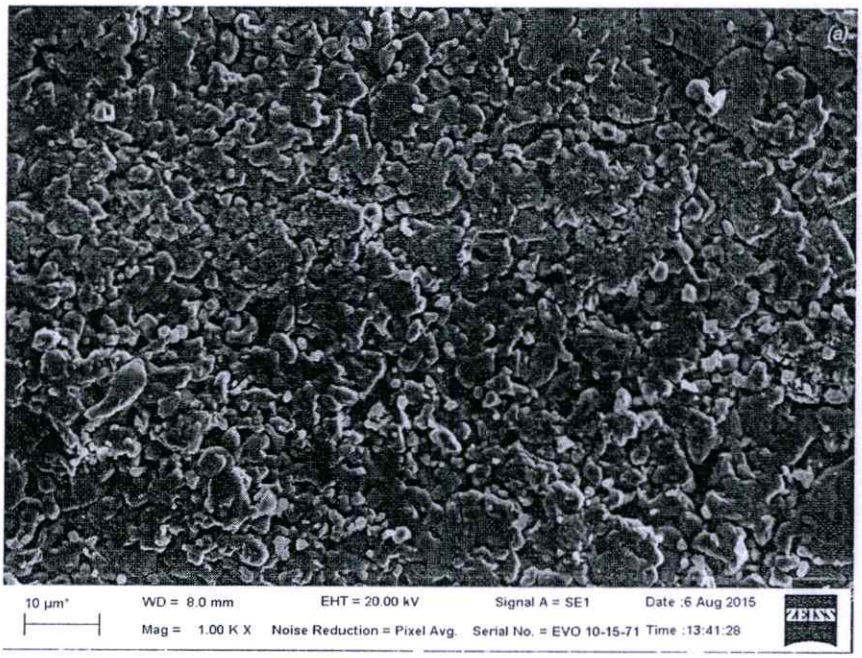

Figure 4.19 Scanning Electron Microscope image of $CuFe_{0.9}Al_{0.1}O_2$

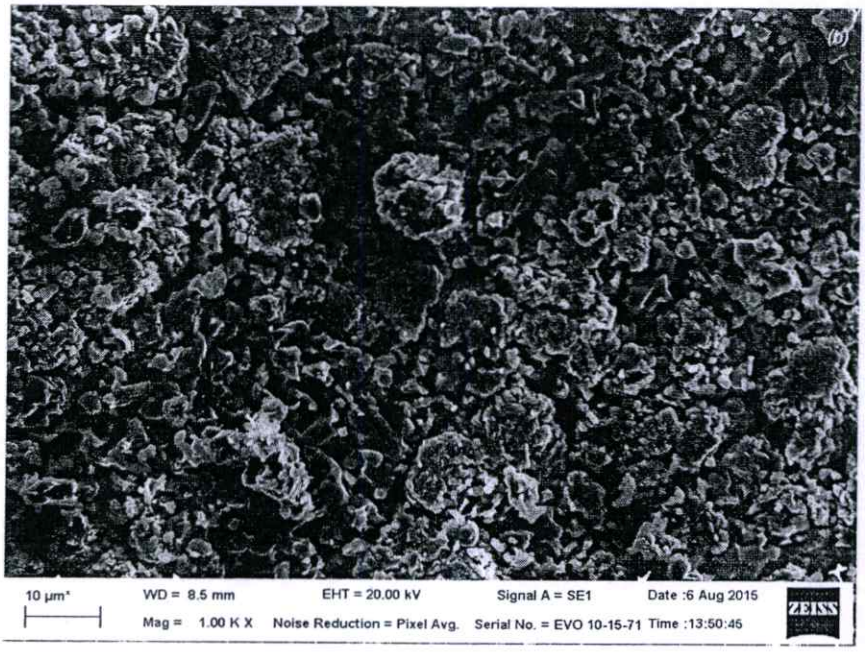

Figure 4.20 Scanning Electron Microscope image of $CuFe_{0.7}Al_{0.3}O_2$

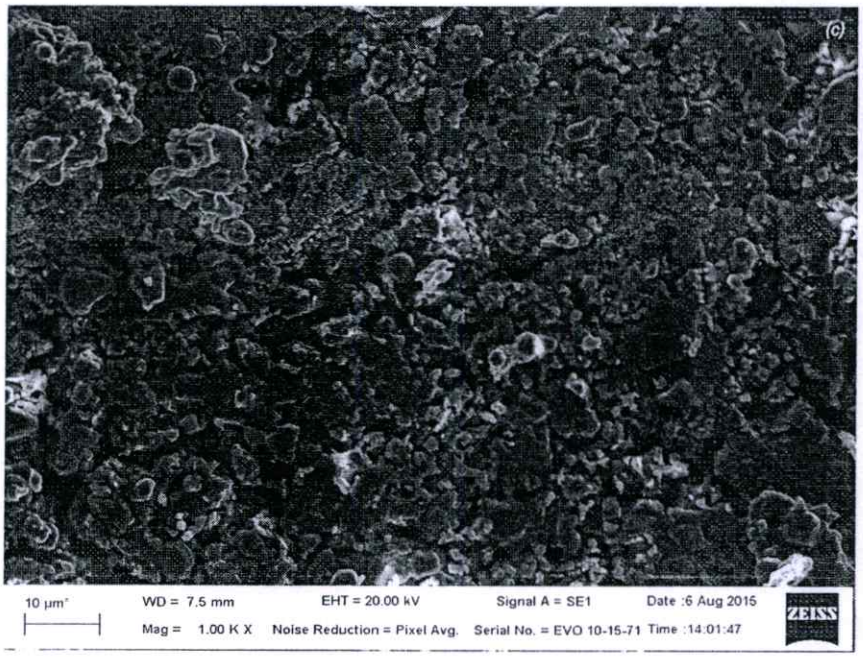

Figure 4.21 Scanning Electron Microscope image of $CuFe_{0.5}Al_{0.5}O_2$

4.2.1.2 Discussion of Thermal Conductivity by Substitution Atom to Difference Mass or Strain in the Lattice

The above reason of results were showed the grain boundary less effective to the properties of thermal conductivity because grain boundary of series $CuFe_{1-x}Al_xO_2$ slightly small than $CuFe_{1-x}Ga_xO_2$. But the results ofthermal conductivity showed $CuFe_{1-x}Al_xO_2$ more than $CuFe_{0.5}Ga_{0.5}O_2$, so grain boundary did not effect to thermal conductivity.Next determine effect of material (Ga and Al) substitution into iron using general expression equation 4.1.

$$K = \frac{1}{\kappa} = (A + BT) \qquad (4.1)$$

Where K is the thermal resistivity, A and B are the phonon scattering by A is thermal resistivity by substitution impurity defect. B is intrinsic thermal resistivity and T is the absolute temperature. figure 4.22 and 4.23show thermal resistivity (K) of series $CuFe_{1-x}$(Ga, and Al)$_xO_2$ when x=0.0, 0.1, 0.3 and 0.5 respectively.

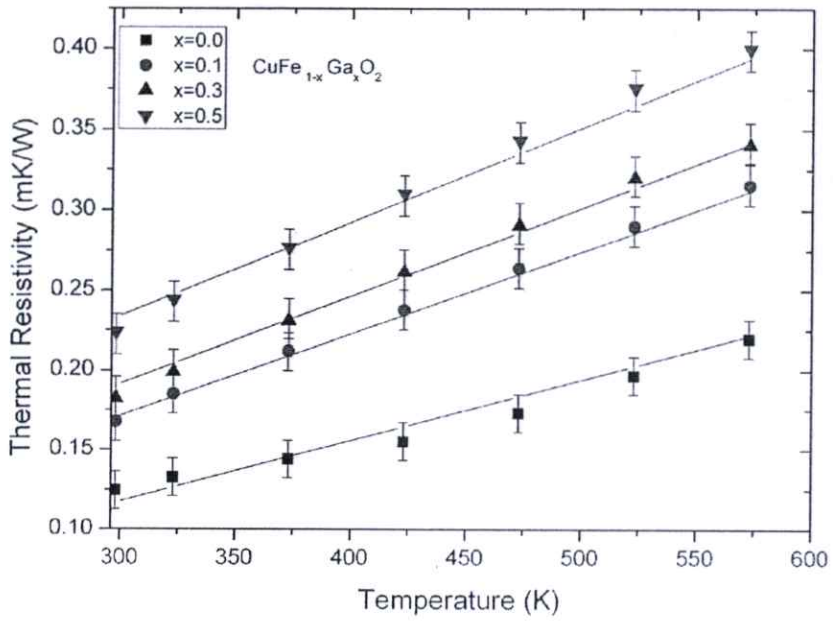

Figure 4.22 Thermal resistivity of the $CuFe_{1-x}Ga_xO_2$ (x=0, 0.1, 0.3 and 0.5)

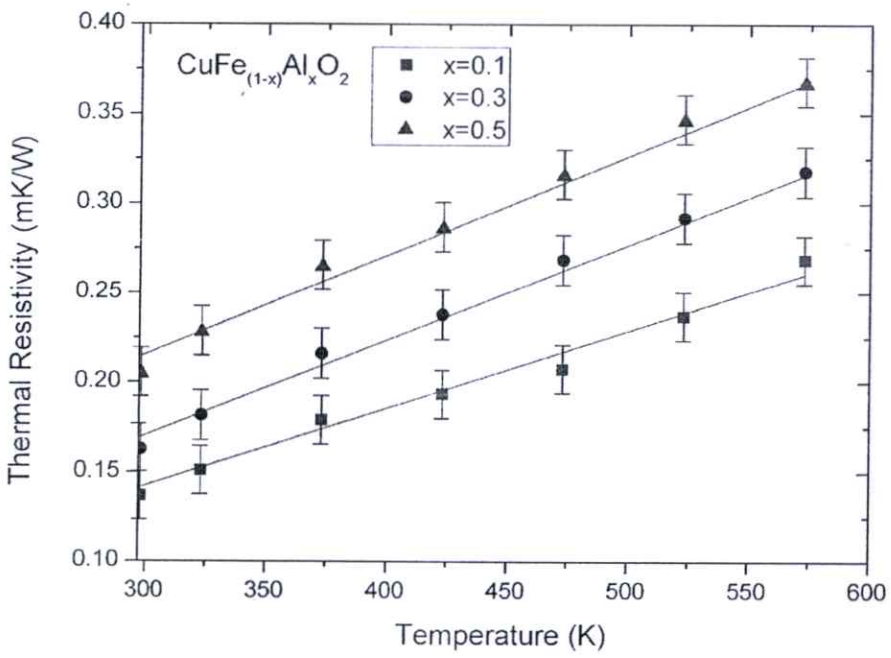

Figure 4.23 Thermal resistivity of the $CuFe_{1-x}Al_xO_2$ (x=0.1, 0.3 and 0.5)

The according to V. Ambegaoker [39], J. Francl and coworker [72], T. Nozaki and coworker [73] the A term of K relation can be approximate by

$$A = \frac{\pi^2 V\theta}{3h\upsilon^2}\Sigma_i\Gamma_i$$

Where V is the average atomic volume, θ is the Debye temperature, *h* is Plank's constant and υ is the velocity of sound in sample. $\Sigma_i\Gamma_i$ is the summation of the cross section of all phonon scatting processes to

$$\Sigma_i\Gamma_i = \Gamma_0 + \Gamma_m + \Gamma_s$$

where Γ_0 is the contribution from the normal defect of the non-dope, here $CuFeO_2$. Γ_m is the contribution from mass difference show in equation 4.2 and Γ_s is contribution from lattice strain show in equation 4.3.

$$\Gamma_m = x(1-x)\left(\frac{M_I - M_{II}}{xM_I + (1-x)M_{II}}\right)^2 \qquad (4.2)$$

$$\Gamma_s = x(1-x)\varepsilon\left(\frac{\delta_I - \delta_{II}}{x\delta_I + (1-x)\delta_{II}}\right)^2 \qquad (4.3)$$

Where M_I, M_{II} is the atomic mass of Fe and Ga or Al. And δ_I, δ_{II} is atomic radius of Fe and Ga or Al. The ε is a constant given as 39 (P.G. Klemens [71]). The values of atomic mass and atomic radius of Fe (55.847 and 0.645A°), Ga (69.732 and 0.625 A°) and Al (26.981 and 0.534A°).

Table 4.2 Scattering cross-section by mass difference and lattice strain

$CuFe_{(1-x)}Ga_{(x)}O_2$ Ga content x	Γ_m	Γ_s
0.0	0	-
0.1	0.0037	0.0036
0.3	0.0094	0.0082
0.5	0.0122	0.0097
$CuFe_{(1-x)}Al_{(x)}O_2$ Al content x	-	-
0.1	0.0841	0.1455
0.3	0.1377	0.3135
0.5	0.1214	0.3456

The results of table 4.2 showed thecontribution of mass flucation anharmonic, which causes from the difference atomic mass. In case of difference atomic radius of Ga and Al affect to arrange in the lattice (lattice strain). Both of atomic mass and atomic radius contributed to effectfor the thermal conductivity to decrease.

The table 4.2 and thermal conductivity results of 2-series samples showed inconsistent. The results showed that the lowest thermal conductivity of this thesis was $CuFe_{0.5}Ga_{0.5}O_2$, which contrast with results of table 4.2. The lattice strain of Al series was dominate reduce thermal conductivity more than Ga. In this cases were explained the according to Klemens concept or Keyes relation [48-74] , as showed in equation 4.4.

$$\kappa_l = A\left(\frac{1}{T}\right)\left(\frac{T_m^{\frac{3}{2}}\rho^{\frac{2}{3}}}{M^{\frac{7}{6}}}\right) \qquad (4.4)$$

Where A is the proportionality constant, T_m is the melting point, ρ is the density and M is average atomic mass.

The equation 4.4 shows the relation of density and melting point of materials, that the density and the average atomic mass of Al are less than Ga but

the melting point of Al is higher than Ga, so the totally effect to compare between Ga to thermal conductivity more than Al materials, Therefore affect to the thermal conductivity of $CuFe_{0.5}Ga_{0.5}O_2$ less than $CuFe_{0.5}Al_{0.5}O_2$.

4.3 Results and discussion of Seebeck Coefficient and Electrical Conductivity

4.3.1 Seebeck Coefficient Results and Discusion

The Seebeck coefficient is a measurement of the entropy per carrier in a material. All of samples measured by ULVAC ZEM-3, temperature between 469-849 K. In case $CuFeO_2$ reference result from Chesta and coworker [17]. The results of seebeak coefficient show in figure. 4.24 and 4.25.

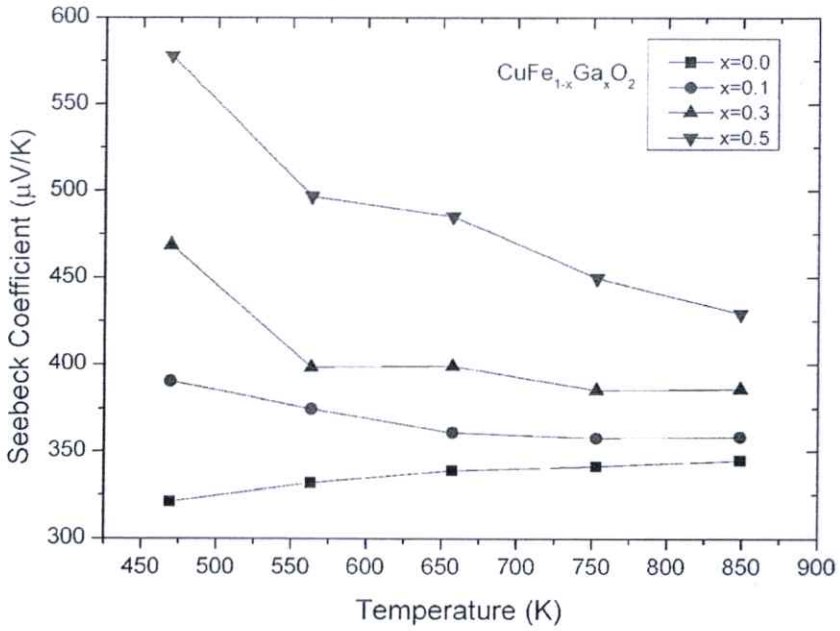

Figure 4.24 Seebeck Coefficient of the $CuFe_{1-x}Ga_xO_2$ (x=0.1, 0.3 and 0.5)

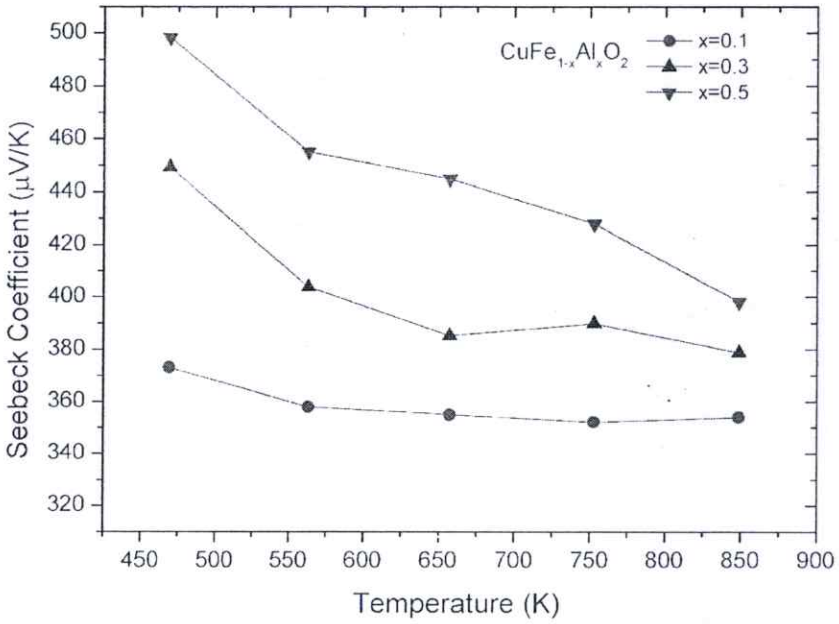

Figure 4.25 Seebeck Coefficient of the $CuFe_{1-x}Al_xO_2$ (x=0.1, 0.3 and 0.5)

The results showed that the Seebeck coefficients are positive sign over the range of temperature for all of samples. These reveal that the all of samples are p-type conductor due to the hole carriers. The $CuFe_{0.5}Ga_{0.5}O_2$ and $CuFe_{0.5}Al_{0.5}O_2$ samples displayed Seebeck coefficient higher than that value of the series.

Refers to First Law of Thermodynamics [75] showed in equation 4.5

$$Q = \Delta U + W_d \tag{4.5}$$

When Q is heat add to a system, ΔU is internal energy and W_d is work of the system.

And refer definition of specific heat (C).

$$C = \frac{1}{m}\frac{dQ}{qT} \tag{4.6}$$

when m is mass. Thus specific heat at constant volume and constant pressure is.

$$dQ = mC_v dT \tag{4.7}$$

$$dQ = mC_p dT \tag{4.8}$$

When C_v is specific heat at constant volume and C_p is specific heat at pressure constant.

In case specific heat at constant volume, the pressure increases when heat add to the system but the volume constant effect to work done is zero ($dW_d = 0 = pdV$). Therefore $dU = mC_v dT$.

In case specific heat at constant pressure, the volume increases when heat add to the system. Effect to work done is ($dW_d = pdV$).

Therefore

$$mC_p dT = dU + dW_d \text{ or } mC_p dT = mC_v dT + pdV \tag{4.9}$$

Refers to Second Law of Thermodynamics showed in equation 4.10

$$dS_{entropy} = \frac{dQ}{\mathrm{T}} \tag{4.10}$$

When $S_{entropy}$ is entropy of the system. Thus replace equation 4.8 to 4.9 and to 4.10.

$$\Delta S_{entropy} = \int \frac{dQ}{T} = \int \frac{mC_p dT}{T} = \int \frac{mC_v dT + pdV}{T} \tag{4.11}$$

The results of specific heat were measured by NETZSCH LFA 477 Nano-Flash thermal diffusivity analyzer at room temperature to 573 K. The results of all samples show figure 4.26 and 4.27. The results of each point of Ga and Al series showed difference maximum at 0.068 J/gK and 0.144 J/gK respectively, therefore the entropy effect of according to equation 4.11 was very slight as shown in figure 4.26 and 4.27. These results were confirmed entropy of each sample in the each series to approximate equal because difference maximum of specific heat a little bit difference can be insignificant.

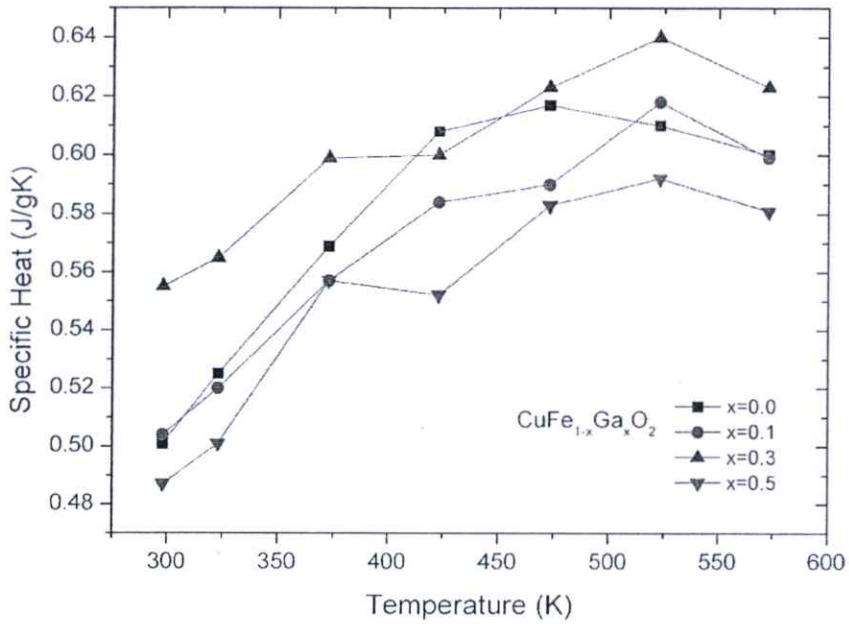

Figure 4.26 Specific Heatof the $CuFe_{1-x}Ga_xO_2$ (x=0.0, 0.1, 0.3 and 0.5)

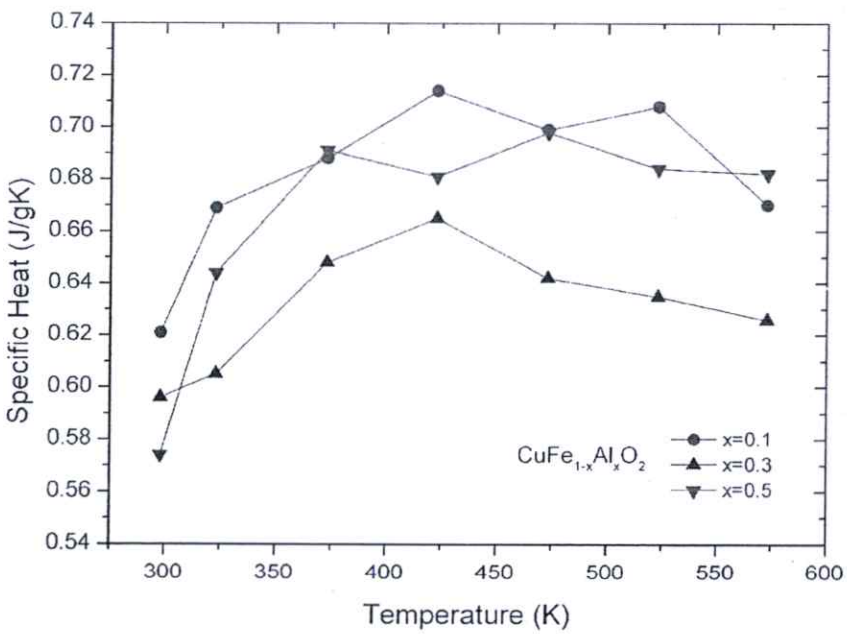

Figure 4.27 Specific Heat of the $CuFe_{1-x}Al_xO_2$ (x=0.1, 0.3 and 0.5)

The according to results of specific heat affect to entropy showed no significant to Seebeck coefficient effect. Therefore the reason of Seebeck coefficient increases because the decreasing of carriers. The density of carrier (n) of each element dependent density and atomic weight showed in equation 4.12.

$$n = \frac{Density \times Avogadro\ Number}{Atomic\ Weight} \tag{4.12}$$

Table 4.3 Ratio of number of carrier per unit volume

Element	Fe	Ga	Al
Density (Kg/m^3)	7874	5904	2700
Atomic Weight	55.84	69.72	26.98
$(Ga/Fe)^{3+}$	0.60		
$(Al/Fe)^{3+}$	0.71		

4.3.2 Electrical Conductivity Results and Discusion

The electrical conductivity of Ga and Al series showed figure 4.28 and 4.29.

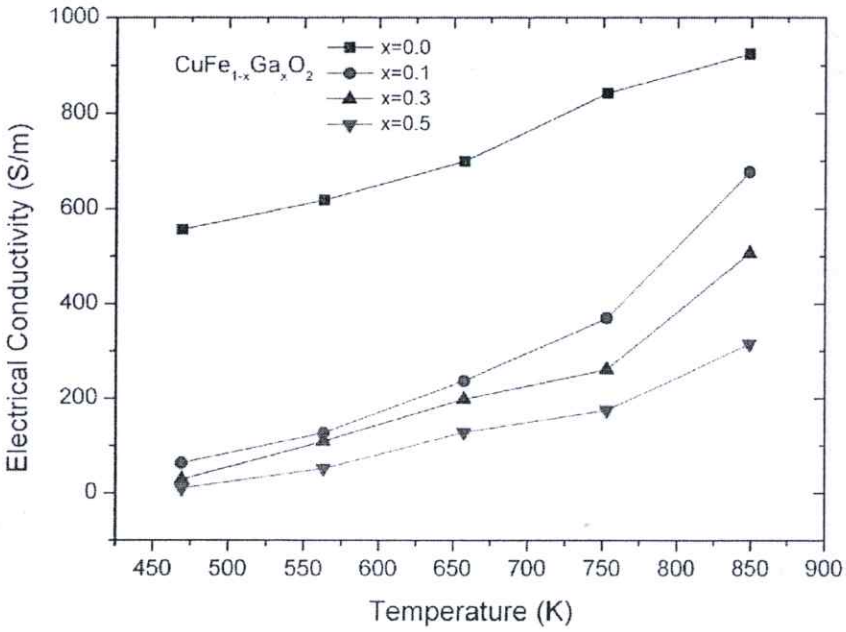

Figure 4.28 Electrical Conductivity of the $CuFe_{1-x}Ga_xO_2$ (x=0.1, 0.3 and 0.5)

The electrical conductivity decreased when the increasing x contents of both series showed in these results. Main effect of decreases of electrical conductivity was displayed in figure 4.28 at temperature 469 K that corresponding to carrier concentration decreases and it increases when temperature increasing. The Effects of increase in electrical conductivity were two possible ways. That was increases of mobility and carrier concentration. According to Brian J. Ingram and coworkers [76] explained the mobility increases estimate 20 S/m, moreover the effect from increasing was carrier. Form to density of state and Fermi-Dirac distribution function, the carrier is function temperature, as showed in equation 4.12 and this supported of measurement results.

$$n = 2\left(\frac{2\pi m_e kT}{h^3}\right)^{3/2} \exp(-\frac{E_c - E_F}{kT}) \quad \textit{for electron}$$

$$p = 2\left(\frac{2\pi m_p kT}{h^3}\right)^{3/2} \exp\left(-\frac{E_F - E_v}{kT}\right) \quad \textit{for hole} \qquad (4.12)$$

The sources of increasing carrier [75] were tramp impurities, oxygen interstitial and cation vacancies. But main of this effect was cation vacancy and oxygen interstitial due to non-stoichiometry and oxygen exceed [16, 76, 77] and performed to confirm tramp impurity slightly effect by Conam Kawin, Inc. using ASTM E 663 tested method.

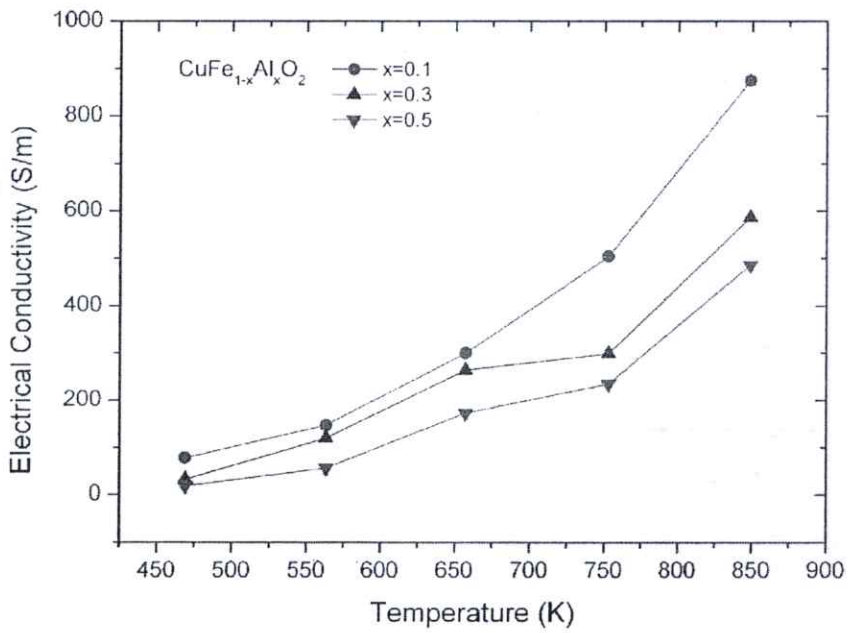

Figure 4.29 Electrical Conductivity of the $CuFe_{1-x}Al_xO_2$ (x=0.1, 0.3 and 0.5)

In case of $CuFeO_2$, the effect of slightly increased in Seebeck coefficient when the temperature was increased, so that the entropy increases. Finally the affect to Seebeck coefficient increases. Similar the increasing in electrical conductivity was the increases in temperature when the increase in the mobility, respectively. The increasing in mobility of $CuFeO_2$ were the properties of non-crystal defect by impurity (from Ga and Al) and non-disturb structure case from difference atomic radius (from

substitution Ga and Al) and non-anharmomic of lattice vibration effect from mass difference.

4.4 Results and discussion of X-ray Photoelectron Spectroscopy

X-ray Photoelectron Spectroscopy (XPS) for study composition of element and binning energy can be interprets to oxidation state of each element. The measurement results of X-ray Photoelectron Spectroscopy survey type showed in figure 4.30-4.36. The signal response of Cu 2p, Fe 2p, Ga and Al were 932 eV, 710 eV, 1117 eV and 74 eV, respectively.

The high-resolution XPS spectra, which binding energy of Cu and Fe compound showed figure 4.37-4.41, which spectrum of Cu of all samples showed Cu^{1+} and Cu^{2+}. In sample $CuFe_{1-x}Ga_xO_2$series spectrum of Cu^{1+}, Cu^{2+} at x=0.0, 0.1, 0.3, and 0.5 was 932.5 and 933.9, 932.7 and 934.0, 932.8 and 934.2, 932.5 and 934.3 eV respectively. In Al series $CuFe_{1-x}Al_xO_2$ spectrum of Cu^{I}, Cu^{II} at x=0.1, 0.3, and 0.5 is 932.3 and 933.7, 932.3 and 933.8, 932.5 and 933.9 ev respectively.

In similarity, the high-resolution XPS spectra, which binding energy of Fe all samples showed Fe^{II} and Fe^{III}. In sample $CuFe_{1-x}Ga_xO_2$ series spectrum of Fe^{II} and Fe^{III} at x=0.0, 0.1, 0.3, and 0.5 was 709.4 and 710.5, 709.9 and 711.4, 710.4 and 711.6, 710.3 and 711.4 eV respective. In Al series $CuFe_{1-x}Al_xO_2$ spectrum of Fe^{II} and Fe^{III} at x=0.1, 0.3, and 0.5 was 709.9 and 711.0, 710.0 and 711.5, 709.5 and 711.1 ev respectively.

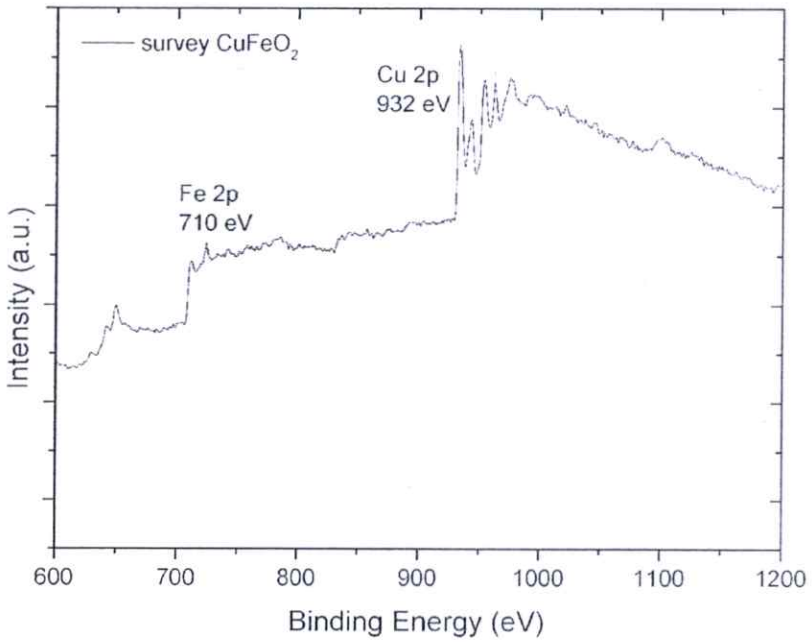

Figure 4.30 XPS spectrum survey of the $CuFeO_2$

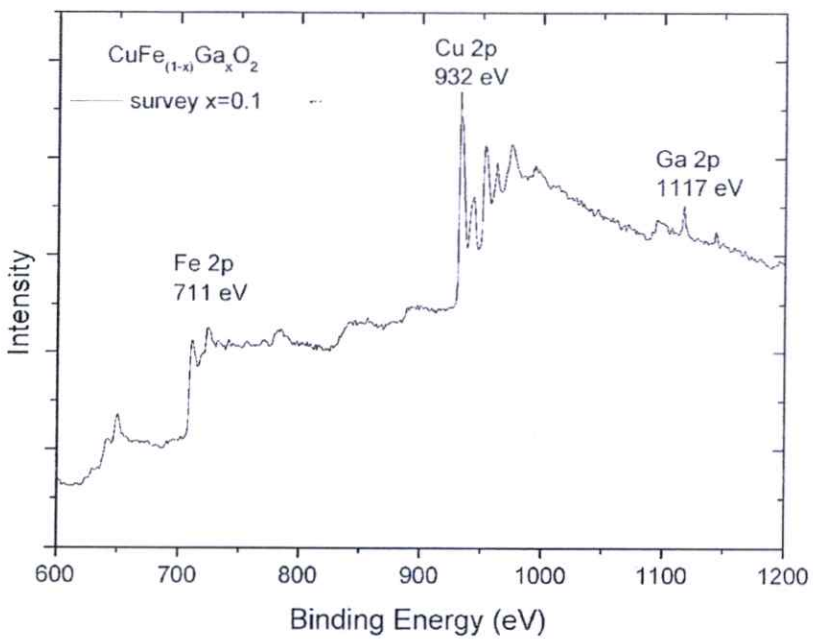

Figure 4.31 XPS spectrum survey of the $CuFe_{0.9}Ga_{0.1}O_2$

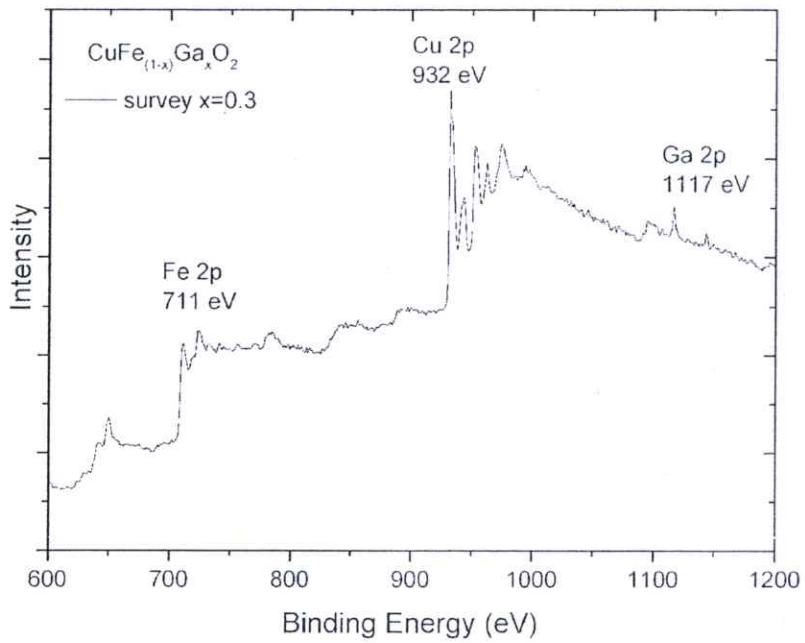

Figure 4.32 XPS spectrum survey of the $CuFe_{0.7}Ga_{0.3}O_2$

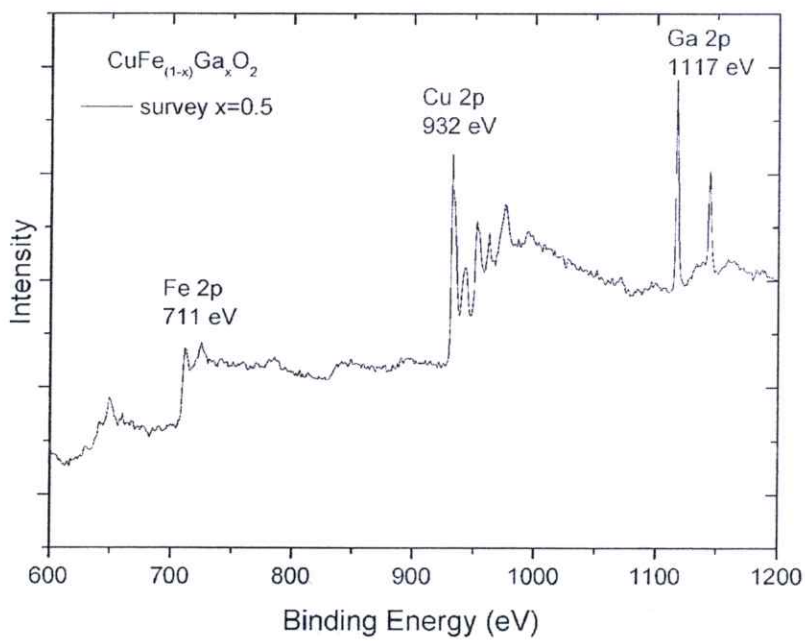

Figure 4.33 XPS spectrum survey of the $CuFe_{0.5}Ga_{0.5}O_2$

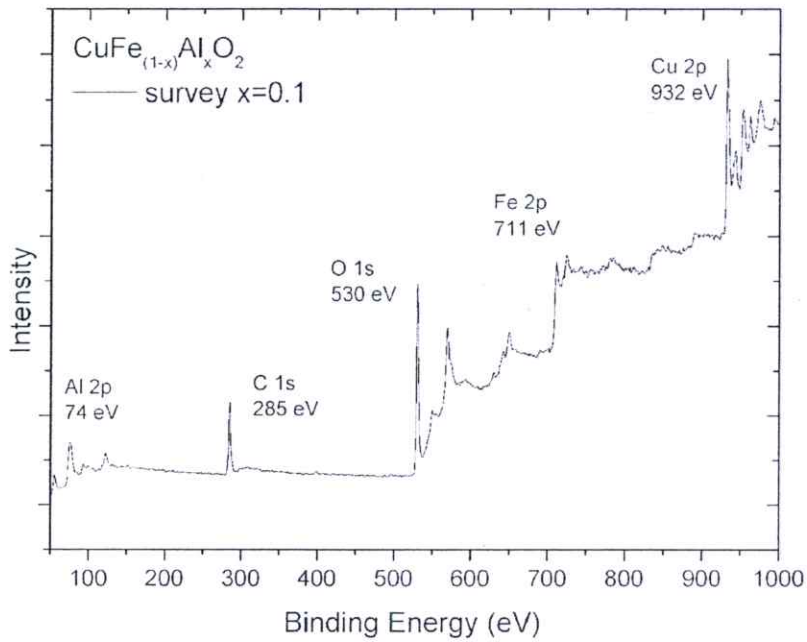

Figure 4.34 XPS spectrum survey of the $CuFe_{0.9}Al_{0.1}O_2$

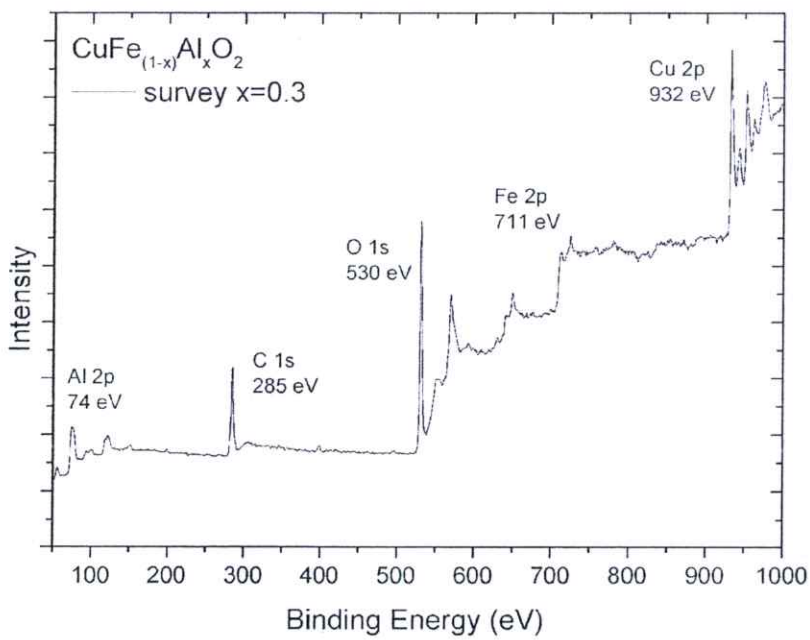

Figure 4.35 XPS spectrum survey of the $CuFe_{0.7}Al_{0.3}O_2$

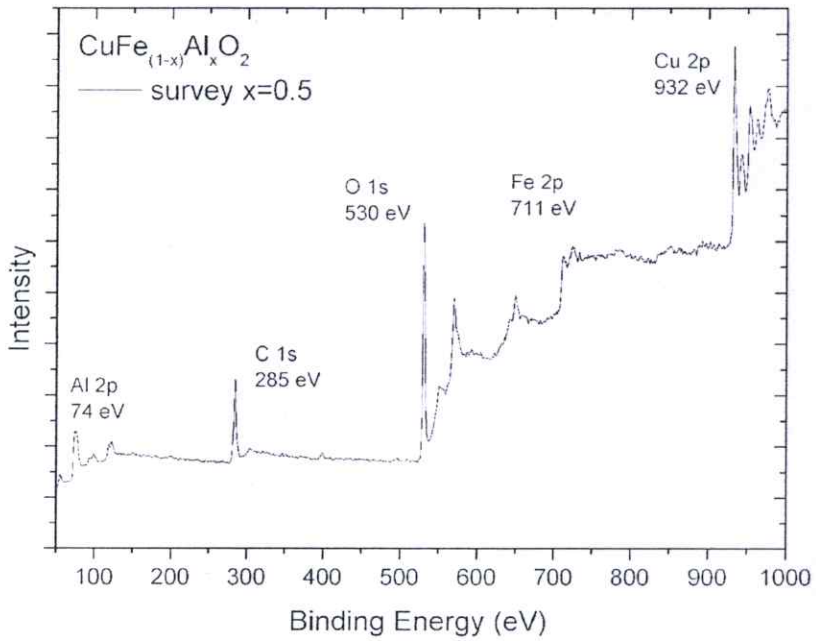

Figure 4.36 XPS spectrum survey of the $CuFe_{0.5}Al_{0.5}O_2$

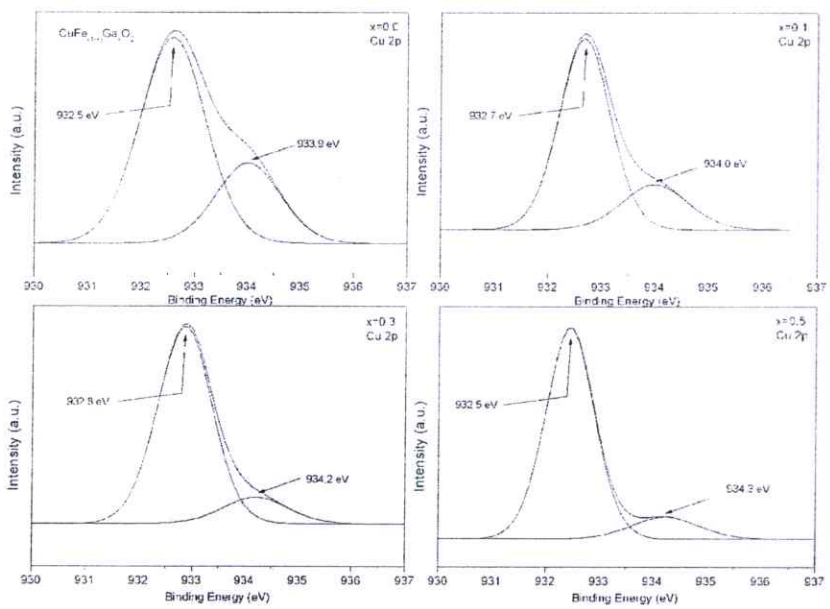

Figure 4.37 XPS spectrum of Cu of $CuFe_{(1-x)}Ga_{(x)}O_2$ (x=0.0, 0.1, 0.3 and 0.5)

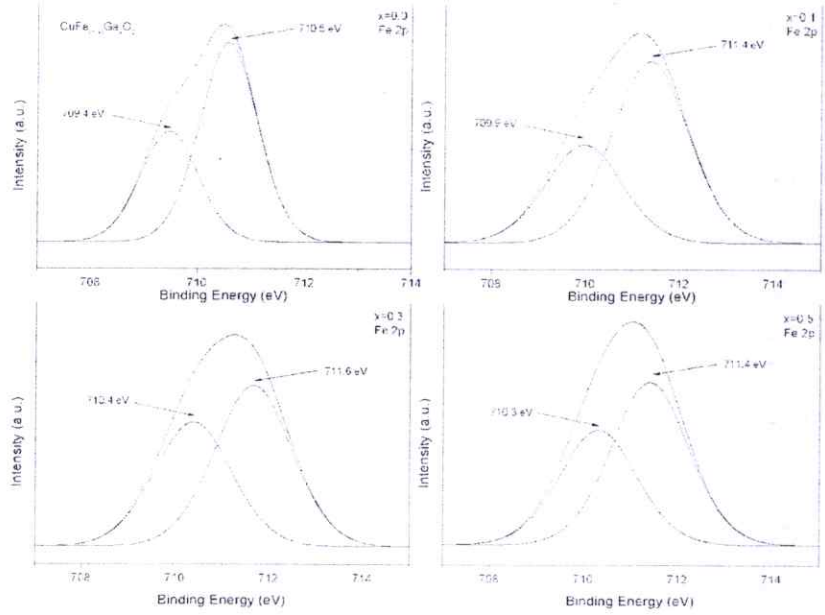

Figure 4.38 XPS spectrum of Fe of $CuFe_{(1-x)}Ga_{(x)}O_2$ (x=0.0, 0.1, 0.3 and 0.5)

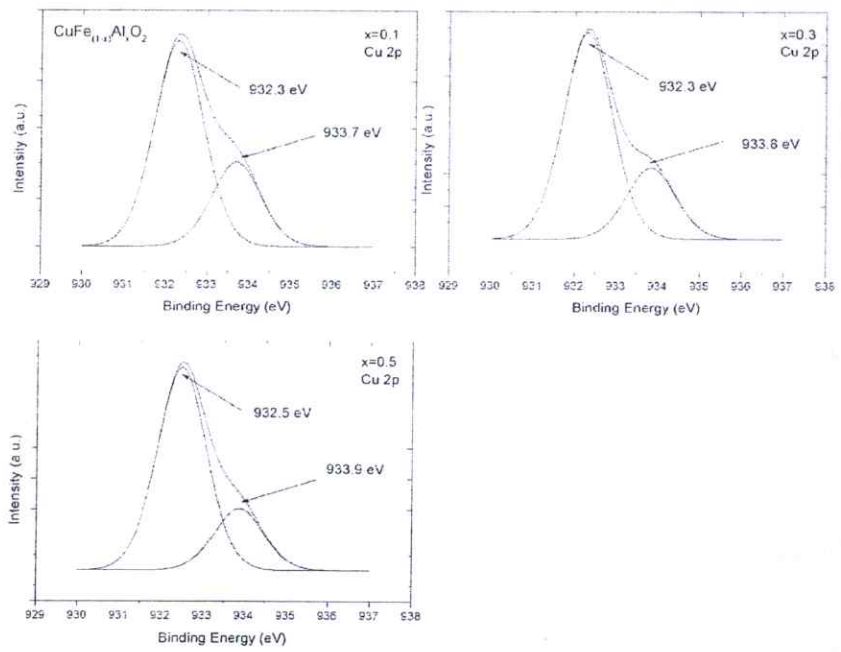

Figure 4.39 XPS spectrum of Cu of $CuFe_{(1-x)}Al_{(x)}O_2$ (x=0.1, 0.3 and 0.5)

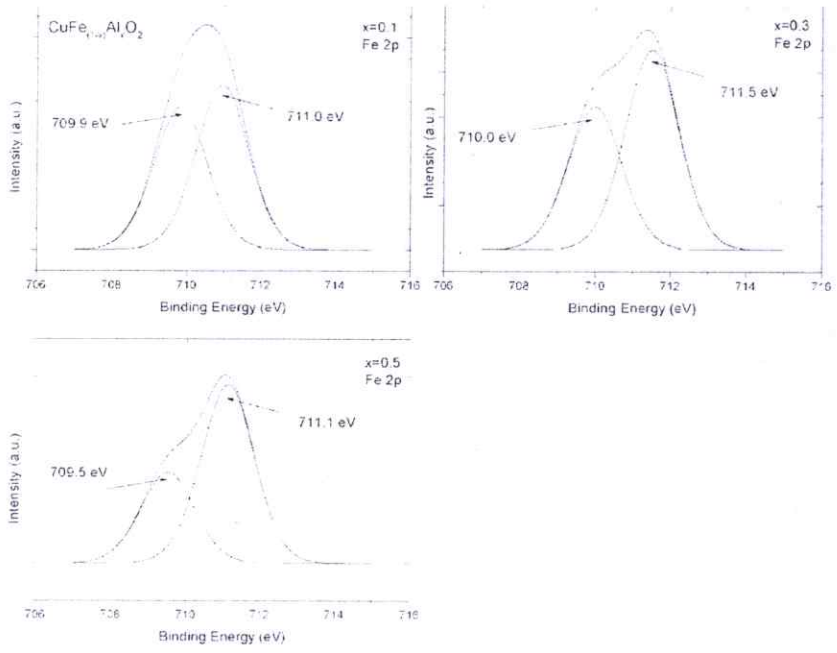

Figure 4.40 XPS spectrum of Fe of $CuFe_{(1-x)}Al_{(x)}O_2$ (x=0.1, 0.3 and 0.5)

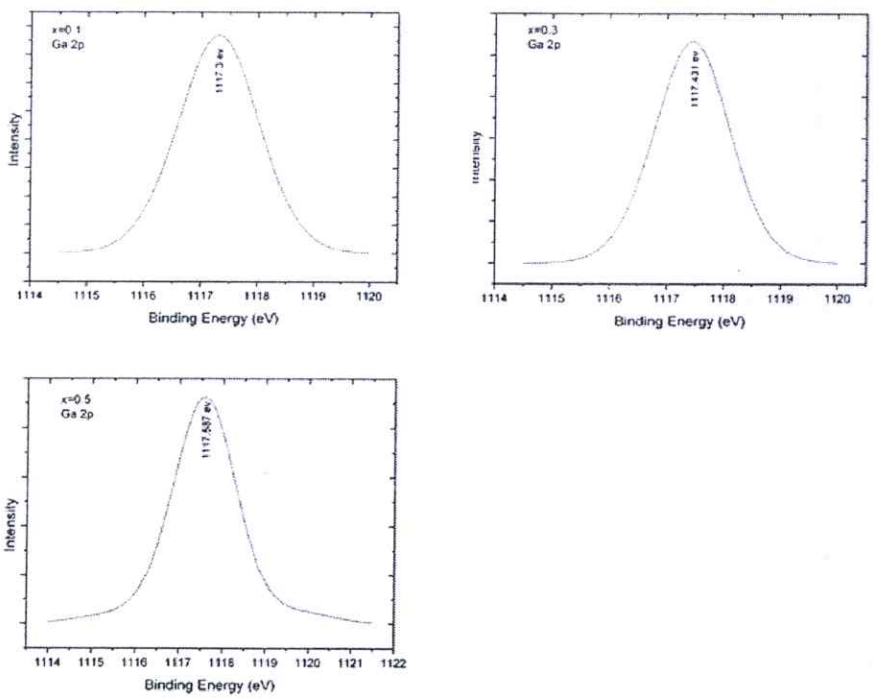

Figure 4.41 XPS spectrum of Ga of $CuFe_{(1-x)}Ga_{(x)}O_2$ (x=0.0, 0.1, 0.3 and 0.5)

The all of sample results of XPS spectrum showed binding energy of Cu^{1+}, Cu^{2+}, Fe^{2+}, Fe^{3+}. This confirms mixed valence between Cu^{1+} / Cu^{2+} and Fe^{2+}/Fe^{3+} which Ga and Al showed one oxidation state, due to the nature of material is 3+.

4.5 Power Factor and Dimensionless Figure of Merit (ZT)

The power factor is defined from Seebeck coefficient and electrical resistivity showed in equation (4.13) and the results showed in figure 4.42 and 4.43.

$$Power\ Factor = \frac{(Seebeck\ coefficient)^2}{Electrical\ Resistivity} \qquad (4.13)$$

The power factor for all sample increased by the increasing temperature. The $CuFeO_2$ sample displays power factor between 0.57×10^{-4} to 1.1×10^{-4} W/m-K^2. Other samples, in the series of Ga higher was $CuFe_{0.9}Ga_{0.1}O_2$ 0.87×10^{-4} W/m-K^2 at 849 K and series of Al higher was $CuFe_{0.9}Al_{0.1}O_2$ 0.87×10^{-4} 1.1×10^{-4} W/m-K^2 at 849 K.

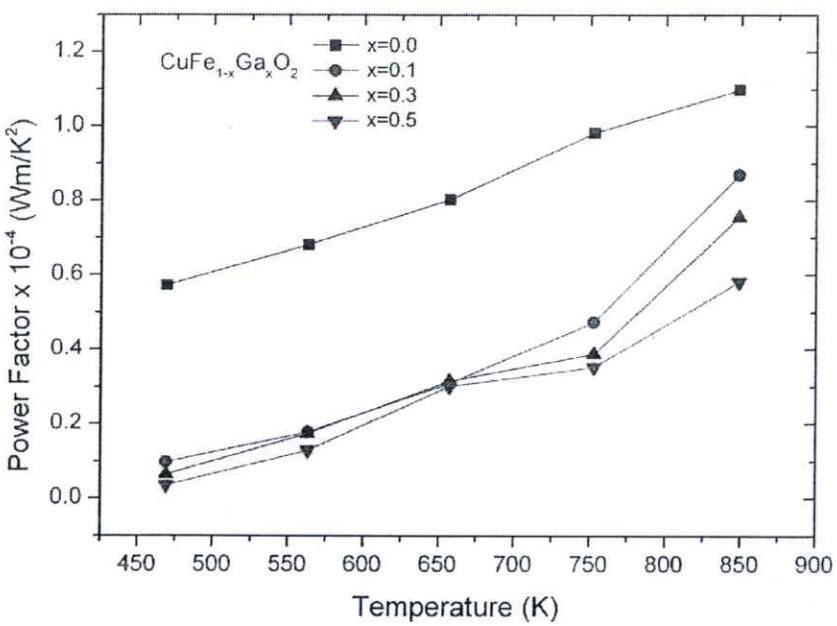

Figure 4.42 Power Factor of the $CuFe_{1-x}Ga_xO_2$ (x=0.1, 0.3 and 0.5)

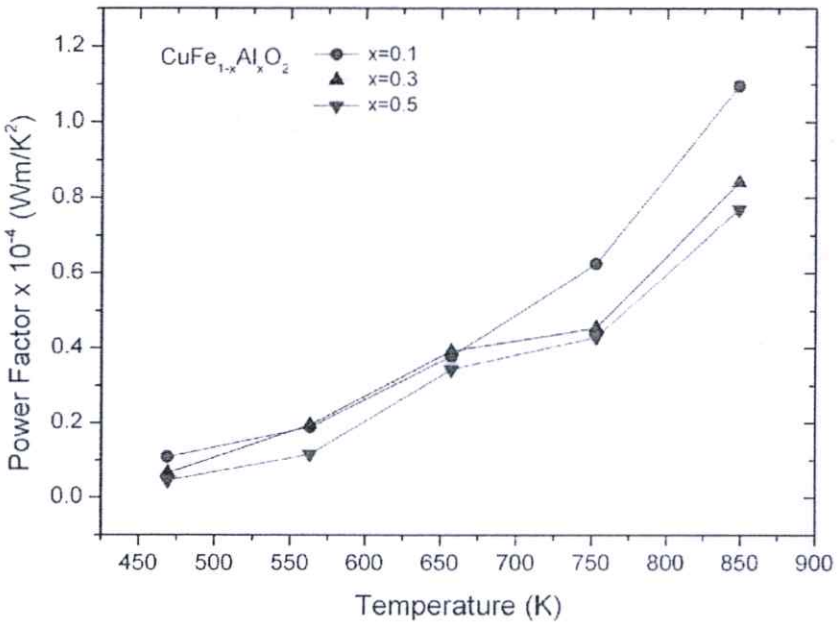

Figure 4.43 Power Factor of the $CuFe_{1-x}Al_xO_2$ (x=0.1, 0.3 and 0.5)

Dimensionless Figure of Merit (ZT)

The Dimensionless Figure of Merit is calculated from the Seebeck coefficient, electrical resistivity and thermal conductivity, as showed in equation 4.14 and the results showed in figure 4.44 and 4.45.

$$ZT = \frac{S^2}{\rho\kappa}T \qquad (4.14)$$

The Dimensionless Figure of Merit dependence with temperature and that calculate range from 469 to 563 K. The results showed that value of $CuFeO_2$ (ZT=0.0086) are higher than the value of Ga and Al series. In Ga series, the higher of this series was $CuFe_{0.7}Ga_{0.3}O_2$ (ZT=0.0033) and the higher of Al series was $CuFe_{0.7}Al_{0.3}O_2$ (ZT=0.0035).

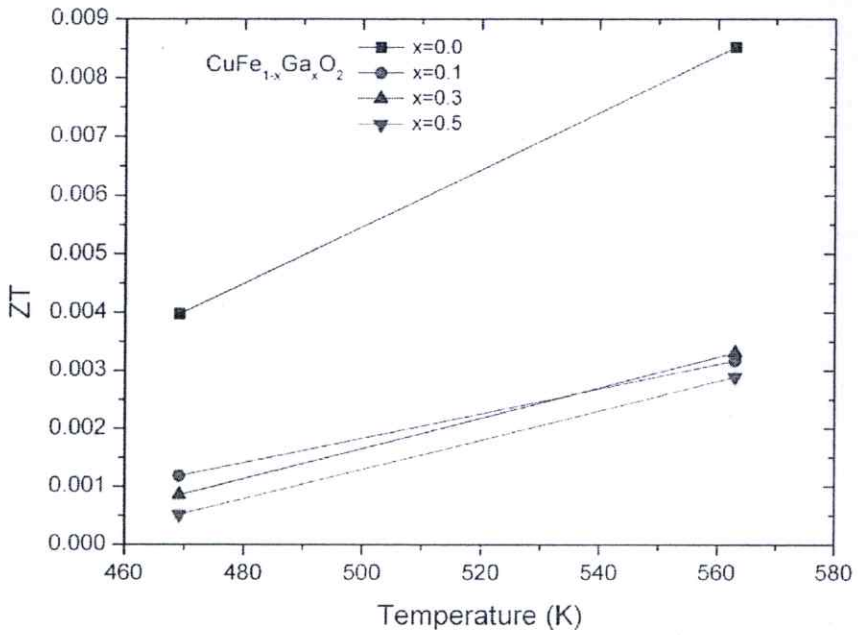

Figure 4.44 Dimensionless Figure of Merit (ZT) of the $CuFe_{1-x}Ga_xO_2$ (x=0.1, 0.3 and 0.5)

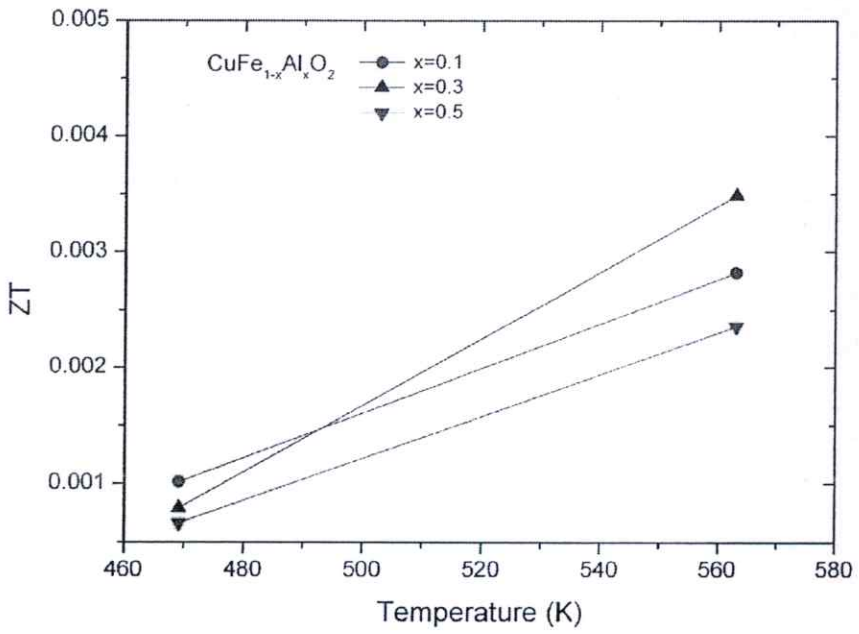

Figure 4.45 Dimensionless Figure of Merit (ZT) of the $CuFe_{1-x}Al_xO_2$ (x=0.1, 0.3 and 0.5)

Chapter 5

Conclusion and Suggestion

5.1 Conclusion

1. The structure all samples characterize by X-ray Diffraction (XRD), the results show delafossite structure in accordance JCPDS 39-0246. And not found impurity phase or remaining starting material.

2. The element all samples characterize by Energy Dispersive X-ray Spectroscopy (EDX), the results show element purposes.

   2.1 In case Ga series

   The energy dispersive x-ray spectroscopy results of Ga each x contents (0.1, 0.3 and 0.5) all samples show oxygen exceed 8-9%, iron 100%, 94% and 95%, copper 91%, 90% and 89%, gallium 100%, 93% and 90% at x=0.1, 0.3 and 0.5 respectively.

   2.2In case Al series

   The energy dispersive x-ray spectroscopy results of Al each x contents (0.1, 0.3 and 0.5) all sample show oxygen exceed 7-8%, iron 102%, 136% and 135%, copper 85%, 70% and 68%, aluminum 70%, 97% and 108% at x=0.1, 0.3 and 0.5 respectively.

3. The thermal conductivity decreased with increasing Ga or Al content and temperature.

   3.1 Incase Ga series

   The thermal conductivity of the sample decreases with increasing Ga content and temperature. The lowest of thermal conductivity was $CuFe_{0.5}Ga_{0.5}O_2$ (2.5 W/mK) at 573 K.

3.2 Incase Al series

The thermal conductivity of the sample decreases with increasing Al content and temperature. The lowest of thermal conductivity was $CuFe_{0.5}Al_{0.5}O_2$ (2.75 W/mK) at 573 K.

4. The Seebeck coefficient increased with Ga or Al content increases and decreases with temperature increasing.

4.1 Incase Ga series

The Seebeck coefficient of the sample increases with increasing of Ga content and decreases with temperature increasing. Higher of this series is $CuFe_{0.5}Ga_{0.5}O_2$ (578 μV/K) at 469 K.

4.2 Incase Al series

The Seebeck coefficient of the sample increases with increasing of Al content and decreases with temperature increasing. Higher of this series is $CuFe_{0.5}Al_{0.5}O_2$ (498 μV/K) at 469 K.

5. The electrical conductivity decreased with Ga or Al increases and increases with temperature increasing.

5.1 Incase Ga series

The electrical conductivity of the sample decreased with increasing of Ga content and increases with temperature increasing. Higher of this series is $CuFe_{0.9}Ga_{0.1}O_2$ (677 $\Omega^{-1}m^{-1}$) at 849 K.

5.2 Incase Al series

The electrical conductivity of the sample decreased with increasing of Al content and increases with temperature increasing. Higher of this series is $CuFe_{0.9}Al_{0.1}O_2$ (875 $\Omega^{-1}m^{-1}$) at 849 K.

6. The power factor

6.1 Incase Ga series

The power factor of the sample decreased with increasing of Ga content and increases with temperature increasing. Higher of this series is $CuFe_{0.9}Ga_{0.1}O_2$ ($0.87x10^{-4}$ W/mK^2) at 849 K.

6.2 Incase Al series

The electrical conductivity of the sample decreased with increasing of Al content and increases with temperature increasing. Higher of this series is $CuFe_{0.9}Al_{0.1}O_2$ ($1.1x10^{-4}$ W/mK^2) at 849 K.

7. Dimensionless Figure of Merit (ZT)

7.1 Incase Ga series

The Dimensionless Figure of Merit of the sample decreased with increasing of Ga content and increases with temperature increasing. Higher of this series is $CuFe_{0.7}Ga_{0.3}O_2$ ($33x10^{-4}$) at 536 K.

7.2 Incase Al series

The Dimensionless Figure of Merit of the sample decreased with increasing of Al content and increases with temperature increasing. Higher of this series is $CuFe_{0.7}Al_{0.3}O_2$ ($1.1x10^{-4}$) at 536 K.

5.2 Suggestion

1. The thermal conductivity measurement over a temperature range of 300-573 K, ought to measure over this (estimate 1000 K). Because in the high temperature umklapp process is mains reduce thermal conductivity, expected the thermal conductivity must to low.
2. Refer the thermal conductivity measurement results, shall selected new element for reduce thermal conductivity by increases atomic mass,

because effect of atomic mass over atomic radius. Although theory effect of atomic radius affect to thermal conductivity but at high temperature atomic mass more effect.

References

1. Taylor David Sparks, Harvard Uni 2012, Oxide Thermoelectric: The role of crystal structure on thermo power in strongly correlated spinals, Massachusetts.
2. Hubbert, M.K. (1956) Nuclear Energy and the Fossil Fuels. Spring Meeting of the Southern District, American Petroleum Institute, Plaza Hotel, San Antonio, Texas.
3. U.S. Energy Information Administration Annual Energy Outlook 2011 with Projections to 2035. DOE/EIA-0383(2011).
4. U.S. Energy Information Administration Electric Power Monthly January 2010. DOE/EIA-0226(2010/01).
5. Lawrence Live more National Laboratory Wind turbines: In the wake of the wind. Science Daily (2011)
6. G.S. Nolas, J. Sharp, H.J. Goldsmid, Thermoelectrics, Thermoelectric, Basic principle and new material development, Springer, New York, NY, 2001.
7. Gordon B. Haxel, James B. Hedrick, and Greta J. Orri, 2002 Rare earth elements: Critical resources for high technology 2002, USGS Washington, D.C.
8. K. Park, K.Y. Ko, H.-C. Kwon, S. Nahm, 2007, Improvement in Thermoelectric Properties of $CuAlO_2$ by adding Fe_2O_3. J. Alloys and Compounds.
9. Goldsmid, H. Julian, Introduction to Thermoelectricity, Springer series in material Science 121, 2009 edition, ISBN-10 3642007155.
10. I. Terasaki, Y.Sasago, K. Uchinokura, Phys. Rev. B56 (1997) R12685.
11. R.D. Shannon, D.B. Rogers and C.T. Prewitt. Inorganic Chemistry. Volume 10, No. 4, 1971. 713-718.
12. C.T. Prewitt, R.D. Shonnon, and D.B. Rogers. Inorganic Chemistry. Volume 10, No. 4, 1971. 719-723.
13. M. Grundmann, The Physics of Semiconductor, 2 nd edn. (Springer, Berlon, 2010).
14. Masashi Hasegawa, Ikuolnagawa, Masayuki Tanaka, Ichimin Shirotani, Humihiko Takei., Thermoelectric Power of delafossite-type metallic oxide $PdCoO_2$. Solid State Communication Volume 121, Issue 4, 14 Jan 2002, Page 203-205.

15. Tohru Higuchi, Daisuke Baba, Yoshiro Yokoyama, Masashi Hasegawa, Humihiko Takei, Akiko Fukushima, Shik Shin and Takeyo Tsukamoto., Electronic Structure of Delafossite-Type Oxide $PtCoO_2$ by Resonant-Photoemission Spectroscope., Japan journal of Applied Physics, Volume 42, Part 1, Number 9A.
16. M. Lalanne, A. Barnabe, F. Mathieu and Ph. Tailhades. Synthesis and Thermostructure Studies of a $CuFe_{1-x}Cr_xO_2$ Delafossite Solid Solution with $0 \leq x \leq 1$. Inorg. Chem. 2009, 48, 6065-6071.
17. Tngram, B.J. Mason, T.O. Shahriari, D.Y Barnabe, A.Ko, D.Poeppelmeier, K.R. Chem. Mater. 2004, 16, 5616-5622.
18. Thomas, G. Nature 1997, 389, 907-908.
19. Masayuki Tanaka, Masashi Hasegawa, Thoru Hiuchi, Takeyo Tsukamoto, Yasushisa Tezuka, Shi Shin, Humihiko Takei. Origin of the metallic conductivity in PdCoO2 with delafossite structure. J, Physica B 245 (1998) 157-163.
20. Chesta. R, Aree. W, Wutthisak, P, Anucha. Y, Anek. C, Tosawat, S. Journal, Thermoelectric Properties of $Cu_{1-x}Pt_xFeO_2$ ($0.0 \leq x \leq 0.05$) delafossite-type transition oxide. Alloys and Compounds, 509, 4588-4594 (2011).
21. Kei HAYASHI, Tomohiro NOZAKI and Tsuyoshi KAJITANI. Japan J of Apply Physics Vol. 46, No.8A, 2007. Pp 5226-5229.
22. Stanley W. Angrist 1978, Direct Energy Conversion 3rd, Allyn and Bacon, Inc., 470 Atlantic: Avenue, Boston, Massachusetts.
23. Francis J. DiSalvo. www. Sciencemag.org, SCIENCE VOL 285, 30 July 1999.
24. A.F. Ioffe, Infosearch limited, London, 1957.
25. R. Bruce Gall, Nathan Ashmore, Meagen A. Marquardt, Xiaoli Tan, David P. Cann, J. Alloys Compd. 391, 261-266 (2005).
26. C.M. Bhandari, D.M. Rowe 1988, Thermal Conduction in Semiconductor, John Wiley & Sons Inc. New York, USA.
27. Terry M. Tritt, Recent Trends in Thermoelectric Materials Research III, Vol 71.
28. Heikes, R. R. & Ure, R. W. Thermoelectricity: science and engineering. (Interscience Publishers: 1961).
29. C Wood, Rep, Prog. Phys. 51(1988) 459-539. Printed in the UK.
30. J.M.Ziman, Principles of the Theory of Solids 2nd Cambridge at the university press 1972.

31. M A Wahab, Solid State Physics 2nd, Alpha Science Internation Ltd., Harrow, U.K.
32. C.M. Bhandari and D.M. Rowe, 1995. CRC Handbook of Thermoelectrics, Boca Raton, Taylor&Francies.
33. R. Berman, Thermal Conduction in Solid, Clarendon Press. Oxford 1976.
34. Slack GA 1995 New materials and performance limits for thermoelectric cooling. In: Rowe DM (ed) CRC Handbook of Thermoelectrics, CRC Press, Boca Raton.
35. T.M.Tritt, Thermoelectric Material: Principles, Structure, Properties and Applications. Elsevier Science 2002, ISBN: 0-08-043152-6, pp.1-11.
36. Charles Kittel, Herbert Kroemer 2nd 1980, W.H. Freeman and Compant, ISBN 0-7167-1088-9.
37. C. Wood, High Temperature Thermoelectric Energy Conversion-I. Theory, Energy Convers. Mgmi, Vol 24, No. 4 pp. 317-329, 1984.
38. P.G. Klemens, in Solod State Physics, vol. 7, ed. By F. Seitz, D. Turnbull (Academic, New York, 1958), p.1.
39. V. Ambegaoker, Phys. Rev. 114, 488 (1959).
40. P.G. Klemens, The Scattering of Low-Frequency Lattice Waves by Static Imperfections, 1955 pp. 1113-1128.
41. Berman, R., 1953, Advances in Physics (Phil. Mag. Suppl.), 2, 103.
42. J.A. Krumhansl and W.S. Williams. Thermoelectricity (edited by P.H. Egli), p. 77. Wiley, New York (1960).
43. R. Peierls, Ann, Physik 3, 1055 (1929).
44. J.S. Dugdale and D.K.C. MacDonald, Phys. Rev. 98, 1751 (1955).
45. G. Liebfried and E. Schlomann, Nachr. Akad. Wiss. Goettingen II Math-Physik. Kl. 2a, 71 (1954).
46. D.P. Spitzer, J.Phys. Chem.k Sol. 31, 19 (1970).
47. P.G. Klemens, Phys. Rev. 119, 507 (1960).
48. R.W. Keyes, Phys. Rev. 115, 564 (1959).
49. G.A. Slack, Solid State Phys, 34, 1 (1979).
50. J. Tavernier, C.R. Acad. Sci., Paris 24, 3427 (1959).
51. H.J. Goldsmid, Thermoelectric Refrigeration, Plenum, New York (1964).

52. Vorgelegt von, Stefan Gotzendorfer, Aus Schweinfurt. *Synthesis of Copper-Based Transparent Conductive Oxides with Delafossite Structure via Sol-Gel Processing. Wurzburg 2010.*
53. H. Hahn, C.De Lorent, Z. Anorg. Allg. Chem. 1955, 279, 281.
54. D.J. Aston, D.J. Payne, A.J.H. Green, R.G. Egdell, D.S.L. Law, J. Guo, P.A. Glans, T. Learmonth, K.E. Smith, Phys. Rev. B 2005, 72, 195115.
55. T. Okuda, N. Jufuku, S. Hidaka, N. Terada, Phys. Rev. B 2005, 72, 144403.
56. W. Dannhauser, P.A. Vaughan. J. Am. Chem. Soc. 1955, 77, 896.
57. A. P. Ramirez, R. Jager-Waldau, T. Siegrist, Phys. Rev. B 1991, 43,10461.
58. H. Haas, E. Kordes, Z. Kristallogr. 1969, 129, 259.
59. E. Mugnier, A. Barnabe, P. Tailhades, Solid State Ionics 2006, 177, 607.
60. T.-R. Zhao, M. Hasegawa, H. Takei, J. Cryst. Growth 1995, 154, 322.
61. F. A. Benko, F. P. Koffyberg, Phys. Stat. Sol. 1986, 94, 231.
62. Y. Takahashi, H. Matsushita, A. Katsui, Mater. Sci. Forum 2007, 534-536, 1081.
63. Joint Committee on Power Diffraction Standard (JCPDS), Card No. 39-0246.
64. B.D. Culity, Elements of X-Ray Diffraction 2nd, Addison-Wesley Pub Com Inc, 1978, ISBN 0-201-01174-3.
65. www.zeiss.com
66. www.netzsch.com
67. www.ulvac-riko.co.jp/en/
68. www.kratos.com
69. Joint Committee on Power Diffraction Standard (JCPDS), Card No. 77-2495.
70. Joint Committee on Power Diffraction Standard (JCPDS), Card No. 75-2361.
71. P.G. Klemens, in Solid State Physics, Vol. 7, ed. By F.Seitz, D Turnbull (Academic, New York, 1958).
72. J. Francl, W.D. Kingery, J. Am. Ceram. Soc. 37, 99 (1954).
73. T. Nozaki, K. Hayashi, T. Kajitani, J. Electron. Mater. 38 (79), 1282-1286 (2009).
74. Y. Hongaromkij, C. Rudradawong, A. Wichainchai& C. Ruttanapun, J integrated Ferroelectrics, 165: 73-80, 2015.
75. Young & Freedman, University Physics 11th ed, Addison Wesley.
76. Brain J. Ingram, Gabriela B. Gonzalez and Thomas O. Mason. J Chem. Mater, 2004, 16, 5616-5622.
77. Hong-Ying Chen, Jia-Hao Wu, J Applied Surface Science 258 (2012) 4844-4847.

Appendix

Appendix A

Publication to International Journals *Integrated Ferroelectrics*, 165:73-80, 2015

ISSN: 1058-4587 (Print)

1607-8489 (Online)

DOI: 10.1080/10584587, 2015.1062685

Title Improvement of Thermoelectric Material by Reduction Thermal Conductivity of SN-doped $CuFeO_2$ Delafossite Compound

Author Y. Hongaromkij, C. Rudradawong, A. Wichainchai & C. Ruttanapun

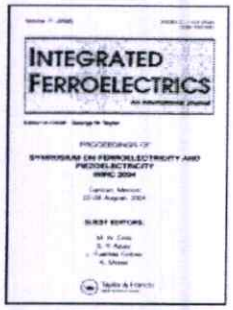

Integrated Ferroelectrics
An International Journal

ISSN: 1058-4587 (Print) 1607-8489 (Online) Journal homepage: http://www.tandfonline.com/loi/ginf20

Improvement of Thermoelectric Material by Reduction Thermal Conductivity of Sn-doped $CuFeO_2$ Delafossite Compound

Y. Hongaromkij, C. Rudradawong, A. Wichainchai & C. Ruttanapun

To cite this article: Y. Hongaromkij, C. Rudradawong, A. Wichainchai & C. Ruttanapun (2015) Improvement of Thermoelectric Material by Reduction Thermal Conductivity of Sn-doped $CuFeO_2$ Delafossite Compound, Integrated Ferroelectrics, 165:1, 73-80, DOI: 10.1080/10584587.2015.1062685

To link to this article: http://dx.doi.org/10.1080/10584587.2015.1062685

Published online: 22 Oct 2015.

Integrated Ferroelectrics, 165:73–80, 2015

ISSN: 1058-4587 print / 1607-8489 online
DOI: 10.1080/10584587.2015.1062685

Taylor & Francis
Taylor & Francis Group

Improvement of Thermoelectric Material by Reduction Thermal Conductivity of Sn-doped $CuFeO_2$ Delafossite Compound

Y. HONGAROMKIJ, C. RUDRADAWONG, A. WICHAINCHAI, AND C. RUTTANAPUN*

Department of Physics, Faculty of Science, King Mongkut's Institute of Technology Ladkrabang, Bangkok, 10520, Thailand

In this work, the polycrystalline $CuFe_{1-x}Sn_xO_2$ ($x = 0.005, 0.01, 0.03$) were synthesized by a solid state reaction method with sintering temperature at 1323K for 40 hours. The XRD pattern and TGA results showed the crystal structure of hexagonal delafossite-type structure for space group $R\bar{3}m$ *(166). Thermal conductivity was decreased because the large atomic mass of the Sn substituted to the Fe sites of $CuFeO_2$. This caused phonon scattering by the point defect of the mass difference between Sn atom and Fe atom. The minimal value of the thermal conductivity was 2.1 W/mK at 573K for Sn = 0.03.*

Keywords $CuFeO_2$; thermoelectric oxide; delafossite structure; lattice thermal conductivity; mass fluctuation

1. Introduction

The performance of thermoelectric material is related to the dimensionless figure of merit ($ZT = (S^2\sigma T)/\kappa$) that depends on Seebeck coefficient, electrical conductivity and thermal conductivity [1]. In order to, obtain a high ZT, it requires large Seebeck coefficient, high electrical conductivity and low thermal conductivity. Seebeck coefficient and electrical conductivity properties are related to charge carrier. Thermal conductivity is associated with charge carrier and phonon because of thermal transport mechanism. In semiconductor, thermal transport mechanism mainly causes more phonon than charge carrier [1]. Thus, thermoelectric material has low thermal conductivity when is composed it of heavy atomic mass such as Bi_2Te_3, Sb_2Te_3, PbTe and Mg_2Sn [2, 3].

The $CuFeO_2$ compound is classified as a semiconductor [1, 4]. It has a unit cell structure of hexagonal and a primitive cell structure of rhombohedral called delafossite structure (space group: $R\bar{3}m$) This structure is formed as alternative stacking layers of monovalent Cu^{1+} linear and trivalent Fe^{3+} octahedral along with the c- axis [4-11]. The $CuFeO_2$ interesting studies on thermoelectric material [1, 4], catalytic hydrogen production [5], magnetic [6, 7], and optical materials [8]. Moreover the $CuFeO_2$ compound is an interesting thermoelectric material because it is inexpensive and non-toxic appropriated for

Received December 22, 2014; in final form May 22, 2015.
*Corresponding author. E-mail: chesta.ruttanapun@gmail.com, krchesta@kmitl.ac.th
Color versions of one or more of the figures in the article can be found online at www.tandfonline.com/ginf.

industry. In this work, the $CuFeO_2$ compound was doped by SnO_2 in contents of 0.5%, 1% and 3%. The effect was investigated on crystal structure and thermal conductivity.

2. Experimental Details

Polycrystalline bulks of $CuFe_{1-x}Sn_xO_2$ (x = 0.005, 0.01 and 0.03) compound were prepared by solid state reaction method, according to the following equation (1). High purity power of starting material, CuO (99%), Fe_2O_3 (99%) and SnO_2 (99%) was mixed and ground in an agate mortar for an hour for being homogeneous. The mixed powder was pressed into a pellet of the 12 mm in diameter and of 2 mm in thick and sintered at 1323K in air atmosphere for 20 hours. Then, the sintered samples were rapidly quenched at the room temperature. The samples were reproduced using the same procedures of grinding, pelleting and sintering 2 times.

$$2CuO + (1 - x)Fe_2O_3 + 2(x)SnO_2 \rightarrow 2CuFe_{(1-x)}Sn_{(x)}O_2 + 1/2O_2 \quad (1)$$

Crystal structure phases of the sample were characterized by the X-ray diffractrometer (XRD) of the Bruker, D8 Advance, with the diffraction intensities in the range of $2\theta = 10^{\circ} - 80^{\circ}$ degree using stepping interval of 0.02°. Lattice parameters were calculated from the plan indexing of XRD peaks according to the equation (2).

$$\frac{1}{d^2} = \frac{4}{3}\left(\frac{h^2 + hk + l^2}{a}\right) + \frac{l^2}{c^2} \quad (2)$$

Morphology of the samples was observed using a scanning electron microscope (SEM) of the Zeiss, EVO MA10. Thermo Gravimetric Analysis (TGA) technique was used for thermal analysis in the temperature range of 325 Kto 1373K in air atmosphere using the NETZSCH STA 449F3 Jupiter. The thermal conductivity was evaluated in the range of 298 K to 573 K based on the method of the laser flash analyzer of the NETZSCH LFA 447 Nano-Flash.

3. Results and Discussion

The XRD patterns of the $CuFe_{1-x}Sn_xO_2$ (x = 0.005, 0.01 and 0.03) samples are shown in Fig. 1. All major peaks were presented the characteristic to the delafossite structure with space group $R\bar{3}m$ relating to the reference JCPDS 39-0246. This confirmed that the $CuFe_{1-x}Sn_xO_2$ samples form phased of the delafossite structure. Impurity peak of Fe_3O_4 was found in a small amount for all samples as corresponding to the reference JCPDS 19-0629.

According to the equation (2), the lattice parameters: *a* and *c* of the $CuFe_{1-x}Sn_xO_2$ samples were calculated as show in the Table 1. The results demonstrate that the change in *a* parameter for all samples when Sn content increasing is minute while the charge in the *c* parameter is large. This implies that the Sn substitution in $CuFeO_2$ distorts the structure in the Z direct. From the XRD results, the broad peaks were raised from the crystal imperfection and the distortion. This affects the lattice strain. The relation for the lattice strain with the peak indexing of XRD results was given by the Williamson- Hall equation expression as:

$$\beta_{hkl}\cos\theta = \frac{K\lambda}{D} + 4\varepsilon\sin\theta \quad (3)$$

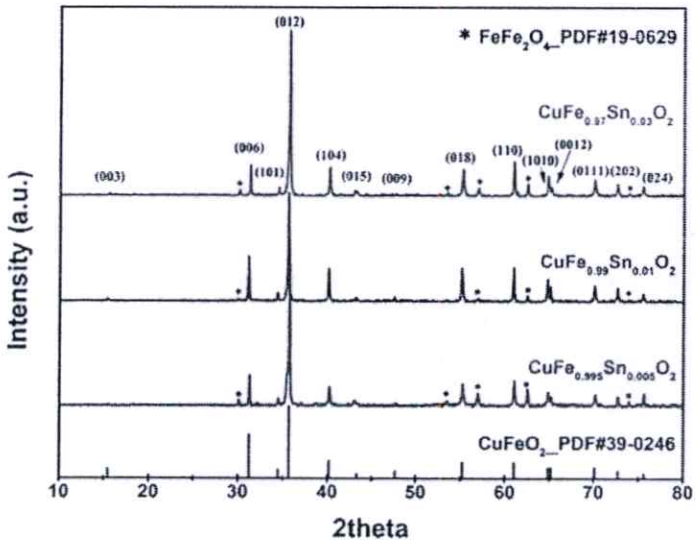

Figure 1. XRD patterns of the $CuFe_{1-x}Sn_xO_2$ (x = 0.005, 0.01 and 0.03) samples.

where β_{hkl}, D, ε, λ, θ and K are the full width at half maximum (FWHM) intensity of the diffraction peak, the sample grain size, the micro lattice strain, the wavelength of CuK_α, the angle and the Scherrer constant, respectively [12]. The results of ε is shown in Table 1. The values of sample grain size were observed from the SEM image. Fig. 2 shows the morphology from SEM of the $CuFe_{1-x}Sn_xO_2$ samples and the approximated value of grain boundaries were displayed in the Table 1. The results shown that the sizes of grain boundaries of the sample were increased with x increase from x = 0 to 0.01, while x = 0.03, the sizes of grain boundaries were decreased with x increase. This implied that the effect of lattice stain was impact in range of the Sn content from 0 to 0.01.

Fig. 3 shows the TGA results of all samples. The results showed that the total%mass of all samples increases from 700K to 1300K and then it drops sharply between 1300 K to 1330 K. This is unique of $CuFeO_2$ because the melting point of $CuFeO_2$ is at 1363K. The increase of%mass was caused by the O_2 absorption from ambient environment. The results implied that the sample at lower temperature, less than 700K, was not suffered from the O_2 absorption.

Fig. 4 shows the total thermal conductivity (κ) of the $CuFe_{1-x}Sn_xO_2$ (x = 0.005, 0.01 and 0.03) samples. The results of κ decrease when Sn and temperature increase. In

Table 1
Crystal properties of the $CuFe_{1-x}Sn_xO_2$ (x = 0.005, 0.01 and 0.03) samples

	Lattice parameter (Å)		Volume cell	Grain size	
$CuFe_{1-x}Sn_xO_2$	a	c	(Å^3)	(μm)	Lattice strain
x = 0.000[1]	3.0300	17.1400	136.28	5	0.00046
x = 0.005	3.0342	17.1876	137.03	10	0.0017
x = 0.010	3.0360	17.2603	137.78	14	0.0007
x = 0.030	3.0379	17.1936	137.41	6	0.0012

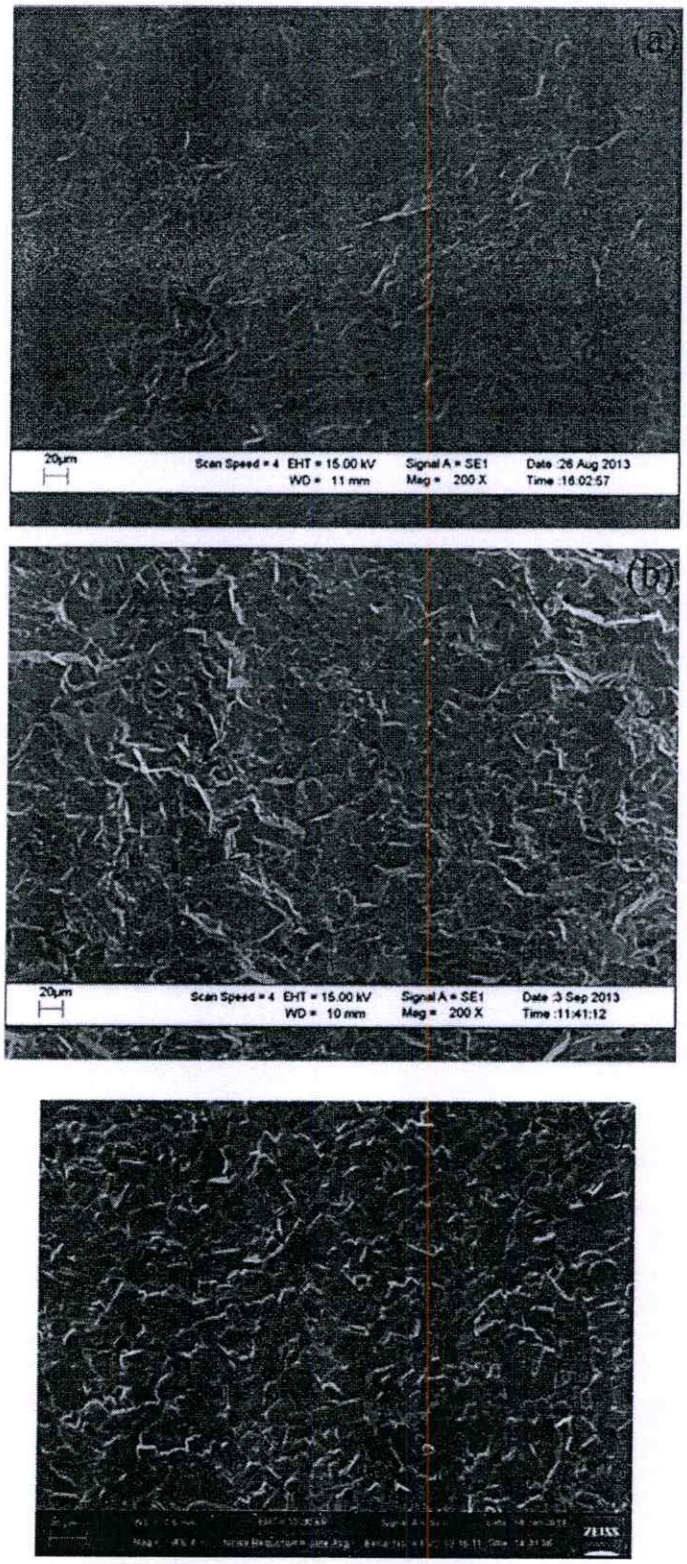

Figure 2. Image SEM of the $CuFe_{1-x}Sn_xO_2$ (a) x = 0.005 (b) 0.01 and (c) 0.03 samples.

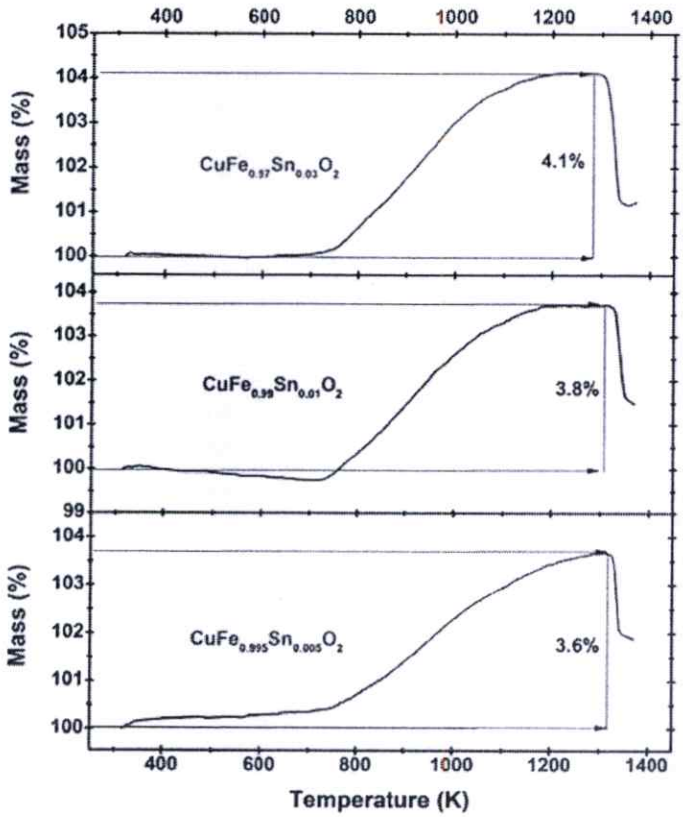

Figure 3. TGA analysis of the $CuFe_{1-x}Sn_xO_2$ (x = 0.005, 0.010 and 0.030) samples.

general, this κ is consisted of the thermal conductivity from electronic charge (κ_e) and thermal conductivity from phonon (κ_l). The κ_e is estimated from the Wiedemann-Franz law [1]. The κ_l is calculated from the relation of $\kappa_l = \kappa - \kappa_e$. Fig. 5 shows the electronic and the phonon thermal conductivity. The κ_e values of the $CuFe_{1-x}Sn_xO_2$ were lower than 0.03 W/mK. This implied that the major part of κ was controlled by the phonon mechanism. Totally, the κ_l values of the $CuFe_{1-x}Sn_xO_2$ samples were decreased when Sn content increased. The reduction of the κ value was caused by point defect, which is the effect on phonon-impurity scattering. It is caused from the Sn substitution for Fe sites in the structure due to the difference of the atomic radius and the mass of Sn^{4+} (0.69Å, 118.71 amu) and Fe^{3+} (0.645Å, 55.84 amu). The minimum κ_l value was 2.1 W/mK for x = 0.03 at 573K.

Nozaki et al. [13] assumed the cross-section of phonon scattering (Γ) as consisting of $\Gamma = \Gamma_m + \Gamma_s$, where Γ_m and Γ_s are the cross-section due to mass difference and bond length difference, respectively.

The relation of the Γ_m and Γ_s is shown below:

$$\Gamma_m = x(x-1)\left[\frac{M_1 - M_2}{xM_1 + (1-x)M_2}\right]^2, \quad \Gamma_s = x(x-1)(\beta)\left[\frac{\delta_1 - \delta_2}{x\delta_1 + (1-x)\delta_2}\right]^2, \quad (4)$$

where M_1, M_2, δ_1, δ_2 are the atomic mass and radius of the Fe and Sn, respectively, and β is the strain parameter equal 39. The results of Γ_m and Γ_s are shown in the Table 2. The values of the Γ_m were higher than the values of the Γ_s. This implied that the scattering of

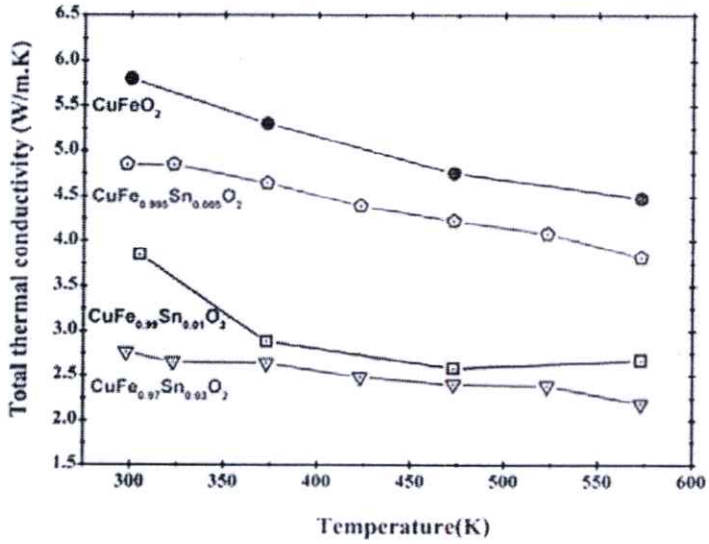

Figure 4. Total thermal conductivity of the $CuFe_{1-x}Sn_xO_2$ (x = 0.005, 0.010 and 0.030) samples.

lattice phonon causing by point effect was strongly controlled by the mass difference and weakly depended on the bond length difference. These results were corresponded with the lattice thermal conductivity (κ_l) by Keyes's relation [14] as written by equation (5)

$$\kappa_l = B\left(\frac{T_m^{3/2}\rho^{2/3}}{M^{7/6}}\right)\frac{1}{T},\ B = \frac{R^{3/2}}{(3\gamma^2 E^3 N_o^{1/3})} \tag{5}$$

where B is the proportionality constant, T_m is the melting point of temperature, M is the average atomic mass, ρ is the density of material, T is the temperature, γ is the Grüneisen constant, E is the fractional amplitude of inter-atomic thermal vibration, R is the gas constant, N_o is Avogadro number. This relation described that the κ_l can be reduced by the large M and high T. Thus, this experiment can be summarized that the large atomic mass of Sn substitution for Fe sites caused to reduce thermal conductivity for $CuFe_{1-x}Sn_xO_2$ affecting from the major part of the mass fluctuation.

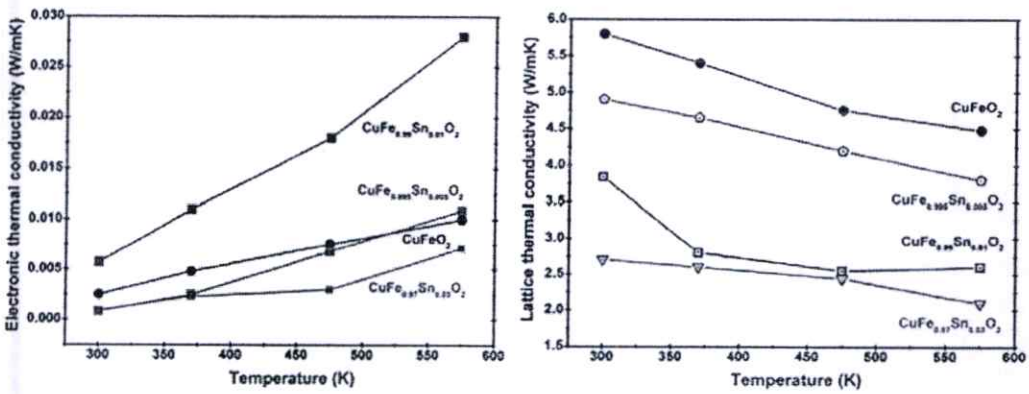

Figure 5. Electronic and lattice thermal conductivity of the $CuFe_{1-x}Sn_xO_2$ (x = 0.005, 0.010 and 0.030) samples.

Table 2
Cross-section of phonon scattering due to mass difference (Γ_m) and lattice strain (Γ_s)

$CuFe_{1-x}Sn_xO_2$	Γ_m	Γ_s
$x = 0.000$	0	-
$x = 0.005$	0.0062	0.0019
$x = 0.010$	0.0123	0.0039
$x = 0.030$	0.0345	0.0115

4. Conclusions

The polycrystalline $CuFe_{1-x}Sn_xO_2$ ($x = 0.005, 0.01, 0.03$) were synthesized by a solid state reaction method. The XRD pattern confirmed the crystal structure of hexagonal delafossite-type structure. And abrupt weight loss of TGA was observed at the temperature above 1323K indicating the forming phase of the $CuFeO_2$. The SEM image displayed the grain size of more than 5 μm. The thermal conductivity was reduced by the large atomic mass of Sn doped into the $CuFeO_2$. Thermal transport was a major effect from phonon scattering part of the point defect by the mass difference part. Totally, thermal conductivity was decreased from 5.8 to 4.5 W/mK at the temperature from 298 to 573K, and the minimum thermal conductivity was 2.1 W/mK at 573K for Sn = 0.03.

Funding

Financial support was provided by a grant from the KMITL Research Fund of King Mongkut's Institute of Technology Ladkrabang, Ministry of Education, Thailand. C. Ruttanapun would like to acknowledge the Thailand Research Fund (TRF) and King Mongkut's Institute of Technology Ladkrabang (KMITL) (Contract Number: TRG5880013) for financial support.

References

1. C. Ruttanapun, A. Wichainchai, W. Prachamon, A. Yangthaisong, A. Charoenphakdee, and T. Seetawan, *J. Alloy. Comp.*, **509**, 4588–4594 (2011).
2. G. Jiang and J. He, *Adv. Funct. Mater.*, **24**, 3776–3781 (2014).
3. P. Zhu and Y. Imai, *Materials Transactions.*, **45**, 3102–3105 (2004).
4. T. Nozaki, K. Hayashi, and T. Kajitani, *J. Chem. Eng. Jpn.*, **40**, 1205–1209 (2007).
5. M. Younsi, A. Aider, A. Bouguelia, and M. Trari, *Sol. Energy.*, **78**, 574–580 (2005).
6. O. A. Petrenko, G. Balakrishnan, M. R. Lees, D. M. Paul, and A. Hoser, *Phys Rev B.*, **62**, 8983–8988 (2000).
7. S. Yamanaka, H. Kobayashi, and K. Kurosaki, *J Alloy Comp.*, **349**, 321–324 (2003).
8. C. Ruttanapun, B. Boonchom, N. Vittayakorn, A. Harnwunggmoung and A. Charoenphakdee, *Ferroelectrics*, **453** 75–83 (2013).
9. C. Ruttanapun, P. Jindajitawat, P. Buranasiri, D. Naenkieng, N. Boonyopakorn, A. Harnwunggmoung, W. Thowladda, W. Neeyakorn, C. Thanachayanont, and A. Charoenphakdee, *Integrated Ferroelectrics*, **156** 102–114, (2014).
10. C. Ruttanapun, *J. Solid State Chem.*, **215**. 43–49 (2014).

11. C. Ruttanapun, P. Jindajitawat, P. Buranasiri, A. Harnwunggmoung, A. Charoenphakdee, and V. Amornkitbamrung, (2015), *Journal of the American Ceramic Society*, **98**, 437–442, (2015).
12. A. K. Zak and W. H. Majid, *Solid State Sci.*, **13**, 251–256 (2011).
13. T. Nozaki, K. Hayashi, and T. Kajitani, *J Elec Mat.*, **39**, 1798–1802 (2010).
14. R.W. Keyes, *J. Phys Rev.*, **115**, 564–567 (1959).

Appendix B

Publication to International Journals	*Journal of Materials Science: Material in Electronics*, June 2016, Volume 27, Issue 6, pp 6438-6444
	ISSN: 0957-4522 (Print version)
	ISSN 1573-482X (Electronic version)
	DOI: 10.1007/s10854-016-4583-5
Title	Effect of *Ga*-substitution for *Fe* sites of delafossite $CuFe_{1-x}Ga_xO_2$ (x=0.0, 0.1, 0.3, 0.5) on thermal conductivity
Author	Yuttana Hongaromkij, Chalermpol Rudradawong & Chesta Ruttanapun

Effect of Ga-substitution for Fe sites of delafossite $CuFe_{1-x}Ga_xO_2$ (x = 0.0, 0.1, 0.3, 0.5) on thermal conductivity

Yuttana Hongaromkij, Chalermpol Rudradawong & Chesta Ruttanapun

Journal of Materials Science: Materials in Electronics

ISSN 0957-4522

J Mater Sci: Mater Electron
DOI 10.1007/s10854-016-4583-5

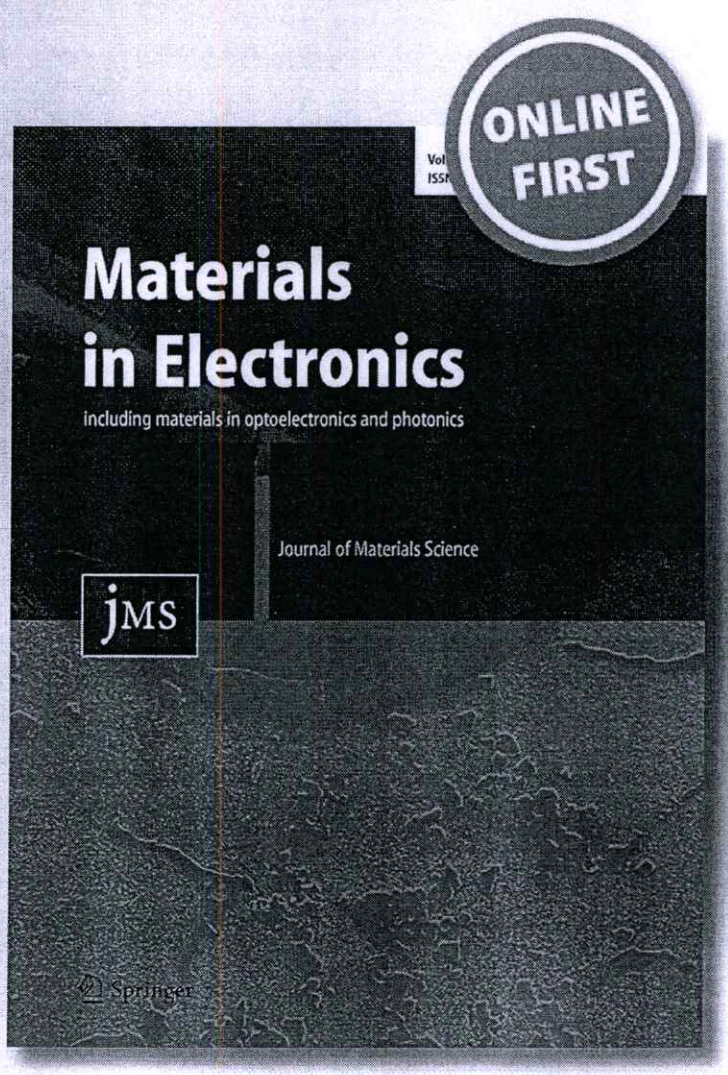

Springer

J Mater Sci: Mater Electron
DOI 10.1007/s10854-016-4583-5

Effect of Ga-substitution for Fe sites of delafossite $CuFe_{1-x}Ga_xO_2$ (x = 0.0, 0.1, 0.3, 0.5) on thermal conductivity

Yuttana Hongaromkij[1] · Chalermpol Rudradawong[1] · Chesta Ruttanapun[1]

Received: 14 January 2016 / Accepted: 23 February 2016

Abstract This work aimed to study the effect of the Ga^{3+}-substitution of Fe^{3+} sites in $CuFeO_2$ delafossite on its thermal conductivity. $CuFe_{1-x}Ga_xO_2$ (x = 0, 0.1, 0.3, and 0.5) samples were synthesized and their phase structure and ionic composition were characterized by X-ray diffraction (XRD), energy dispersive X-ray spectroscopy (EDX) and X-ray photoelectron spectroscopy (XPS). The thermal conductivity of the samples was measured at a high temperature range of 298–573 K. The XRD results confirmed that the samples were pure phase delafossite with hexagonal structure space group: $R\bar{3}m$ while the EDX results showed composition atomic percent of Ga 100 % of x = 0.1, 93 % of x = 0.3 and 90 % of x = 0.5 and the XPS results revealed Cu^{1+} and Cu^{2+}, Fe^{2+} and Fe^{3+}, and Ga^{3+} ion states in the structure. The Ga-substitution decreased the thermal conductivity of the samples below that of non-doped $CuFeO_2$. The high substitution sample (x = 0.5) exhibited the lowest thermal conductivity, 2.5 W/mK at 573 K. Ga substitution into Fe sites affected the lattice thermal conductivity partly through phonon scattering processes arising from mass difference and lattice strain.

1 Introduction

Typical delafossite-type oxides have the chemical formula ABO_2, in which A = Cu, Pt, Pd, Ag and B = Cr, Fe, Al, Co, Ga, and so on [1, 2]. The unit cell of this structure is hexagonal; the oxygen atoms are bonded to the A site atoms in a dumbbell configuration and the edge sharing layer B atoms are octahedrally configured as BO_6 [3]. The advantages of this material structure are its low toxicity and low cost, and it can be used to convert thermal energy into electrical energy (thermoelectric effect). The efficiency of a thermoelectric material depends on its figure of merit (Z),

$$Z = \frac{S^2\sigma}{\kappa},$$

where S is its Seebeck coefficient, σ is its electrical conductivity, and κ is its thermal conductivity. κ is the sum of the contribution of electrons to the thermal conductivity, κ_e, and the contribution of phonons to the thermal conductivity, κ_l. The two parameters (S and σ) are inversely proportional. If the Seebeck coefficient is large, the electrical conductivity will be small. The electron thermal conductivity depends on the electrical conductivity. The only parameter used to calculate the figure of merit that does not relate to the other parameters is the phonon thermal conductivity, which is independent of the carrier. To improve thermoelectric properties of the delafossite compounds, their thermal conductivity can be reduced by decreasing the amount of phonons.

According to the work of Gall et al. [4], $CuGaO_2$ exhibits a Seebeck coefficient of 780 μV/K and electrical conductivity of 0.0033 S/cm. From the work of Ruttanapun et al. [5], $CuFeO_2$ exhibits a Seebeck coefficient of 260 μV/K and electrical conductivity of 3.5 S/cm. These two works suggest that substitution with Ga will give a higher Seebeck coefficient than that obtainable with Fe.

In this study, gallium (Ga) was chosen to substitute into the B-site of $CuFeO_2$ to provide a high Seebeck coefficient. We expect that an increased Seebeck coefficient caused by gallium substitution will improve the thermoelectric

✉ Chesta Ruttanapun
chesta.ruttanapun@gmail.com; chesta.ru@kmitl.ac.th

[1] Department of Physics, Faculty of Science, King Mongkut's Institute of Technology Ladkrabang, Chalongkrung Road, Ladkrabang, Bangkok 10520, Thailand

Published online: 05 March 2016

properties of $CuFeO_2$ by reducing its thermal conductivity. Nozaki et al. [6] reported that $CuFe_{0.5}Mn_{0.5}O_2$ delafossite shows the lowest thermal conductivity at room temperature, 2.28 W/mK, owing to its mixed-structure of $R\bar{3}m$ and $C2/m$. To the best our knowledge, however, there have been no reports on the thermal conductivity of $CuFe_{0.5}Ga_{0.5}O_2$ delafossite. Therefore, in this paper, $CuFe_{1-x}Ga_xO_2$ with x = 0.0, 0.1, 0.3, and 0.5 was prepared to investigate the effect of Ga^{3+} substitution for Fe^{3+} sites on the thermal properties of $CuFeO_2$.

2 Experimental details

Polycrystalline samples of $CuFe_{1-x}Ga_xO_2$ (x = 0.0, 0.1, 0.3, and 0.5) were prepared via solid state reaction in argon atmosphere. The starting materials CuO (≥99 %, Sigma-Aldrich), Fe_2O_3 (≥99 %, Sigma-Aldrich), and Ga_2O_3 (≥99.99 %, Sigma-Aldrich) were weighed out to follow the equation

$$2CuO + (1 - x)Fe_2O_3 + (x)Ga_2O_3 \rightarrow 2CuFe_{(1-x)}Ga_{(x)}O_2 + 1/2O_2.$$

then mixed and ground in an agate mortar. The mixture was then pressed into a pellet of 12-mm diameter and 2–3-mm thickness, and the pellet was sintered in an alumina cup furnace at 1050 °C under an argon gas atmosphere for 20 h. Samples were reproduced using the same procedures of grinding, pelleting, and sintering 2 time. The crystal phase of the samples was analyzed by powder X-ray diffraction (XRD) using a BrukerD8 Advance instrument (X-ray source $\lambda CuK\alpha = 1.5406$ Å, $2\theta = 10$–$80°$, step = 0.02°). The composition of the sample was confirmed by energy dispersive X-ray spectroscopy (EDX). Binding energies were characterized by X-ray photoelectron spectroscopy (XPS) using a Kratos Model Axis Ultra DLD. A Zeiss EVO MA10 scanning electron microscope (SEM) was used to observe the morphology of the samples. Thermal characterizations were carried out on flat samples of approximately 12-mm diameter and 2–3-mm thickness using a NETZSCH LFA 477 Nano-Flash thermal diffusivity analyzer. The electrical resistance of the samples was measured at room temperature with a KEITHLEY 2001 multi-meter.

3 Results and discussion

3.1 Material characterization

The material was tested using X-ray diffraction instrument and the x content was varied from 0.0 to 0.5. The X-ray diffraction patterns of all of the fabricated samples are shown in Fig. 1. All of the patterns exhibited the peaks of delafossite with space group $R\bar{3}m$ (166), in accordance with JCPDS 39-0246 [7]. No peaks corresponding to impurity phases or remaining starting material were found, confirming that pure phase delafossite was formed. All XRD peaks were shifted when the x component increased. This happens were resulted from the substitution of gallium into iron sites as causing for the BO_6 octahedral to shrink, which resulted in a decrease in edge length (a-axis decrease) owing to the smaller ionic radius of Ga^{3+} (0.625 Å) as compared with that of Fe^{3+} (0.645 Å) [8]. Moreover, the length of the c-axis decreased due to the shrink of the bond length of the O–A–O layers and the BO_6 octahedral layers became slightly edge distorted [3, 8]. This means that the lattice parameters a and c of $CuFe_{1-x}Ga_xO_2$ decreased with increasing x content [1, 9] as shown in Fig. 2. Therefore, when x component increases, all XRD peaks are shifted or the angle of diffraction increases. Figure 3 shows that the main peak (0 1 2) shifted from 35.84° to 35.96° as the x content increased from 0.0 to 0.5. This was caused by the shortening of the distance between the adjacent (012) planes [10, 11] and the particle size which was calculated by the Scherrer equation of $Size = \frac{0.94\lambda}{\cos\theta\beta_{1/2}}$ as 43 nm (x = 0), 43 nm (x = 0.1), 44 nm (x = 0.3) and 45 nm (x = 0.5). The element (O, Fe, Cu and Ga), percent weight and percent atomic were characterized by EDX. The results were shown in Fig. 4a–c. All samples show oxygen exceed 8–9 %, iron 100, 94 and 95 %, copper 91, 90 and 89 %, gallium 100, 93 and 90 % at x = 0.1, 0.3 and 0.5 respective. Both results of XRD and EDX confirmed that the samples were delafossite structure by substation gallium into iron.

Figure 5a–c shows the XPS results for the $CuFe_{1-x}Ga_xO_2$, x = 0.0, 0.1, 0.3, and 0.5, samples. Before

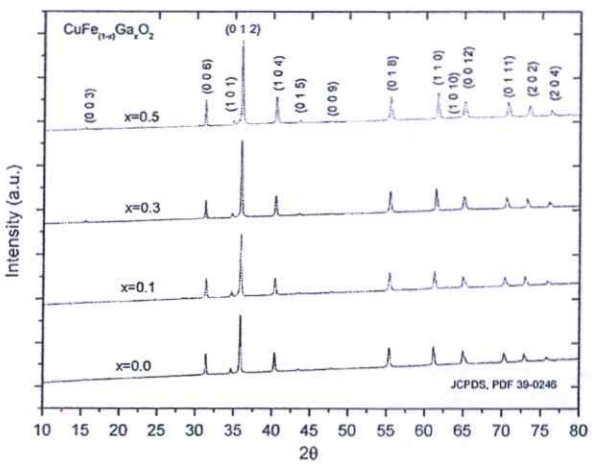

Fig. 1 The XRD pattern of the $CuFe_{(1-x)}Ga_{(x)}O_2$ (x = 0, 0.1, 0.3 and 0.5)

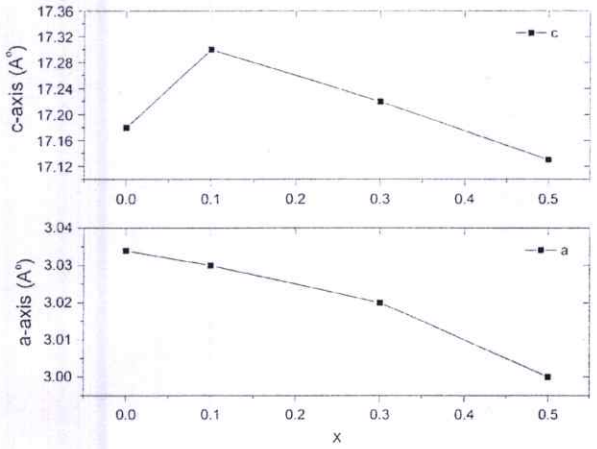

Fig. 2 Lattice parameter a-axis and c-axis functions with Ga (x = 0, 0.1, 0.3, and 0.5)

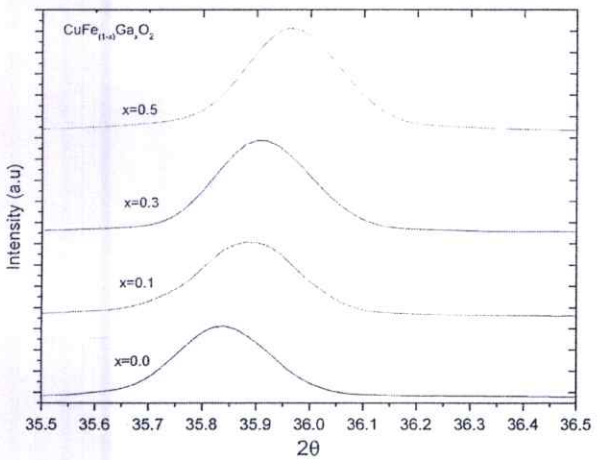

Fig. 3 Main peak (0 1 2) functions with Ga (x = 0, 0.1, 0.3, and 0.5)

characterization, all samples were etched with the mixed of hydrochloric 12 mol 4.87 mL, nitric 15 mol 1.54 mL and distill 30 mL at 70 °C for 10 min [12]. The binding energy was measured up to 1200 eV. The peaks of Fe 2*p* and Cu 2*p* of x = 0.0, 0.1, 0.3 and 0.5 were shown in Fig. 5a–c. In case of the Fe 2*p* state, the binning energy of the samples shown Fe^{2+} and Fe^{3+} ions. The binning energy between 709.8–710.4 eV corresponded to the Fe^{2+} ion and 711.1–711.6 eV corresponded to the Fe^{3+} ions, from the Refs. [12–14]. In cases of the Cu 2*p* state, the binning energy of the samples shown Cu^{1+} and Cu^{2+} ions. The binning energy between 932.5–932.8 eV corresponded to the Cu^{1+} ions and 933.9–934.3 eV corresponded to the Cu^{2+} ions, from the Refs. [12, 15, 16]. For cases of Ga 2*p*, the binding energy was observed between 1117.6–1117.8 eV as corresponding to the Ga^{3+} ions from the Ref. [17].

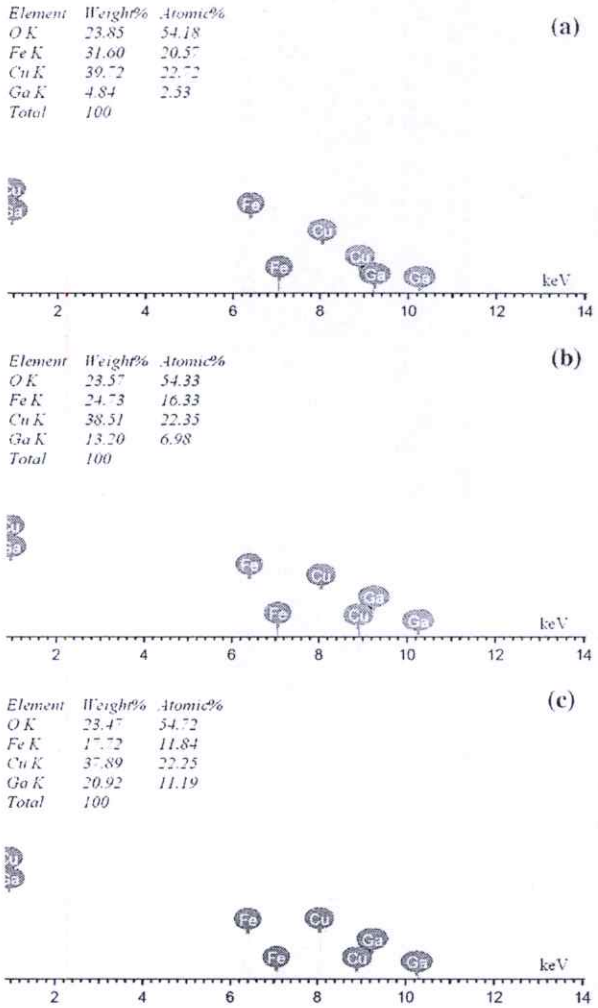

Fig. 4 **a** Energy dispersive spectroscopy of $CuFe_{(1-x)}Ga_{(x)}O_2$ (x = 0.1). **b** energy dispersive spectroscopy of $CuFe_{(1-x)}Ga_{(x)}O_2$ (x = 0.3). and **c** energy dispersive spectroscopy of the $CuFe_{(1-x)}Ga_{(x)}O_2$ (x = 0.5)

Figure 6a–d shows SEM images of the $CuFe_{1-x}Ga_xO_2$, x = 0.0, 0.1, 0.3 and 0.5 samples. The smallest grain size of the samples was approximately 5–8 μm at x = 0.5. The grain size of the x = 0.0, 0.1 and x = 0.3 samples was approximately 6–9 μm. Thus, the grain size of the x = 0.1, 0.3 and 0.5 $CuFe_{1-x}Ga_xO_2$ samples was not expected to significantly affect their thermal conductivity compared with that of $CuFeO_2$.

3.2 Thermal conductivity

Figure 7 shows the total thermal conductivity (κ) of the $CuFe_{1-x}Ga_xO_2$, x = 0.0, 0.1, 0.3, 0.5 samples as a function of temperature. The κ results were evaluated via the relation $\kappa = \alpha\rho C_p$ [14], where α, ρ and Cp are the thermal

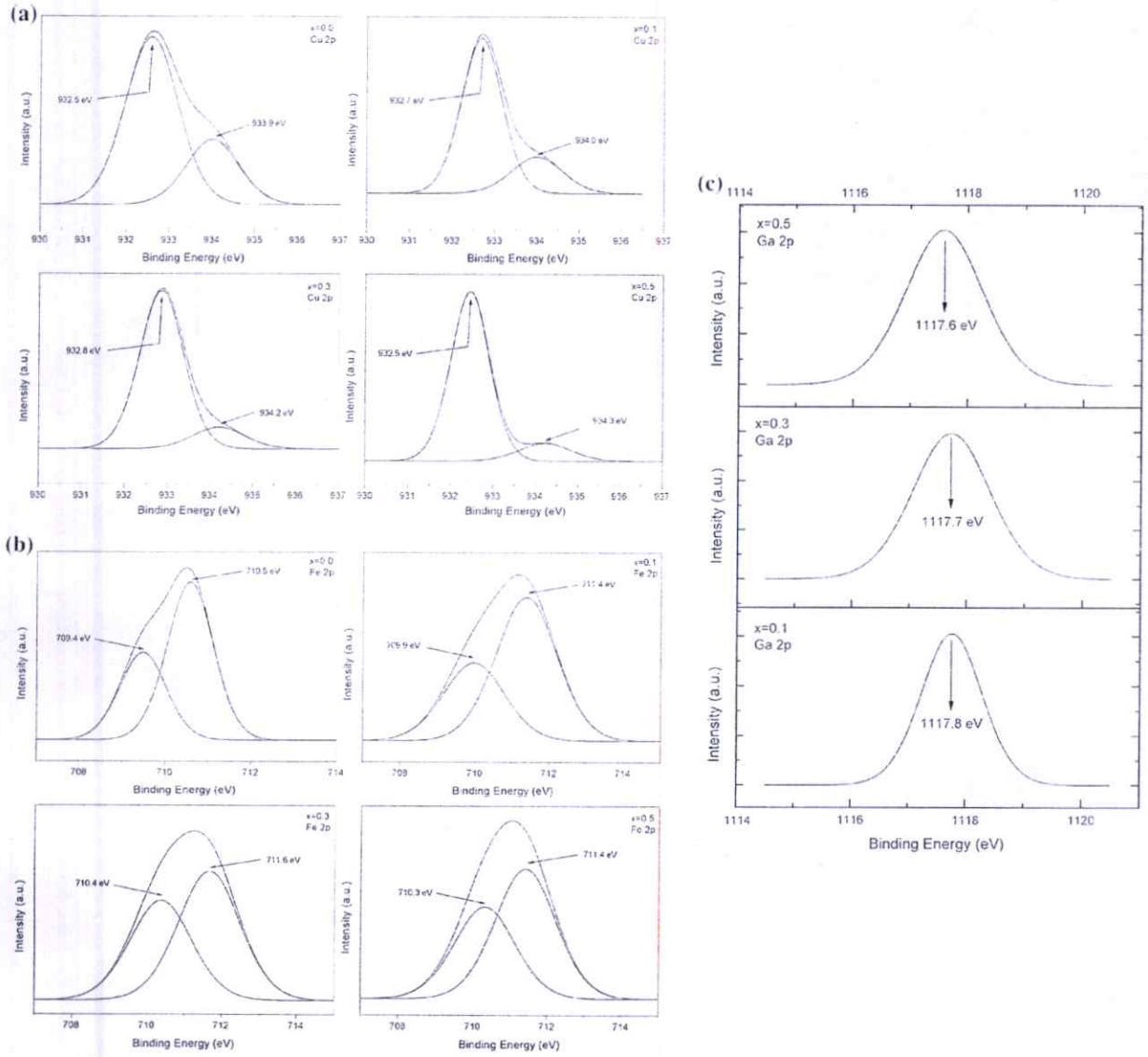

Fig. 5 **a** XPS spectrum of Cu of $CuFe_{(1-x)}Ga_{(x)}O_2$ (x = 0.0, 0.1, 0.3 and 0.5), **b** XPS spectrum of Fe of $CuFe_{(1-x)}Ga_{(x)}O_2$ (x = 0.0, 0.1, 0.3 and 0.5), and **c** XPS spectrum of Ga of $CuFe_{(1-x)}Ga_{(x)}O_2$ (x = 0.1, 0.3 and 0.5)

diffusivity, the density, and the specific heat of the sample, respectively. The values of α and Cp for the samples were obtained by thermal diffusivity measurements over a temperature range of 298–573 K. The bulk density determined by Archimedes method [18] and the % of theoretical density of $CuFe_{1-x}Ga_xO_2$ samples are shown in Table 1. All samples had densities that were estimate between 80–84 % of their theoretical density and correction thermal conductivity results by density as seen in Fig. 7. The κ of the samples decreased with increasing Ga content and temperature. $CuFe_{0.5}Ga_{0.5}O_2$ displayed the lowest κ value in this experiment. κ can be expressed as $\kappa = \kappa_l + \kappa_e$, where is the phonon component of the thermal conductivity (lattice vibration) and is the electronic component of the thermal conductivity. Next will be find case of thermal conductivity decreases because phonon component decreases, electronic component decreases or both. The resistance of the samples was measured using multimeter at room temperature for approximate the value of κ_e. The κ_e can be calculated using the Wiedmann–Franz law [5, 19] as $\kappa_e = L_0 T\sigma$, where $L_0 = 2.45 \times 10^{-8}$ (the Lorenz factor), T is the absolute temperature, σ is the electrical conductivity and results show in Table 1. The κ_e values of all of the samples were found slightly fewer by Ga constant. Therefore, the case of thermal conductivity was decreased comes from phonon component decrease with the ratio of

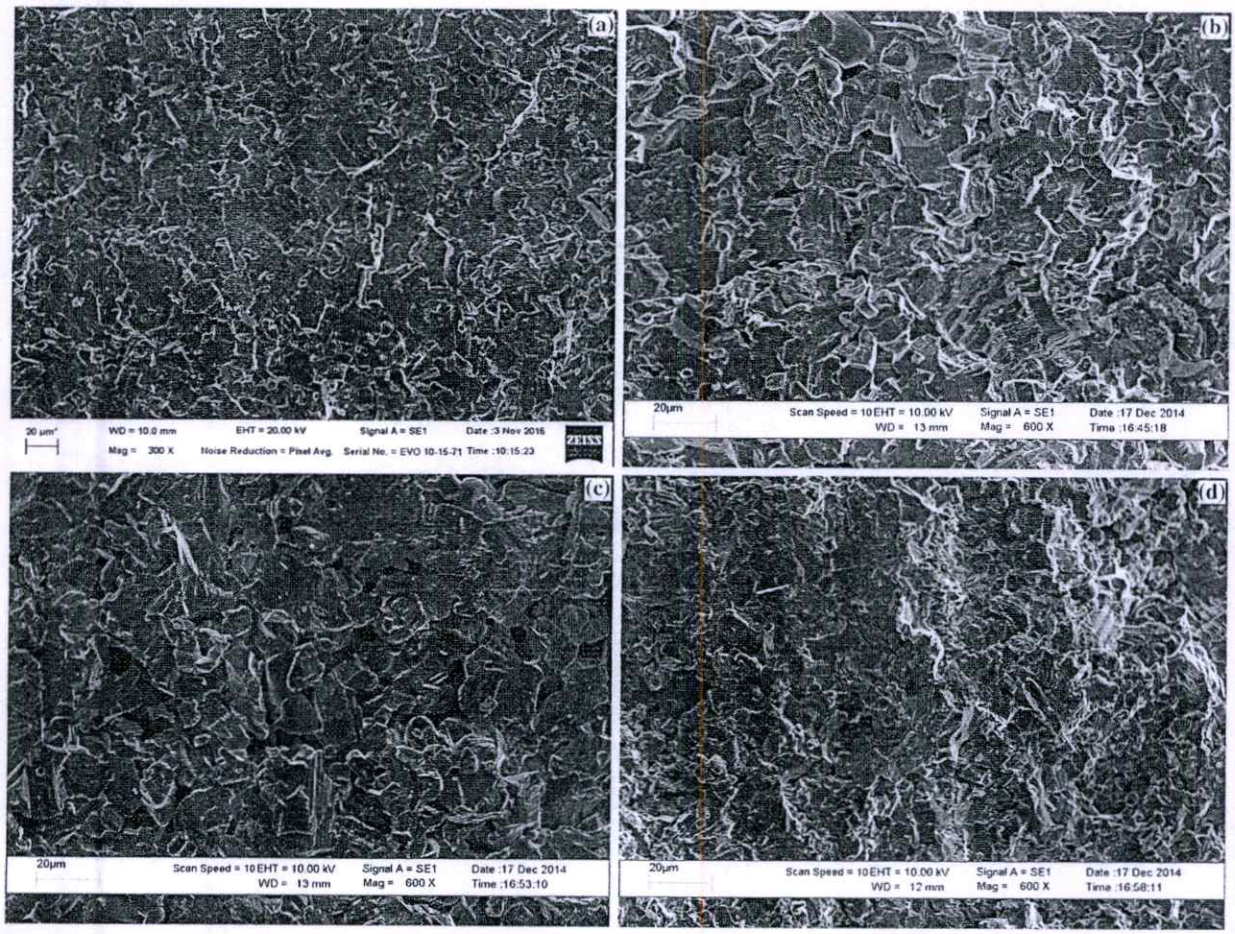

Fig. 6 **a** SEM image of $CuFeO_2$, **b** SEM image of $CuFe_{0.9}Ga_{0.1}O_2$, **c** SEM image of $CuFe_{0.7}Ga_{0.3}O_2$, and **d** SEM image of the $CuFe_{0.5}Ga_{0.5}O_2$

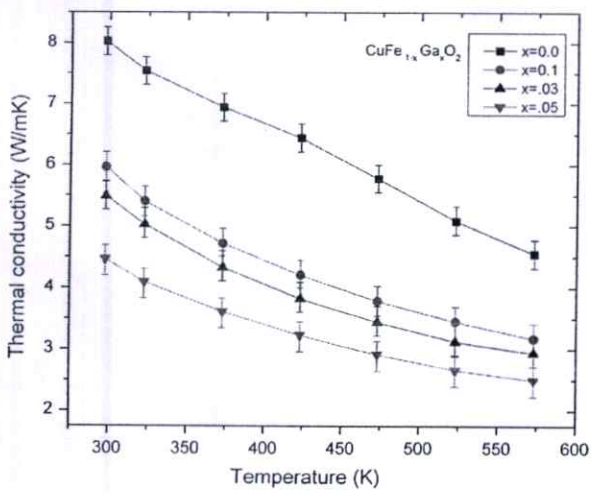

Fig. 7 Thermal conducivity of the $CuFe_{1-x}Ga_xO_2$ (x = 0.0, 0.1, 0.3 and 0.5)

Table 1 Density and thermal conductivity by electronic component of $CuFe_{1-x}Ga_xO_2$ x = 0.0, 0.1, 0.3 and 0.5

$CuFe_{(1-x)}Ga_{(x)}O_2$	Density	$\frac{\rho}{\rho_{theory}}$ (%)	$\kappa_e = L_0 T\sigma$	κ_e (%)
Ga content x				
0	4.35	79.18	0.0294	0.96
0.1	4.73	84.77	0.0216	0.82
0.3	4.83	84.49	0.0226	0.92
0.5	4.75	80.83	0.0230	1.10

electronic component per thermal conductivity around 1 %. This confirmed that the thermal conductivity of the $CuFe_{1-x}Ga_xO_2$, x = 0.1, 0.3, 0.5 samples was controlled by the phonon component [20, 21].

To determine the effect of Ga-substitution on the value of κ, the thermal resistivity (K) of the samples was cal-

culated using the general expression of $K = \frac{1}{\kappa} = (A + BT)$ [6, 19, 22–24], where K is the thermal resistivity, A and B are the phonon scattering by A as thermal resistivity by substitution impurity defect and B as intrinsic thermal resistivity and T is the absolute temperature. Figure 8 shows the K values of the $CuFe_{1-x}Ga_xO_2$, x = 0.0, 0.1, 0.3, 0.5 samples as a function of temperature. The K values for all three Ga contents were linear with temperature and increased with Ga content, indicating that the above expression for $A + BT$ was satisfied. The values of A and B were then determined by linear regression, as shown in Table 2. The value of A was found to increase with Ga content, while the B values were increases and slightly increases with Ga content increases. The A values were higher than the B values by four orders of magnitude. This indicated that the K values of the $CuFe_{1-x}Ga_xO_2$samples were governed by term A.

According to Refs. [6, 19, 23] the A term of the K relation can be approximated by

$$A = \frac{\pi^2 V 0}{3hv^2} \Sigma_i \Gamma_i.$$

where V is the average atomic volume, 0 is the Debye temperature, h is Planck's constant, and v is the velocity of sound in the sample. $\Sigma_i \Gamma_i$ is the summation of the cross section of all phonon scatting processes according [6, 22–24] to.

$$\Sigma_i \Gamma_i = \Gamma_0 + \Gamma_m + \Gamma_s.$$

where Γ_0 is the contribution from the normal defects of the non-doped sample, here $CuFeO_2$, Γ_m is the contribution from mass difference, and Γ_s is the contribution from lattice strain. The value of Γ_0 was taken as constant in all of the samples and was obtained from the thermal resistivity of the $CuFeO_2$ sample via, where, the Debye temperature

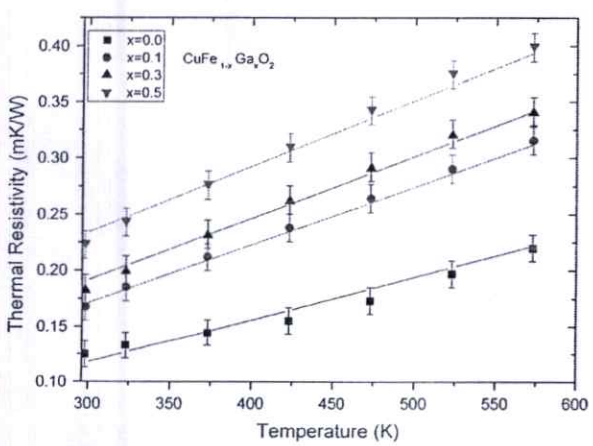

Fig. 8 Thermal resistivity of the $CuFe_{1-x}Ga_xO_2$ (x = 0, 0.1, 0.3 and 0.5)

Table 2 Value of A and B obtained from thermal resistivity data

$CuFe_{(1-x)}Ga_{(x)}O_2$	A (mK/W)	B (m/W)
Ga content x		
0	0.124	0.00036
0.1	0.171	0.00053
0.3	0.185	0.00061
0.5	0.224	0.00063

(0) is 600 K, and the average phonon velocity base Debye estimate is 7.19×10^3 m/s [6, 19, 25]. The values of Γ_m and Γ_s were obtained from $\Gamma_m = x(1-x)\left(\frac{M_I - M_{II}}{xM_I + (1-x)M_{II}}\right)^2$ and $\Gamma_s = x(1-x) \cdot \varepsilon\left(\frac{\delta_I - \delta_{II}}{x\delta_I + (1-x)\delta_{II}}\right)^2$, where M_I, M_{II} and δ_I, δ_{II} are the atomic mass of Fe (55.847) and Ga (69.732) and the atomic radius of Fe (0.645 Å) and Ga (0.625 Å) [8], respectively, and ε is a constant, given as 39 [25]. The results of the calculation of Γ_m and Γ_s are shown in Table 3.

The values of Γ_m were found to equal those of Γ_s for each of the $CuFe_{1-x}Ga_xO_2$, x = 0.1, 0.3, 0.5 samples. This implied that the A values of $CuFe_{(1-x)}Ga_{(x)}O_2$, x = 0.1, 0.3, 0.5 were controlled by half of the Γ_m and Γ_s values. Moreover, the Γ_m and Γ_s value increased with Ga content. This supported the idea that the thermal resistivity of $CuFeO_2$ can be increased by a large amount of Ga-substitution into Fe sites to enlarge both Γ_m and Γ_s. Therefore, the thermal conductivity of the $CuFe_{1-x}Ga_xO_2$, x = 0.1, 0.3, and 0.5 samples was affected by the Ga-substitution. The higher the Ga content, the lower the thermal conductivity, owing to increases in the amounts of mass difference and lattice strain causing increased phonon scattering.

To describe the phonon scattering processes arising from defects by Ga-substitution for Fe^{3+} sits, the phonon mean free path (l) is given by $l = v/A\omega^4$, where v is the velocity of phonon, ω is the phonon frequency. By assuming, the values of v and ω were constant for all x contents. The results in Table 2 showed that the A values were increased with increasing x as a results to the l values decreasing with increasing x [25–27]. This effect was

Table 3 Scattering cross-section by mass difference and lattice strain $CuFeO_2$-based

$CuFe_{(1-x)}Ga_{(x)}O_2$	Γ_m	Γ_s
Ga content x		
0	0	–
0.1	0.0037	0.0036
0.3	0.0094	0.0082
0.5	0.0122	0.0097

arisen from the difference atomic mass and the difference atomic radius of Ga and Fe atoms in the structure. To considering of the 2-D structure of $CuFeO_2$ delafosite which is O linking to Cu likely a dumbbell configuration and the edge sharing layer Fe and O likely an octahedral FeO_6 configuration, the Fe atoms occupied in middle of the octahedral FeO_6 configuration [28]. Therefore, the Ga-substitution for Fe sits caused to the distortion of the octahedral configuration with mass damping in the structure. The results contributed for mass fluctuation anharmonic, which causes from the difference atomic mass of Ga and Fe, and for lattice strain, which causes from the difference atomic radius of Ga and Fe affecting of atom arranging in the lattice. Totally, the reduction of mean free path of $CuFe_{1-x}Ga_xO_2$ (x = 0.1, 0.3, and 0.5) resulted from both effects of the mass fluctuation anharmonic and the lattice strain.

4 Conclusion

The thermal transport and properties of Ga^{3+}-substituted (for Fe^{3+}) $CuFeO_2$ delafossite, a thermoelectric material, were investigated. $CuFe_{1-x}Ga_xO_2$, x = 0.0, 0.1, 0.3, and 0.5 samples were prepared by a conventional solid-state reaction method, and their phase structure, elemental composition, and thermal conductivity were characterized by XRD, EDX, XPS, and thermal measurements, respectively. XRD confirmed that the delafossite $CuFe_{1-x}Ga_xO_2$ structure was obtained for all samples, EDX results show composition atomic percent of Ga 100 % of x = 0.1, 93 % of x = 0.3 and 90 % of x = 0.5 and XPS verified the presence of Cu^{1+} and Cu^{2+}, Fe^{2+} and Fe^{3+}, and Ga^{3+} ions in the structure. Ga substitution into Fe sites was found to reduce the *a* and *c* lattice constants with increasing Ga content. The thermal conductivity also decreased as the Ga content was increased. The main contribution to thermal transport and therefore the thermal properties of the samples was the phonon mechanism via defect of scattering processes. The substitution of Ga into Fe sites resulted in scattering arising from mass difference and lattice strain. Thus, the observed low thermal conductivity of the delafossite $CuFe_{1-x}Ga_xO_2$ was caused by dual defects from the mass difference and the lattice strain introduced by the Ga substitution.

Acknowledgments C. Ruttanapun would like to thank the Thailand Research Fund (TRF) and King Mongkut's Institute of Technology Ladkrabang (KMITL) (Contract Number: TRG5880013) for financial support. The author would like to thank Density Laboratory, Mechanical Department, National Institute of Metrology Thailand for provide measured density value of all samples. Additional financial support was provided by a grant from the KMITL Research Fund of King Mongkut's Institute of Technology Ladkrabang, Ministry of Education, Thailand.

References

1. R.D. Shannon, D.B. Rogers, C.T. Prewitt, Inorg. Chem. **10**(4), 713–718 (1971)
2. C.T. Prewitt, R.D. Shonnon, D.B. Rogers, Inorg. Chem. **10**(4), 719–723 (1971)
3. M. Grundmann, *The Physics of Semiconductor*, 2nd edn. (Springer, Berlin, 2010), p. 54
4. R.B. Gall, N. Ashmore, M.A. Marquardt, X. Tan, D.P. Cann, J. Alloys Compd. **391**, 261–266 (2005)
5. C. Ruttanapun, A. Wichainchai, W. Prachamon, A. Yangthaisong, A. Charoemphakdee, T. Seetawan, J. Alloys Compd. **509**, 4588–4594 (2011)
6. T. Nozaki, K. Hayashi, T. Kajitani, J. Electron. Mater. **39**(9), 1798–1802 (2010)
7. Joint Committee on Powder Diffraction Standards (JCPDS), Card No. 39-0246
8. M. Laianne, A. Barnabe, F. Mathieu, Ph Tailhades, Inorg. Chem. **48**, 6065–6071 (2009)
9. Joint Committee on Powder Diffraction Standards (JCPDS), Card No. 77-2495
10. B.D. Cullity, *Element of X-Ray Diffraction* (Addison-Wesley, Reading, 1978). (**Ch 9 and Appendix**)
11. M.A. Wahab, *Solid State Physics Structure and Properties of Material*, 2nd edn. (Alpha Science, Oxford, 2005), pp. 300–322
12. T. Nozaki, K. Hayashi, T. Kajitani, J. Electron. Mater. **38**(79), 1282–1286 (2009)
13. T. Fujii, F.M.F. de Groot, G.A. Sawatzky, Phys. Rev. B **59**, 3195–3202 (1999)
14. A.P. Grosvenor, B.A. Kobe, M.C. Biesinger, N.S. McIntyre, Surf. Interface Anal. **36**, 1564–1574 (2004)
15. J.P. Tobin, W. Hirschwald, J. Cunningham, Appl. Surf. Sci. **16**, 441–452 (1983)
16. S.W. Gaarenstroom, N. Winograd, J. Chem. Phys. **67**, 3500 (1977)
17. G. Cabello, A. Araneda, L. Lillo, C. Caro, C. Venegas, M. Tejos, B. Chornik, Solid State Sci. **27**, 24–29 (2014)
18. T. Pangviwate, IMEKO TC3 & TC5 & TC22 International Conference, Nov 22–25, Chonburi (2010)
19. J. Francl, W.D. Kingery, J. Am. Ceram. Soc. **37**, 99 (1954)
20. C.G. Sivan Pillai, A.M. George, J. Phys. Chem. Solids **55**, 479 (1994)
21. C. Wood, Rep. Prog. Phys. **51**, 459–539 (1988)
22. A.F. Ioffe, *Semiconductor Thermoelements and Thermoelectric Cooling* (Infosearch Limited, London, 1957)
23. V. Ambegaoker, Phys. Rev. **114**, 488 (1959)
24. G.A. Slack, Solid State Phys. **34**, 1 (1979)
25. P.G. Klemens, in *Solid State Physics*, vol. 7, ed. by F. Seitz, D. Turnbull (Academic, New York, 1958), p. 1
26. B. Abeles, Phys. Rev. **131**(N5), 1906–1911 (1963)
27. C. Ruttanapun, S. Maensiri, J. Phys. D Appl. Phys. **48**, 495103 (2015)
28. C. Ruttanapun, J. Solid State Chem. **215**, 43–49 (2014)

ประวัติผู้เขียน (Biography)

ชื่อ – นามสกุล	ยุทธนา หงษ์อารมณ์กิจ
วัน เดือน ปีเกิด	19 พฤษภาคม 2516 ต. บ้านใหม่ อ.บางใหญ่ จ.นนทบุรี
ที่อยู่	59/258 ต. แสมดำ อ.บางขุนเทียน จ.กรุงเทพ 10150

ประวัติการศึกษา

พ.ศ. 2519-2522	อนุบาล: โรงเรียน ประชาเจริญ คลอง 12 จ. ปทุมธานี
พ.ศ. 2523-2529	ประถมศึกษา: โรงเรียน มงคลประชาราม และโรงเรียน บางขุนเทียนศึกษา
พ.ศ. 2529-2531	มัธยมต้น: โรงเรียนรัตนโกสินทร์สมโภชบางขุนเทียน
พ.ศ. 2531-2533	มัธยมปลาย: โรงเรียนบางมดวิทยา
พ.ศ. 2536-2542	ปริญญาตรี: มหาวิทยาลัยรามคำแหง
พ.ศ. 2542-2546	ปริญญาโท: สถาบันเทคโนโลยีพระจอมเกล้าเจ้าคุณทหารลาดกระบัง

ประสบการณ์การทำงาน

พ.ศ. 2548- ปัจจุบัน	**ตำแหน่ง** นักมาตรวิทยาชำนาญการ **งาน** ห้องปฏิบัติการระยะขีดสเกล ฝ่ายมาตรวิทยามิติ สถาบัน มาตรวิทยาแห่งชาติ 3/4-5 ต. คลองห้า อ. คลองหลวง จ. ปทุมธานี